PHYSICAL-BIOLOGICAL INTERACTIONS AND THE THERMODYNAMICS OF THE UPPER OCEAN

by

Pulysary Ravindran

Submitted in partial fulfillment of the requirements
for the degree of Doctor of Philosophy

at

Dalhousie University
Halifax, Nova Scotia
November, 1995

National Library
of Canada

Acquisitions and
Bibliographic Services Branch

395 Wellington Street
Ottawa, Ontario
K1A 0N4

Bibliothèque nationale
du Canada

Direction des acquisitions et
des services bibliographiques

395, rue Wellington
Ottawa (Ontario)
K1A 0N4

Your file Votre référence

Our file Notre référence

ISBN 0-612-15819-5

Canada

Name RAVINDRAN PULYARY

Dissertation Abstracts International and *Masters Abstracts International* are arranged by broad, general subject categories. Please select the one subject which most nearly describes the content of your dissertation or thesis. Enter the corresponding four-digit code in the spaces provided.

PHYSICAL OCEANOGRAPHY
SUBJECT TERM

0415 UMI
SUBJECT CODE

Subject Categories

THE HUMANITIES AND SOCIAL SCIENCES

COMMUNICATIONS AND THE ARTS
Architecture 0729
Art History 0377
Cinema 0900
Dance 0378
Fine Arts 0357
Information Science 0723
Journalism 0391
Library Science 0399
Mass Communications 0708
Music 0413
Speech Communication 0459
Theater 0465

EDUCATION
General 0515
Administration 0514
Adult and Continuing 0516
Agricultural 0517
Art 0273
Bilingual and Multicultural 0282
Business 0688
Community College 0275
Curriculum and Instruction 0727
Early Childhood 0518
Elementary 0524
Finance 0277
Guidance and Counseling 0519
Health 0680
Higher 0745
History of 0520
Home Economics 0278
Industrial 0521
Language and Literature 0279
Mathematics 0280
Music 0522
Philosophy of 0998
Physical 0523
Psychology 0525
Reading 0535
Religious 0527
Sciences 0714
Secondary 0533
Social Sciences 0534
Sociology of 0340
Special 0529
Teacher Training 0530
Technology 0710
Tests and Measurements 0288
Vocational 0747

LANGUAGE, LITERATURE AND LINGUISTICS
Language
- General 0679
- Ancient 0289
- Linguistics 0290
- Modern 0291

Literature
- General 0401
- Classical 0294
- Comparative 0295
- Medieval 0297
- Modern 0298
- African 0316
- American 0591
- Asian 0305
- Canadian (English) 0352
- Canadian (French) 0355
- English 0593
- Germanic 0311
- Latin American 0312
- Middle Eastern 0315
- Romance 0313
- Slavic and East European 0314

PHILOSOPHY, RELIGION AND THEOLOGY
Philosophy 0422
Religion
- General 0318
- Biblical Studies 0321
- Clergy 0319
- History of 0320
- Philosophy of 0322

Theology 0469

SOCIAL SCIENCES
American Studies 0323
Anthropology
- Archaeology 0324
- Cultural 0326
- Physical 0327

Business Administration
- General 0310
- Accounting 0272
- Banking 0770
- Management 0454
- Marketing 0338

Canadian Studies 0385
Economics
- General 0501
- Agricultural 0503
- Commerce-Business 0505
- Finance 0508
- History 0509
- Labor 0510
- Theory 0511

Folklore 0358
Geography 0366
Gerontology 0351
History
- General 0578
- Ancient 0579
- Medieval 0581
- Modern 0582
- Black 0328
- African 0331
- Asia, Australia and Oceania 0332
- Canadian 0334
- European 0335
- Latin American 0336
- Middle Eastern 0333
- United States 0337

History of Science 0585
Law 0398
Political Science
- General 0615
- International Law and Relations 0616
- Public Administration 0617

Recreation 0814
Social Work 0452
Sociology
- General 0626
- Criminology and Penology 0627
- Demography 0938
- Ethnic and Racial Studies 0631
- Individual and Family Studies 0628
- Industrial and Labor Relations 0629
- Public and Social Welfare 0630
- Social Structure and Development 0700
- Theory and Methods 0344

Transportation 0709
Urban and Regional Planning 0999
Women's Studies 0453

THE SCIENCES AND ENGINEERING

BIOLOGICAL SCIENCES
Agriculture
- General 0473
- Agronomy 0285
- Animal Culture and Nutrition 0475
- Animal Pathology 0476
- Food Science and Technology 0359
- Forestry and Wildlife 0478
- Plant Culture 0479
- Plant Pathology 0480
- Plant Physiology 0817
- Range Management 0777
- Wood Technology 0746

Biology
- General 0306
- Anatomy 0287
- Biostatistics 0308
- Botany 0309
- Cell 0379
- Ecology 0329
- Entomology 0353
- Genetics 0369
- Limnology 0793
- Microbiology 0410
- Molecular 0307
- Neuroscience 0317
- Oceanography 0416
- Physiology 0433
- Radiation 0821
- Veterinary Science 0778
- Zoology 0472

Biophysics
- General 0786
- Medical 0760

EARTH SCIENCES
Biogeochemistry 0425
Geochemistry 0996
Geodesy 0370
Geology 0372
Geophysics 0373
Hydrology 0388
Mineralogy 0411
Paleobotany 0345
Paleoecology 0426
Paleontology 0418
Paleozoology 0985
Palynology 0427
Physical Geography 0368
Physical Oceanography 0415

HEALTH AND ENVIRONMENTAL SCIENCES
Environmental Sciences 0768
Health Sciences
- General 0566
- Audiology 0300
- Chemotherapy 0992
- Dentistry 0567
- Education 0350
- Hospital Management 0769
- Human Development 0758
- Immunology 0982
- Medicine and Surgery 0564
- Mental Health 0347
- Nursing 0569
- Nutrition 0570
- Obstetrics and Gynecology 0380
- Occupational Health and Therapy 0354
- Ophthalmology 0381
- Pathology 0571
- Pharmacology 0419
- Pharmacy 0572
- Physical Therapy 0382
- Public Health 0573
- Radiology 0574
- Recreation 0575
- Speech Pathology 0460
- Toxicology 0383

Home Economics 0386

PHYSICAL SCIENCES
Pure Sciences
Chemistry
- General 0485
- Agricultural 0749
- Analytical 0486
- Biochemistry 0487
- Inorganic 0488
- Nuclear 0738
- Organic 0490
- Pharmaceutical 0491
- Physical 0494
- Polymer 0495
- Radiation 0754

Mathematics 0405
Physics
- General 0605
- Acoustics 0986
- Astronomy and Astrophysics 0606
- Atmospheric Science 0608
- Atomic 0748
- Electronics and Electricity 0607
- Elementary Particles and High Energy 0798
- Fluid and Plasma 0759
- Molecular 0609
- Nuclear 0610
- Optics 0752
- Radiation 0756
- Solid State 0611

Statistics 0463

Applied Sciences
Applied Mechanics 0346
Computer Science 0984
Engineering
- General 0537
- Aerospace 0538
- Agricultural 0539
- Automotive 0540
- Biomedical 0541
- Chemical 0542
- Civil 0543
- Electronics and Electrical 0544
- Heat and Thermodynamics 0348
- Hydraulic 0545
- Industrial 0546
- Marine 0547
- Materials Science 0794
- Mechanical 0548
- Metallurgy 0743
- Mining 0551
- Nuclear 0552
- Packaging 0549
- Petroleum 0765
- Sanitary and Municipal 0554
- System Science 0790

Geotechnology 0428
Operations Research 0796
Plastics Technology 0795
Textile Technology 0994

PSYCHOLOGY
General 0621
Behavioral 0384
Clinical 0622
Developmental 0620
Experimental 0623
Industrial 0624
Personality 0625
Physiological 0989
Psychobiology 0349
Psychometrics 0632
Social 0451

In loving memory of my parents

TABLE OF CONTENTS

LIST OF FIGURES

LIST OF TABLES

ABSTRACT

The effects of phytoplankton-induced changes in the attenuation of solar radiation in the ocean on the evolution of the surface, mixed layer and the heat exchange across the sea surface are examined in this study. A sensitivity analysis of the bulk (depth-integrated) class of mixed-layer models is used to explain the pathways through which the phytoplankton variability can influence the depth and temperature of the mixed layer. Conditions under which this influence can be expected to be significant are identified. The model equation for mixed-layer depth, common to all bulk models, is extended to take into account the spectral dependence of light transmission in the ocean as a function of phytoplankton biomass.

Changes in the potential energy of the upper ocean associated with vertical mixing are balanced against the TKE input to develop a general, bulk model of the oceanic mixed layer. The Kraus-Turner-type, bulk, mixed-layer models can be derived as special cases of this model. Moreover, the essential requirements, common to models of the Kraus-Turner-type, of a temperature discontinuity at the base of the mixed layer and the *a priori* existence of an initial mixed layer, are eliminated in the present formulation. A non-dimensional form of the general, bulk model is used to identify limitations inherent to conventional, bulk, mixed-layer models.

A coupled model of physical-biological interactions in the mixed layer, in the presence of air-sea heat exchange, is developed by combining the general, bulk model of the oceanic mixed layer with an energy-balance model of the atmosphere and a nitrogen-conserving model of net primary production in the mixed layer. This coupled model is used to examine the contributions from seasonal modulations in phytoplankton biomass to the evolution of mixed-layer depth, mixed-layer temperature, air temperature, and heat exchange across the sea surface for a hypothetical station at 50°N latitude. From the results of this analysis, a conceptual model of physical-biological interactions in the mixed layer and the heat exchange between the ocean and the atmosphere is developed as a suite of interacting feedback loops.

LIST OF SYMBOLS

Notation	Quantity and Description	Dimensions	Typical Units
α	Coefficient of thermal expansion	K^{-1}	$°C^{-1}$
α^B	Biomass-normalized initial slope of the P - I curve	$M^{-1}\ T^2$	mg C h^{-1}(W m^{-2})$^{-1}$(mg chl-a)$^{-1}$
β	Solar declination	Radians	Radians
χ	Carbon-chlorophyll ratio	Dimensionless	—
$\delta(z)$	Dirac delta function of depth z	Dimensionless	—
Δ_r	Fractional change in the density caused by solar heating in equation (2.9)	Dimensionless	—
$\gamma(z)$	Attenuation coefficient at depth z	L^{-1}	m^{-1}
γ_e	Attenuation coefficient of the entrainment layer	L^{-1}	m^{-1}
γ_m	Attenuation coefficient of the mixed layer	L^{-1}	m^{-1}
$(\gamma_m)_0$	An arbitrary value of γ_m	L^{-1}	m^{-1}
γ_i	Attenuation coefficient of the i^{th} sub-layer	L^{-1}	m^{-1}
Γ	A function of day number J defined as $\Gamma = 2\pi(J-1)/365$	Dimensionless	—
$\hbar$	The depth through which a phytoplankton cell sinks during one day	L	m
κ	Absorptivity of shortwave radiation in the atmosphere	Dimensionless	—
λ	Wavelength	L	nm
Λ	Change in the potential energy resulting from the removal of stratification at the base of the mixed layer in equation (3.42)	$M\ T^{-2}$	Kg s^{-2}
$\phi(z_1, z_2)$	Depth-integrated change in the potential energy for unit area of a layer of thickness $(z_2 - z_1)$, produced by vertical mixing	$M\ T^{-2}$	J m^{-2}
$\phi(0, h_m)$	Depth-integrated change in the potential energy for unit area	$M\ T^{-2}$	J m^{-2}

	of the surface layer, produced by vertical mixing		
$\phi(0, h_m^+)$	Depth-integrated change in the potential energy for unit area of an entraining mixed layer, produced by vertical mixing	$M\ T^{-2}$	$J\ m^{-2}$
$\phi(h_m, h_m^+)$	Depth-integrated change in the potential energy for unit area of the entrainment layer, produced by vertical mixing	$M\ T^{-2}$	$J\ m^{-2}$
$\tilde{\phi}(0, h_m^+)$	Depth-integrated change in the potential energy resulting from mixing between the surface layer and the entrainment layer of unit area	$M\ T^{-2}$	$J\ m^{-2}$
Φ	Heaviside step function	Dimensionless	—
ψ	Latitude	Degree	Degree
ρ	Density of sea water	$M\ L^{-3}$	$Kg\ m^{-3}$
$\rho(T)$	Density of sea water as a function of temperature T	$M\ L^{-3}$	$Kg\ m^{-3}$
$\rho(z)$	Density of sea water as a function of depth z	$M\ L^{-3}$	$Kg\ m^{-3}$
$\overline{\rho}$	Depth-averaged density of a given layer in the ocean	$M\ L^{-3}$	$Kg\ m^{-3}$
ρ_a	Density of the atmosphere	$M\ L^{-3}$	$Kg\ m^{-3}$
ρ_b	Density at the base of the mixed-layer at the beginning of a time step	$M\ L^{-3}$	$Kg\ m^{-3}$
$\rho_e(z)$	Density at depth z in the entrainment layer at the beginning of a time step	$M\ L^{-3}$	$Kg\ m^{-3}$
ρ_m	Density of the surface layer at the beginning of a time step	$M\ L^{-3}$	$Kg\ m^{-3}$
$\Delta\rho_m$	Density difference between the mixed layer and the underlying water	$M\ L^{-3}$	$Kg\ m^{-3}$
$\rho'(z)$	Density of the surface layer and the entrainment layer after internal mixing	$M\ L^{-3}$	$Kg\ m^{-3}$
$\overline{\rho}^e$	Depth-averaged density of the entrainment layer at the end of a time step	$M\ L^{-3}$	$Kg\ m^{-3}$
$\overline{\rho}^m$	Depth-averaged density of the surface layer at the end of a time step	$M\ L^{-3}$	$Kg\ m^{-3}$
σ	The Stefan-Boltzmann constant	$M\ T^{-3}K^{-4}$	$W\ m^{-2}\ K^{-4}$
τ	Wind stress	$M\ L^{-1}T^{-2}$	Pascal
θ	Optical depth of a layer, defined as the product of the	Dimensionless	—

	attenuation coefficient and the thickness of the layer		
θ_1	The lower bound of θ in equation (3.34)	Dimensionless	—
θ_2	The upper bound of θ in equation (3.34)	Dimensionless	—
ζ	Transfer coefficient of sensible heat	$M\ T^{-3}K^{-1}$	$W\ m^{-2}\ °C^{-1}$
ζ'	Relative vorticity	T^{-1}	s^{-1}
a	Linear gradient in the density profile in the entrainment layer	$M\ L^{-4}$	$Kg\ m^{-4}$
A	A scale-factor in the expression for daily, mixed-layer primary production	$M\ L^{-2}$	$mg\ C\ m^{-2}$
B	Phytoplankton biomass	$M\ L^{-3}$	$mg\ chl\text{-}a\ m^{-3}$
ΔB	Change in the phytoplankton biomass (in the mixed layer) during one day	$M\ L^{-3}$	$mg\ chl\text{-}a\ m^{-3}$
C_a	Specific heat of air at constant pressure	$L^2T^{-2}K^{-1}$	$J\ kg^{-1}\ °C^{-1}$
C_d	Drag coefficient	Dimensionless	—
C_p	Specific heat of sea water at constant pressure	$L^2T^{-2}K^{-1}$	$J\ kg^{-1}\ °C^{-1}$
c_E	Bulk coefficient of evaporation of water	$M\ T^{-3}$	$W\ m^{-2}$
d	Day length	T	h
D	Depth-integrated rate of dissipation of TKE	$M\ T^{-3}$	$J\ m^{-2}\ s^{-1}$
	per unit area of the mixed layer		
e_a	Thermal emissivity of the atmosphere	Dimensionless	—
e_o	Thermal emissivity of the ocean	Dimensionless	—
e_p	Planetary (thermal) emissivity	Dimensionless	—
$E(0)$	Latent heat flux across the sea surface	$M\ T^{-3}$	$W\ m^{-2}$
f	Planetary vorticity	T^{-1}	s^{-1}
f_{h_e}	A function of γ_e in equation (3.25)	Dimensionless	—
f_{h_m}	A function of γ_m in equation (2.34)	Dimensionless	—
$f_{h_m^+}$	The function f_{h_m} based on h_m^+	Dimensionless	—

$f^n_{h_m}$	A function of γ_i in equation (2 48)	Dimensionless	—
f_{T_m}	A function of γ_m in equation (2 37)	Dimensionless	—
$f^n_{T_m}$	A function of γ_i in equation (2 49)	Dimensionless	—
F	A function representing the contribution from solar heating to the change in potential energy of the mixed layer (equation (2 5))	$M\ T^{-3}$	$W\ m^{-2}$
F'	A function derived from F	$M\ T^{-2}L^{-1}$	$J\ m^{-3}$
g	Gravitational acceleration	$L\ T^{-2}$	$m\ s^{-2}$
G	Depth-integrated rate of generation of TKE per unit area of the mixed layer	$M\ T^{-3}$	$J\ m^{-2}s^{-1}$
h_a	Height of the model atmosphere	L	m
h_e	Depth of the entrainment layer	L	m
h_m	Depth of the mixed layer	L	m
$(h_m)_\infty$	Depth of the mixed layer when $\gamma_m \to \infty$	L	m
$(h_m)_0$	Depth of the mixed layer when $\gamma_m \to 0$	L	m
h^+_m	Depth of the mixed layer at the end of a time step	L	m
$H(0)$	Total heat flux at the sea surface, $H(0) = Q(0) + I(0)$	$M\ T^{-3}$	$W\ m^{-2}$
$H(-h_a)$	Total heat flux at the top of the atmosphere, $H(-h_a) = R(-h_a) + L(-h_a)$	$M\ T^{-3}$	$W\ m^{-2}$
i	Summation index for sub-layers used in the derivation of $f^n_{h_m}$ and $f^n_{T_m}$ $(1 \le i \le n)$	Dimensionless	—
$I(0)$	Penetrative component of solar radiation at the sea surface	$M\ T^{-3}$	$W\ m^{-2}$
$I(z)$	Penetrative component of solar radiation at depth z	$M\ T^{-3}$	$W\ m^{-2}$
$I_d(z)$	Daily solar radiation at depth z	$M\ T^{-3}$	$W\ m^{-2}$
$I_l(z)$	A form of $I(z)$ that decays linearly through the mixed layer	$M\ T^{-3}$	$W\ m^{-2}$
$I^m(0)$	Daily-maximum (noon) value of $I(0)$	$M\ T^{-3}$	$W\ m^{-2}$

$\hat{I}(0)$	Non-penetrative component of solar radiation at the sea surface	$M\ T^{-3}$	$W\ m^{-2}$
I_k	Photoadaptation parameter defined as: $I_k = P_m^B/\alpha^B$	$M\ T^{-3}$	$W\ m^{-2}$
I_*^m	Dimensionless form of $I(0)$, defined as: $I_*^m = I(0)^m/I_k$	Dimensionless	—
j	Summation index for sub-layers used in the derivation of $f_{h_m}^n$ and $f_{T_m}^n$ $(1 \leq j \leq i-1)$	Dimensionless	—
J	Day number	Dimensionless	—
K_m	Half-saturation coefficient for nitrogen uptake	$M\ L^{-3}$	$mmol\ N\ m^{-3}$
$L(-h_a)$	Long-wave radiation at the top of the atmosphere	$M\ T^{-3}$	$W\ m^{-2}$
$L(0)$	Long-wave radiation at the sea surface	$M\ T^{-3}$	$W\ m^{-2}$
l_T^B	Carbon equivalent of the biomass-specific loss of phytoplankton from the mixed layer through respiration, excretion, grazing and sedimentation, averaged over the day and over the layer depth, $l_T^B = l_R^B + l_E^B + l_G^B + l_S^B$	T^{-1}	$mg\ C\ (mg\ chl\text{-}a)^{-1}\ h^{-1}$
l_G^B	Carbon equivalent of the biomass-specific loss of phytoplankton from the mixed layer through zooplankton grazing, averaged over the day and over the layer depth	T^{-1}	$mg\ C\ (mg\ chl\text{-}a)^{-1}\ h^{-1}$
l_R^B	Carbon equivalent of the biomass-specific loss of phytoplankton from the mixed layer through respiration, averaged over the day and over the layer depth	T^{-1}	$mg\ C\ (mg\ chl\text{-}a)^{-1}\ h^{-1}$
l_E^B	Carbon equivalent of the biomass-specific loss of phytoplankton from the mixed layer through excretion, averaged over the day and the layer depth	T^{-1}	$mg\ C\ (mg\ chl\text{-}a)^{-1}\ h^{-1}$
l_S^B	Carbon equivalent of the biomass-specific loss of phytoplankton from the mxied layer through sedimentation, averaged over the day	T^{-1}	$mg\ C\ (mg\ chl\text{-}a)^{-1}\ h^{-1}$

	and the layer depth		
$l_{h_m,24}$	Total loss of organic carbon from the phytoplankton community in the mixed layer integrated over the day (24h) and the layer depth	M L^{-2}	mg C m^{-2}
M	Optical transmittance of the mixed layer defined as $M = e^{-\gamma_m h_m}$	Dimensionless	—
n	Total numbers of sub-layers used in in the derivation of $f^n_{h_m}$	Dimensionless	—
$N(z)$	Nitrogen concentration at depth z	M L^{-3}	mmol N m^{-3}
N_m	Nitrogen concentration in the mixed layer at the beginning of the time step	M L^{-3}	mmol N m^{-3}
ΔN_m	Change in the nitrogen concentration in the mixed layer during the time step	M L^{-3}	mmol N m^{-3}
N^+_m	Nitrogen concentration in the mixed layer at the end of the time step	M L^{-3}	mmol N m^{-3}
N_e	Daily input of nitrogen to the mixed layer through entrainment	M L^{-3}	mmol N m^{-3}
ΔN_e	Change in the nitrogen concentration in the entrainment layer during the time step	M L^{-3}	mmol N m^{-3}
$p_k\|_{(k=1\cdots5)}$	Coefficients used in the rational-polynomial approximation of equation (3.34)	Dimensionless	—
P^B_m	Biomass specific maximum production at saturating light	T^{-1}	mg C (mg chl-a)$^{-1}$ h^{-1}
$P_{h_m,d}$	Total production of organic carbon by phytoplankton in the mixed layer integrated over the day length and the layer depth	M L^{-2}	mg C m^{-2}
$P^N_{h_m,d}$	Total production of organic carbon by phytoplankton in the mixed layer integrated over the day length and the layer depth in the presence of nutrient limitation	M L^{-2}	mg C m^{-2}
q	Potential vorticity	T^{-1}	s^{-1}
$Q(0)$	Non-penetrative heat flux across the sea surface averaged over the day, $Q(0) = \hat{I}(0) + L(0) + E(0) + S(0)$	M T^{-3}	W m^{-2}
$R(0)$	Total solar radiation at the sea surface	M T^{-3}	W m^{-2}

	averaged over the day $R(0) = I(0) + \hat{I}(0)$		
$R(-h_a)$	Total solar radiation the top of the atmosphere averaged over the day	M T^{-3}	W m^{-2}
$R(-h_a, t)$	Solar radiation at the top of the atmosphere at time t	M T^{-3}	W m^{-2}
$R^m(-h_a)$	Daily maximum value of total solar radiation at the top of the atmosphere	M T^{-3}	W m^{-2}
R_D	Coefficient representing the change in the dark respiration of phytoplankton per unit change in growth rate	Dimensionless	—
R_L	Coefficient representing the increase in respiration of phytoplankton in the presence of light	Dimensionless	—
R_s	Solar constant	M T^{-3}	W m^{-2}
R_0^B	Respiration in the absence of growth	T^{-1}	mg C (mg chl-a)$^{-1}$ h^{-1}
$S(0)$	Sensible heat flux from the sea surface averaged over the day	M T^{-3}	W m^{-2}
t	Time	T	s
Δt	Time step of integration	T	s
ΔT	Change in the mixed-layer temperature at the end of a time interval of Δt	K	°C
$(\Delta T)_{\gamma_m}$	Increase in temperature of a shallowing mixed layer for an arbitrary γ_m	K	°C
$(\Delta T)_0$	Increase in temperature of a shallowing mixed layer for the limiting case of $\gamma_m \to 0$	K	°C
ΔT_a	Change in the air temperature at the end of a time interval of Δt	K	°C
$T(z)$	Temperature at depth z	K	°C
T_b	Temperature at the base of the mixed layer	K	°C
T_m	Temperature of the mixed layer	K	°C
T_m^+	Temperature of the mixed layer at the end of the time step	K	°C
$(T_m)_\infty$	Temperature of the mixed layer when $\gamma \Rightarrow \infty$	K	°C

$(T_m)_0$	Temperature of the mixed layer when $\gamma \Rightarrow 0$	K	°C
U	Wind speed	$\mathrm{L\,T^{-1}}$	$\mathrm{m\,s^{-1}}$
v	Relative humidity of the atmosphere	Dimensionless	—
w	Vertical velocity below the mixed layer	$\mathrm{L\,T^{-1}}$	$\mathrm{m\,s^{-1}}$
X_0	Zeroth order coefficient in the quardratic approximation of equation (3.25)	Dimensionless	—
X_1	First order coefficient in the quardratic approximation of equation (3.25)	Dimensionless	—
X_2	Second order coefficient in the quardratic approximation of equation (3.25)	Dimensionless	—
Y_0	Zeroth order coefficient in equation (3.35)	Dimensionless	—
Y_1	First order coefficient in equation (3.35)	Dimensionless	—
Y_2	Second order coefficient in equation (3.35)	Dimensionless	—
z	Depth	L	m
Δz_i	Thickness of the i^{th} sub-layer	L	m

ACKNOWLEDGEMENTS

This thesis represents a milestone in my educational life. At this point, appreciation keenly felt prompts the acknowledgement of indebtedness to the several teachers, colleagues, friends and family members who have helped and encouraged me throughout the journey of my education. In particular, I would like to thank Dr. Trevor Platt and Dr. Shubha Sathyendranath for their patient and dedicated guidance on all aspects, and at all stages of my thesis work. Also, I thank Dr. Kenneth L. Denman, Dr. Jon Grant, Dr. Barry Ruddick and Dr. Daniel G. Wright for their valuable suggestions and constructive comments on the thesis.

CHAPTER 1

General Introduction

The heat capacity of the top three meters of the world ocean is greater than that of the entire atmosphere overlying it (Gill, 1982). The oceans are the major source of the water vapour in the atmosphere. The heat flux across the ocean-atmosphere interface is a function of the temperature difference between the ocean and the atmosphere. These are some of the characteristic features that make the surface layer of the ocean an important contributor to the global climate.

The effect of variability in the sea-surface temperature on atmospheric processes has been the subject of several investigations in the past. Such studies have revealed for example that in the tropical regions atmospheric processes such as storms, disturbances and organized convection tend to occur in those regions where the sea-surface temperature is above 28°C (Webster, 1994). Statistical analyses have indicated that the intensity of many of the atmospheric processes can be correlated with sea-surface temperature patterns (Rasmusson and Carpenter, 1983; Joseph *et al.*, 1991). Numerical studies using general circulation models of the atmosphere have shown that model evolution is sensitive to perturbations in the prescribed values of sea-surface temperature with respect to its climatological mean value (Palmer, 1985; Kershaw, 1988). The effect of spatial and temporal variability in the sea-surface temperature on global climate has been the focus of studies of El Niño, which is characterized by the large-scale warming of the tropical Pacific waters by more than 1.5°C for three consecutive months (Halpern, 1983). All these points suggest that improvements in our ability to model the seasonal evolution of sea-surface temperature will definitely lead to improvements in our understanding of large-scale climatic processes.

The sensitivity of atmospheric processes to the sea-surface temperature has prompted researchers to study the factors responsible for changes in the temperature and to develop numerical models for accurate prediction of its spatial and temporal variability. International projects such as TOGA (Tropical Ocean and Global Atmosphere) were undertaken in recognition of the important role played by the sea-surface temperature in driving atmospheric processes. One of the goals set by the TOGA program is to obtain an accuracy of 0.3°C in measurements of the sea-surface temperature over a $2° \times 2°$ spatial grid with a temporal resolution of 15 days (Anonymous, 1983). This goal underlines the significance of accurate information on variability in the sea-surface temperature for climatic studies.

In the past decades, several mixed-layer models have been developed to describe the seasonal evolution of the sea-surface temperature and mixed-layer depth (Kraus and Turner, 1967; Denman, 1973; Mellor and Yamada, 1974; Mellor and Durbin, 1975; Niiler and Kraus, 1977; Garwood, 1977; Price *et al.,* 1986; Gaspar, 1988). Many of these models have been coupled to upper-ocean circulation models (Rosati and Miyakoda, 1988; Schopf and Harrison, 1983; McCreary and Kundu, 1989; Cherniawsky *et al.,* 1990). Comparison of several mixed-layer models with long-term observations has shown that, even though these models are generally successful in reproducing the seasonal evolution of the sea-surface temperature (Martin, 1985; Gaspar, 1988; Kantha and Clayson, 1994; Large *et al.,* 1994), the accuracy of model results is not always satisfactory. Further improvements in mixed-layer modelling are therefore required.

Much of the research devoted to improve the performance of mixed-layer models has addressed the parameterization of the turbulent kinetic-energy budget used in these models (Garwood, 1977; Garwood, 1979; Zilitinkevich *et al.,* 1979; Gaspar, 1988; Kantha and Clayson, 1994). However, the lack of a significant improvement in model performance has forced modelers to search for alternative ways of refining the models. One issue that has received attention in the recent past is the effect

of optical variability on the evolution of the mixed-layer temperature (Dickey and Simpson, 1983; Simpson and Dickey, 1981; Woods and Barkmann, 1986). Because phytoplankton is the major source of changes in the optical properties in the open ocean, the effects of phytoplankton variability on the upper-ocean thermal structure have received special consideration (Lewis *et al.*, 1983; Kirk, 1988; Simonot *et al.*, 1988; Sathyendranath *et al.*, 1991; Platt *et al.*, 1994; Sathyendranath and Platt, 1994).

Recent advances in satellite oceanography offer the possibility of obtaining synoptic maps of phytoplankton distribution in the ocean. Methods have also been developed to model the optical properties of the upper ocean as a function of phytoplankton biomass (Sathyendranath and Platt, 1988; Morel, 1991; Morel and Antoine, 1994). Moreover, our ability to model the coupled evolution of physical and biological processes in the upper ocean has also improved (Wroblewski 1976; Simonot *et al.*, 1988; Taylor *et al.*, 1991). These developments offer efficient means of incorporating the effect of phytoplankton variability into upper-ocean thermodynamic models. The general approach is to model the joint evolution of optical and thermodynamic processes in the upper ocean either by incorporating satellite-derived data on phytoplankton distribution directly into mixed-layer models (Sathyendranath *et al.*, 1991), or by coupling a biological model of the upper ocean to a mixed-layer model (Simonot *et al.*, 1988; Stramska and Dickey, 1993; Platt *et al.*, 1994; Sathyendranath and Platt, 1994).

It is well known that the depth of the mixed layer of the ocean affects the growth of phytoplankton in the layer (Sverdrup, 1953, Platt *et al.*, 1991). On the other hand, phytoplankton concentration modifies the attenuation of solar radiation in the mixed layer, which in turn, affects the mixed-layer depth and temperature. Thus there is a potential for positive feedback between mixed-layer biology and mixed-layer physics. This picture is further complicated by the existence of another feedback between the ocean and the atmosphere through the interdependence of sea-surface temperature and air-sea heat flux. In this thesis I examine some selected

aspects of these feedback processes with special emphasis on the effect of biological feedback on mixed-layer physics and on the heat exchange between the ocean and the atmosphere.

The main objectives of the thesis are:

1. To identify and describe the physical processes that make mixed-layer models sensitive to changes in the attenuation of solar radiation in the ocean.

2. To develop a mixed-layer model that is free of some of the major limitations of existing models and capable of providing an accurate description of the thermodynamic processes responsible for the evolution of the mixed-layer depth and temperature.

3 To describe the contributions from phytoplankton dynamics to the evolution of mixed-layer depth, mixed-layer temperature, air temperature and the air-sea heat exchange and to identify the factors regulating the feedbacks between mixed-layer physics, mixed-layer biology and atmospheric physics through model simulations.

In Chapter 2, I address the question: how does a given change in the attenuation coefficient of the mixed layer affect the layer depth and temperature predicted by conventional bulk mixed-layer models? Moreover, I identify the conditions under which the models become sensitive to changes in phytoplankton concentration and estimate the magnitude of the sensitivity under various oceanographic conditions. In Chapter 2, I also develop a method to incorporate the depth-dependent changes in the attenuation coefficient for solar radiation into mixed-layer models.

Bulk models of the oceanic mixed layer provide a simple description of the evolution of the layer depth and temperature. They are also the preferred choice as elements of large-scale models of upper-ocean processes and ocean-atmosphere

interactions (Kraus, 1988). However, some of the assumptions used in the development of bulk models are not strictly valid according to observations, and therefore limit their applicability (Mellor and Durbin, 1975). In Chapter 3, I have developed a bulk model of the mixed layer that is free from some of the major limitations associated with existing bulk models. Conventional bulk models can be derived as special cases of this model. A non-dimensional form of the model is used to explain the limitations on the time step of integration of conventional bulk models resulting from the simplifying assumptions used in the formulation of these models.

The mixed-layer model formulated in Chapter 3 is used in Chapter 4 to develop a coupled model of mixed-layer physics, mixed-layer biology and atmospheric physics. In this coupled model, the evolution of mixed-layer depth, mixed-layer temperature, air temperature, heat exchange across the sea surface and phytoplankton biomass are described as parts of feedback loops interacting with each other. This coupled model is used to examine the contributions from biological feedback to the evolution of the mixed-layer physics and atmospheric physics.

A general discussion of the research problem addressed in this thesis is given in Chapter 5. A conceptual model of physical-biological interactions in the ocean-atmosphere system is developed by synthesizing the results from Chapter 2 and Chapter 4. I have also discussed, in Chapter 5, some of the upper-ocean processes that require further study to provide a comprehensive description of the biological feedback on the evolution of upper-ocean physics.

CHAPTER 2

Optical Variability in the Upper Ocean: Implications for Mixed-Layer Modelling

2.1 Introduction

2.1.1 Upper-Ocean Optics and Mixed-Layer Physics

With the exception of a small percentage that is scattered back to the atmosphere, all the solar radiation entering the ocean is absorbed within the top few hundred meters of the water column. Water molecules, the organic compounds dissolved in the sea water, and the particulate material in suspension determine the rate of absorption of solar radiation in the ocean. Outside of the coastal waters, phytoplankton and products derived from them are the most important variable components affecting light absorption in the ocean. Seasonal and regional variabilities in them affect the depth distribution of solar-energy absorption in the ocean (in the spectral range between 400 and 700 nm). The effects of such variabilities can be incorporated into upper-ocean models of thermodynamics by specifying the attenuation coefficient of the mixed layer as a function of phytoplankton concentration.

It is known that the evolution of mixed-layer depth and temperature in the ocean is sensitive to the transparency of the water column. For example, Martin (1985) examined the effect of changes in the light attenuation using data from stations Papa (145°W, 50°N) and November (140°W, 30°N) using two bulk (depth-integrated) models and two turbulent-closure models. He reported significant changes in the layer temperature predicted by these models when the optical

water type was changed from type I of the Jerlov (1976) classification, representing clear open-ocean waters, to type III, representing highly turbid coastal waters. Using a thermodynamic model, Kirk (1988) carried out a sensitivity analysis to examine the effect of changes in the optical properties of the water column on the evolution of the surface temperature. In the absence of surface wind, the temperature of the layer deviated by about 3°C over 24 h simulated time, when the optical properties of the medium were changed from those of clear water to those of highly turbid water.

Simonot *et al.* (1988) used a coupled model of physical-biological interactions in the mixed layer and climatological observations of oceanographic and meteorological variables to simulate the seasonal evolution of mixed-layer depth and temperature at station 'Romeo' (North Atlantic). In this coupled model, the attenuation of solar radiation in the ocean was modelled as a function of the phytoplankton biomass using the Jerlov (1976) classification of the optical water types. Based on the results of the model simulation they reported that seasonal changes in phytoplankton concentration can modify the evolution of the mixed-layer temperature in a thermodynamic-biological-optical coupled model. Sathyendranath *et al.* (1991) carried out a model simulation to examine the effect of phytoplankton variability in the Arabian Sea on the evolution of mixed-layer temperature, when the attenuation coefficient of the mixed layer was parametrized as a function of phytoplankton biomass. Satellite-derived data on monthly-mean phytoplankton distribution together with a spectral-irradiance model of under-water light transmission (Sathyendranath and Platt, 1988) were used in this study to describe the attenuation of solar radiation in the ocean. The authors concluded that the presence of phytoplankton in the Arabian Sea could change the heating rate of the mixed layer more than 3°C per month. Ramp *et al.* (1991) observed strong temperature gradients (up to 4.7 °C between 4 cm and 2 m depths) in the surface layers off central California and suggested that such gradients can occur in the presence of high solar radiation, strong

attenuation of solar radiation associated with high concentration of phytoplankton biomass, and low wind.

Model simulations using turbulent-closure models have also confirmed the effects of phytoplankton-induced changes in the light attenuation in the ocean. Dickey and Simpson (1983) examined the diurnal cycle of upper-ocean thermal structure in coastal and open-ocean waters through model simulations, using a turbulent-closure model. The author concluded that the incorporation of optical variability associated with biological processes in the ocean may improve the performance of global climate models. Using high-resolution physical and biological data and a turbulent-closure model, Stramska and Dickey (1993) have also demonstrated the effects of phytoplankton variability on the thermal structure and stability of the upper ocean during a Spring phytoplankton bloom in high latitude seas.

The above results show that thermodynamic models are sensitive to changes in the light attenuation in the ocean. What are the factors that make thermodynamic models sensitive to changes in light attenuation? Under what conditions can the changes in light attenuation be expected to play an important role in the evolution of mixed-layer depth and temperature? These are two of the questions addressed in the following sections. Some background information on the model used in the analysis is presented first.

2.1.2 The Choice of Model

Over the last two decades, various one-dimensional models of upper-ocean thermodynamic and dynamic processes have been developed for simulating the evolution of mixed-layer depth and temperature with time (see Zilitinkevich, *et al.*, 1979; Martin, 1985 and Archer, 1990 for reviews). There are significant differences among these models, conceptually as well as in the details of their implementation. But

they can be divided into two groups: bulk models and turbulent-closure models (Martin 1985). Because of their modest computational requirements, bulk models are preferred for long-term simulations and as elements of large-scale numerical models (Kraus, 1988). Therefore I decided to carry out this study using a bulk mixed-layer model.

Bulk models share a common physical foundation, introduced by Kraus and Turner (1967), but they differ in the details of implementation and in the choice of parameters. Some of the major differences lie in the parametrizations of the generation and dissipation of turbulent kinetic energy (TKE) and in the parametrization of the depth distribution of solar energy absorption in the ocean (Zilitinkevich *et al.*, 1979; Garwood, 1979; Gaspar, 1988).

From all the bulk models available, I have selected the Denman (1973) model as the basis for a sensitivity analysis. The Denman scheme for parametrization of solar radiation in the ocean, or an approximation to it, is used in many bulk thermodynamic models (Kraus and Turner, 1967; Kim, 1976; Niiler and Kraus, 1977). Furthermore, this model has been used in several theoretical and field studies in the past (Denman, 1973; Denman and Miyake, 1973; Thompson, 1976; Zilitinkevich *et al.*, 1979, Shetye, 1986, McCormick, 1988), and its merits and limitations are well known.

2.1.3 The Model Equations

The model equations are derived by integrating the equations for conservation of heat and mechanical energy over the mixed-layer depth. The evolution of the depth and temperature of the mixed layer are described by the equations (Denman, 1973):

$$\Phi \cdot \left(w + \frac{dh_m}{dt}\right) = 2\Big\{\frac{(G-D)}{\rho\alpha g h_m} +$$

$$\frac{1}{\rho C_p}\Big[\frac{1}{h_m}\int_0^{h_m} I(z)dz - \frac{(I(0)+I(h_m))}{2}\Big] - \frac{1}{\rho C_p}\frac{Q(0)}{2}\Big\}(T_m - T_b)^{-1}, \qquad (2.1)$$

and

$$\frac{dT_m}{dt} = \frac{2}{h_m^2}\Big[-\frac{(G-D)}{\rho\alpha g} + \frac{Q(0)h_m + \int_0^{h_m}(I(0)-I(z))dz}{\rho C_p}\Big], \qquad (2.2)$$

respectively. Here, h_m and T_m are the depth and temperature of the mixed layer, T_b is the temperature just below the mixed layer, C_p is the specific heat of sea water at constant pressure, α is the coefficient of thermal expansion, ρ is the density of sea water and g is the acceleration due to gravity.

The shallowing and deepening phases of the mixed-layer evolution are considered separately by incorporating a Heaviside step function Φ in equation (2.1), defined as:

$$\Phi = 1 \text{ if } \left(w + \frac{dh_m}{dt}\right) > 0 \quad \text{(entraining mixed layer)}, \qquad (2.3)$$

and

$$\Phi = 0 \text{ if } \left(w + \frac{dh_m}{dt}\right) \leq 0 \quad \text{(detraining or stable mixed layer)}. \qquad (2.4)$$

In equations (2.1) and (2.2), $Q(0)$ denotes the total non-penetrative heat input across the sea surface: it includes contributions from the latent heat flux, $E(0)$, sensible heat flux, $S(0)$, net, longwave, back radiation, $L(0)$, and the non-penetrative component of solar radiation, $\hat{I}(0)$. The total solar radiation at the sea surface $R(0)$ is the sum of the penetrative component $I(0)$ and the non-penetrative component $\hat{I}(0)$. Note that the partition of solar radiation into penetrative and non-penetrative

components makes the specification of solar radiation in the model compatible with that in a spectral-irradiance model to be discussed later. In this respect the present analysis deviates from the Denman (1973) model, which combines $\hat{I}(0)$ and $I(0)$ into one term. The absorption of infrared radiation is dominated by water molecules and therefore the effect of phytoplankton on the absorption of infrared radiation is negligible (Stramska and Dickey, 1993).

The term $(G - D)$ represents the net generation of TKE (the difference between the total TKE generated and that dissipated) within the mixed layer. A variety of schemes exist to parametrize the generation and dissipation of TKE as functions of routinely-measured oceanographic and meteorological variables. The merits and limitations of many of these schemes have been examined in the past (see, for example, Zilitinkevich, *et al.*, 1979 Martin, 1985; Gaspar, 1988). A fundamental assumption inherent in the analysis in the following sections is that the net generation of TKE represented by the term $(G-D)$ is independent of the buoyancy input to the mixed layer.

2.2 Optical Variability and Bulk Models of Upper-Ocean Thermodynamics

The evolution of the mixed layer in the upper ocean is determined by the balance between the input of buoyancy and the difference between the generation and dissipation of TKE within the water column. Major sources of buoyancy in the upper ocean are the net fresh water input associated with the hydrological cycles and the heat input. To isolate the effect of optical variability on the buoyancy input and the evolution of the mixed layer, I have neglected the effect of hydrological cycles. The action of wind at the sea surface generates TKE in the water column. Solar heating is not limited to the air-sea interface but is a continuous function of depth. This is important because the energy budget of the mixed layer is affected not only

by the amount of solar energy entering the ocean, but also by its distribution within the water column.

In equation (2.1), the contribution from the penetrative component of solar radiation to the evolution of the mixed-layer depth is accounted for by the second term on the right, i.e. in a function (say F) of the form:

$$F = \frac{1}{h_m}\int_0^{h_m} I(z)dz - \frac{(I(0)+I(h_m))}{2}. \tag{2.5}$$

This functional form is common to a number of bulk mixed-layer models developed from the basic theory presented in Kraus and Turner (1967), including those of Kim (1976), Garwood (1977) and Gaspar (1988). Equation (2.5) can be written as

$$F = \frac{1}{h_m}\int_0^{h_m} \Big(I(z) - I_l(z)\Big)dz, \tag{2.6}$$

where $I_l(z)$ is a function that decays linearly through the mixed layer from $I(0)$ to $I(h_m)$.

The right side of equation (2.6) is proportional to the change in potential energy of the mixed layer associated with the penetrative component of solar radiation. To demonstrate this, let us consider the integral F′ defined as,

$$F' = \Delta t \frac{g\alpha}{C_p h_m}\int_0^{h_m} z\,\frac{\partial}{\partial z}\Big(I(z) - I_l(z)\Big)dz, \tag{2.7}$$

where Δt is the time step under consideration. Integrating equation (2.7) by parts and applying the condition $I(h_m) = I_l(h_m)$, we see that F' is related to F as

$$F' = -\Big(\Delta t \frac{g\alpha}{C_p}\Big)F, \tag{2.8}$$

where the factors inside the parentheses are all constants. Now the partial derivative in equation (2.7) denotes the vertical divergence of $(I(z) - I_l(z))$ at depth z. The divergence in irradiance at a given depth indicates the irradiance absorbed at that depth and therefore determines the rate of heating. Noting that the net heating

rates over the interval $[0, h_m]$ associated with $I(z)$ and $I_l(z)$ are identical and that the heating associated with $I_l(z)$ is depth-independent, we see that equation (2.7) can be written as

$$F' = \frac{g}{h_m} \int_0^{h_m} z \, \Delta_r \left[\rho(z) - \overline{\rho}^m \right] dz, \tag{2.9}$$

or

$$F' = \frac{g}{h_m} \Delta_r \int_0^{h_m} z \left[\rho(z) - \overline{\rho}^m \right] dz, \tag{2.10}$$

where Δ_r represents the fractional change in the density during the time interval Δt due to heating by the penetrative component of radiation, and $\overline{\rho}^m$ is the mean density of the mixed layer. Equation (2.10) therefore denotes the change in the potential energy of the mixed layer associated with the penetrative component of radiative heating.

The physical significance of the function F is easily understood. When $I(z)$ and $I_l(z)$ are plotted as functions of z, if the profile of $I(z)$ lies above and to the left of the profile of $I_l(z)$, the upper parts of the mixed layer will be heated more strongly than the lower parts. This will be the case, for example, when $I(z)$ is an exponential function. Consequently, the top of the mixed layer will become less dense than the bottom, and the center of gravity of the layer will be lowered relative to that associated with the linear profile. The layer thus will tend to become stably stratified. On the other hand, if the profile of $I(z)$ lies below and to the right of the profile of $I_l(z)$, then the the upper parts of the mixed layer will be heated less strongly than the lower parts, raising the center of gravity of the layer and tending to render it statically unstable. Consequently, the layer may be internally mixed even in the absence of TKE input. A strongly absorbing layer at the base of a mixed layer would, in the absence of other effects, become statically unstable and mix with the overlying mixed layer. This condition may occur in the presence of a nonuniform vertical distribution of phytoplankton biomass in the ocean (Lewis *et al.*, 1983).

Changes in the concentration of light-absorbing substances in the water, which modify the attenuation coefficient of the medium, affect the contribution of solar heating to the thermodynamic balance in the upper ocean in two ways: 1) they modify the balance between the TKE and the buoyancy inputs to the mixed layer; and 2) they determine the amount of solar energy penetrating the base of the mixed layer. An increase in the attenuation coefficient of the water column increases the absorption close to the sea surface, which tends to stratify that portion of the water column. The TKE generated by the action of wind works against this stratification to maintain a well-mixed surface layer. If the TKE exceeds the energy required for vertical mixing of the initial mixed layer, the excess energy will be available for deepening the mixed layer by entraining water across its base.

When there is a strong density gradient at the base of the layer, the energy required to entrain a given amount of water across the lower boundary of the mixed layer is more than that required to entrain the same amount of water in the presence of a weaker density gradient. When the mixed layer is shallow and transparent, strong solar heating in the thermocline reduces the stratification, and thereby decreases the TKE required for entrainment.

If the radiation penetrating the base of the mixed layer is absorbed over a short vertical extent, the resulting increase in T_b may become an important factor determining the thermal stratification at the base. Thus, strong absorption at the base of the mixed layer tends to increase the mixed-layer depth in comparison with weak absorption there. However, the overall effect of the absorption of solar radiation below the mixed layer depends on the stratification in the thermocline; the importance of light absorption below the mixed layer will increase when the initial stratification is weak (that is, when $T_m - T_b$ is small). In the present study, the temperature difference between the mixed layer and its base ($T_m - T_b$) is specified as a parameter of the model so that the effect of changes in the amount of solar

radiation penetrating the base of the mixed layer on T_b is not explicitly considered. This approach makes the analysis less ambiguous.

In the next section I will examine in detail how changes in the attenuation coefficient affect the depth and temperature of the mixed layer. The equations discussed in the previous sections are valid for arbitrary forms of $I(z)$. Bulk models, such as that of Denman (1973), usually assume that the depth distribution of solar radiation follows an exponential profile, which is expressed using a constant attenuation coefficient γ_m as:

$$I(z) = I(0)e^{-\gamma_m z}. \tag{2.11}$$

For this specific form, the integrals appearing in equations (2.1) and (2.2) are easily evaluated. In particular, the equation for mixed-layer depth, (equation (2.1)), and mixed-layer temperature (equation (2.2)) can be written as (Denman, 1973):

$$\Phi \cdot \left(w + \frac{dh_m}{dt} \right) =$$

$$\left\{ \frac{2(G-D)}{\rho \alpha g h_m} + \frac{1}{\rho C_p} \left[\frac{2}{\gamma_m h_m} (I(0) - I(h_m)) - I(h_m) \right] - \frac{1}{\rho C_p} H(0) \right\} (T_m - T_b)^{-1} \tag{2.12}$$

and,

$$\frac{dT_m}{dt} = \frac{2}{h_m^2} \left[-\frac{(G-D)}{\rho \alpha g} + \frac{Q(0)h_m + I(0)(h_m - \gamma_m^{-1}) + \gamma_m^{-1} I(h_m)}{\rho C_p} \right], \tag{2.13}$$

where $H(0) = I(0) + Q(0)$. These equations will be used in the following sections to examine the effect of changes in the attenuation coefficient of the medium on the evolution of the layer depth and temperature. The general approach used in the sensitivity analysis is to examine the changes in the mixed-layer depth and temperature predicted by the model over a single time step, as a function of the optical properties

of the medium. Attenuation of solar radiation in the ocean is a wavelength-, and depth-dependent process. Therefore, the use of a depth-independent attenuation coefficient for describing the attenuation of solar radiation in the ocean may introduce some errors in model results. In a later section I will examine the consequences of relaxing the assumption that γ_m is independent of depth.

2.3 Sensitivity Analysis

2.3.1 Shallowing Mixed Layer: The Layer Depth

The depth of the mixed layer is determined by the balance between the net generation of TKE and the input of buoyancy. For a given initial mixed-layer depth, if the net TKE generation is not sufficient to maintain vertical mixing throughout the layer, the layer will retreat to a shallower depth within which the net TKE generation balances the buoyancy input. This process is described by the Denman (1973) model equation for a shallowing mixed layer, obtained by setting $\Phi = 0$ in equation (2.12). That is, h_m is determined by

$$\frac{2(G-D)}{\rho\alpha g h_m} + \frac{2}{\rho C_p}\left[\frac{I(0)-I(h_m))}{\gamma_m h_m} - I(h_m)\right] - \frac{Q(0)+I(0)-I(h_m)}{\rho C_p} = 0. \quad (2.14)$$

The first term represents the net kinetic energy input from wind. The terms inside the square brackets represent the effect of differential heating on density stratification produced by the absorption of solar radiation within the mixed layer. The last term represents the net input of buoyancy into the mixed layer from the solar and surface fluxes.

Case I: Strong absorption

An assumption used in the development of some bulk mixed-layer models is that all the energy is absorbed within the mixed layer (eg. Kraus and Turner, 1967). This implies that the optical depth of the layer (defined as the product of the attenuation coefficient and the thickness of the layer) is large, i.e., the attenuation coefficient is large or the layer is very deep. Under this assumption, equation (2.14) becomes

$$\frac{2(G-D)}{\rho\alpha g h_m} + \frac{I(0)}{\rho C_p}\frac{2}{\gamma_m h_m} - \frac{H(0)}{\rho C_p} = 0. \tag{2.15}$$

In the above equation, the last term on the left represents the increase in stratification if all the heating occurred at the surface of the layer, whereas the first term represents the TKE available for working against the stratification. The second term accounts for the reduction in stratification resulting from the distributed absorption of solar radiation within the mixed layer rather than at the sea surface. When $\gamma_m h_m$ is very large, the contribution of the second term to the reduction of stratification is negligible. On the other hand, as the optical depth of the layer decreases, more energy penetrates to the lower levels of the mixed layer, reducing the stratification.

For high values of the attenuation coefficient, the depth of the equilibrium layer is given by the balance between the net generation of TKE and the buoyancy input across the sea surface. For the limiting case when $\gamma_m h_m \to \infty$, the equilibrium depth $(h_m)_\infty$ is given by

$$\frac{2(G-D)}{\rho\alpha g (h_m)_\infty} - \frac{H(0)}{\rho C_p} = 0, \tag{2.16}$$

or

$$(h_m)_\infty = \left[\frac{2(G-D)}{\rho\alpha g}\right]\left[\frac{H(0)}{\rho C_p}\right]^{-1}. \tag{2.17}$$

Once the net generation of TKE in the water column is specified, the above equation is similar to that for the classical Monin-Obukhov depth (see for example, Kundu, 1990). Equation (2.17) is independent of $\gamma_m h_m$ since all the energy is absorbed at the surface.

Case II: Weak absorption

As the attenuation of light in the mixed layer decreases, more solar radiation is transferred to the lower levels of the water column. This results in a decrease in the tendency for stratification within the mixed layer. Thus a decrease in the attenuation coefficient of the water column results in a decrease in the buoyancy input to the mixed layer and in a decrease in the TKE required for redistribution of solar heating within the mixed layer. Both of these factors affect the balance between the TKE and buoyancy inputs into the mixed layer, resulting in an increase in the layer depth for a given heat input.

Consider the limiting case of $\gamma_m \to 0$, which represents complete transmission of solar radiation through the mixed layer. Under this condition, there would be no contribution from solar heating to the density stratification of the water column and therefore the equilibrium depth, $(h_m)_0$, would be independent of the penetrative solar radiation in the ocean.

Note that the equilibrium depth is valid only in the case of a shallowing mixed layer ($\Phi = 0$). In the absence of solar radiation, for constant TKE input, shallowing of the mixed layer requires that $Q(0) > 0$. Thus, $(h_m)_0$ is defined only when $Q(0) > 0$.

Under such conditions, the depth of the shallowing mixed layer can be calculated from equation (2.14) by setting $I(0) = 0$:

$$(h_m)_0 = \left[\frac{2(G-D)}{\rho\alpha g}\right]\left[\frac{Q(0)}{\rho C_p}\right]^{-1}, \tag{2.18}$$

where $Q(0)$ is the total non-penetrative heat flux to the ocean.

From equations (2.17) and (2.18) we have

$$\frac{(h_m)_\infty}{(h_m)_0} = \frac{Q(0)}{H(0)} = 1 - \frac{I(0)}{H(0)}. \tag{2.19}$$

Equation (2.19) shows that the ratio of the two limiting cases of equilibrium depth is a simple non-dimensional function of the penetrative component of solar radiation scaled to the net heat flux at the surface. This simple equation reflects the fact that for $\gamma_m \to \infty$, I(0) represents an additional contribution to non-penetrative surface heating.

The total range of variability in the layer depth caused by changes in the attenuation coefficient of a shallowing mixed layer is bounded by the two limiting cases of $(h_m)_0$ and $(h_m)_\infty$. Since $(h_m)_\infty$ has a lower bound of zero, the range of variability is determined in practice by $(h_m)_0$.

Case III: Arbitrary attenuation coefficient

From equation (2.14) we have

$$\frac{1}{i_m} = \left[\frac{H(0)}{\rho C_p} - \frac{I(0)}{\rho C_p}\frac{2}{\gamma_m h_m}(1 - e^{-\gamma_m h_m}) + \frac{I(0)}{\rho C_p}e^{-\gamma_m h_m}\right]\left[\frac{\rho\alpha g}{2(G-D)}\right]. \tag{2.20}$$

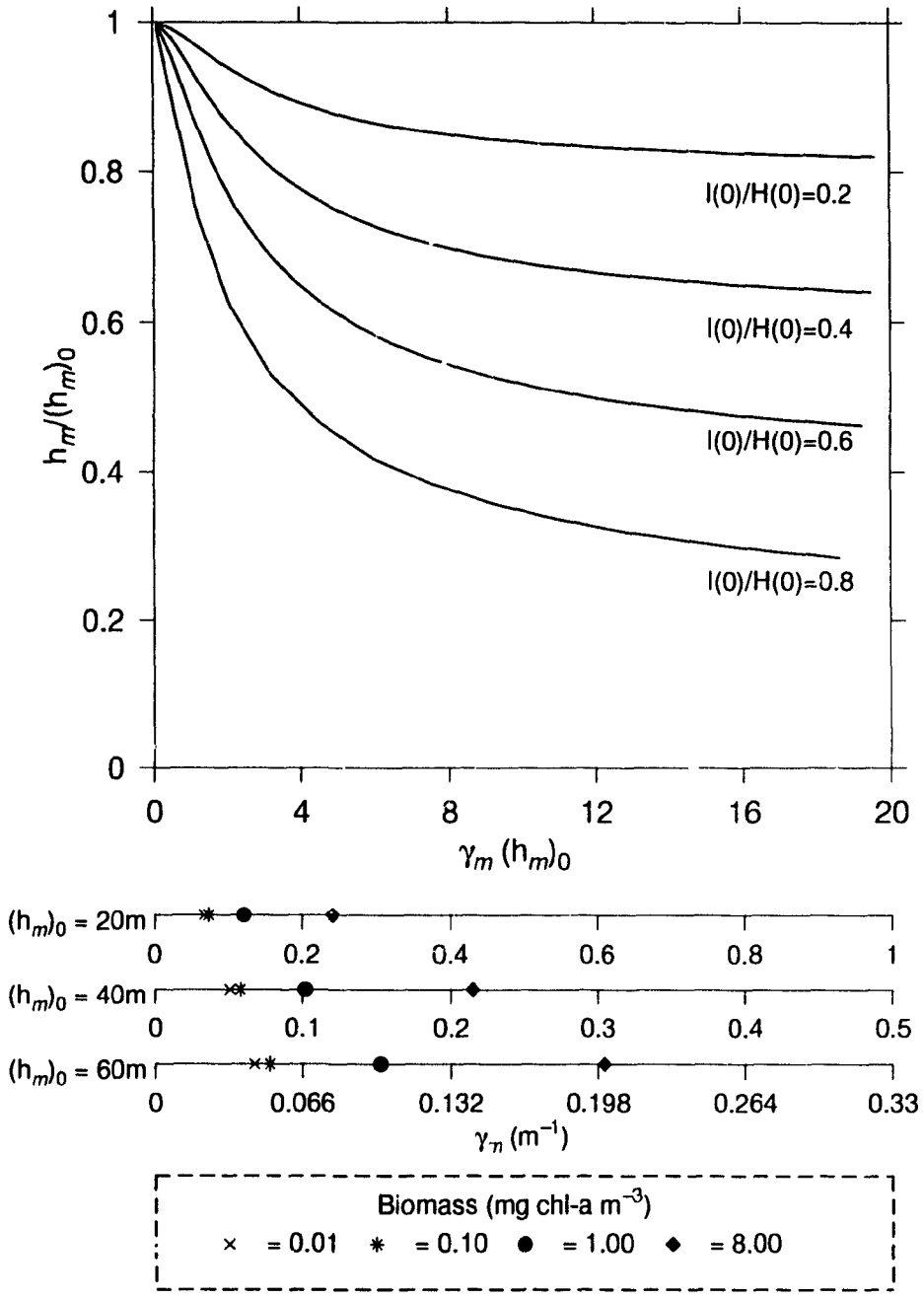

FIGURE 2.1. Dependence of the equilibrium depth on $\gamma_m(h_m)_0$, based on equation (2.21). In this figure, $h_m/(h_m)_0$ is plotted as a function of $\gamma_m(h_m)_0$ for different values of $I(0)/H(0)$ (dimensionless). The distribution of $h_m/(h_m)_0$ as a function of γ_m for different values of $(h_m)_0$ can also be estimated from the figure using the additional axes. The mixed-layer mean attenuation coefficients corresponding to phytoplankton concentrations of 0.01, 0.1, 1.0 and 8.0 mg chl-a m^{-3} estimated using a spectral irradiance model of under-water light transmission (Sathyendranath and Platt, 1988) are also given.

The depth of the equilibrium layer for an arbitrary value of γ_m, compared with the corresponding depth for $\gamma_m = 0$, can be obtained by combining equations (2.20) and (2.18) and rearranging:

$$\frac{h_m}{(h_m)_0} = \frac{\left[1 - I(0)/H(0)\right]}{1 - \left[I(0)/H(0)\right]\left[\frac{2}{\gamma_m h_m}(1 - e^{-\gamma_m h_m}) - e^{-\gamma_m h_m}\right]}. \tag{2.21}$$

The ratio $h_m/(h_m)_0$ from the equation (2.21) is plotted in Figure 2.1 as a function of $\gamma_m(h_m)_0$ for different values of the ratio $I(0)/H(0)$. The figure shows that for high values of γ_m, the equilibrium depth for any given value of $I(0)/H(0)$ becomes independent of γ_m. It can also be noticed from the figure that the relative importance of the penetrative component of solar radiation compared with the total heat flux, given by $I(0)/H(0)$, is an important factor determining the effect of changes in γ_m. I have added three additional axes corresponding to different values of $(h_m)_0$ to highlight the dependence of h_m on the attenuation coefficient. The attenuation coefficients corresponding to 0.01, 0.1, 1.0 and 8.0 mg. chl-a m^{-3} (biomass concentration assuming chlorophyll-a as the index of the phytoplankton biomass), estimated from a spectral irradiance model (see Section 2.4), are shown on these additional axes to help to understand the potential effect of phytoplankton variability on the equilibrium depth. For small values of $(h_m)_0$ (20 m), the entire range of variability in γ_m due to phytoplankton is represented by a narrow region on the abscissa where $h_m/(h_m)_0$ varies rapidly. Therefore the equilibrium depth is sensitive to small changes in γ_m. On the other hand, for large values of $(h_m)_0$ (60 m) the equilibrium depth is not very sensitive to changes in γ_m when $\gamma_m > 0.06 m^{-1}$, and therefore it is less sensitive to changes in the phytoplankton concentration.

In winter, the net heat flux to the ocean may be negative, and therefore the mixed layer may be deep. With the onset of Spring, the net heat flux to the ocean increases, and the mixed-layer depth becomes the equilibrium depth determined

by equation (2.14). In the early stages of the development of stratification, solar radiation dominates the net heat input to the ocean and therefore $I(0)/H(0)$ will be relatively large. Therefore, changes in the attenuation coefficient will have considerable influence on the rate of shallowing of the layer. According to the critical mixing depth theory (Sverdrup, 1953; Platt *et al.*, 1991), such a shallowing mixed layer favours an increase in phytoplankton concentration and hence also in the attenuation coefficient of the mixed layer.

2.3.2 Shallowing Mixed Layer: The Layer Temperature

In this section I examine how the temperature of a shallowing mixed layer is affected by changes in the mean attenuation coefficient. The Denman (1973) model estimates the increase in temperature (ΔT) of a shallowing mixed layer during a given time step (Δt) in terms of the total heat absorbed by the layer during that time step, as:

$$\Delta T = \Delta t \frac{Q(0) + I(0)(1 - e^{-\gamma_m h_m})}{\rho C_p h_m}. \tag{2.22}$$

Note that the effect of solar heating on the temperature of the equilibrium mixed layer depends not only on the amount of solar energy absorbed by the layer but also on the thickness of the layer. As the layer becomes shallower, the energy absorbed within the layer is redistributed over a shorter vertical distance, which favours the subsequent increase in the layer temperature.

As the mean attenuation coefficient of the mixed layer increases, more energy will be trapped within the mixed layer, which will tend to increase the layer temperature. At the same time, the increased stratification resulting from the increase in the amount of solar energy absorbed by the layer will tend to decrease the layer

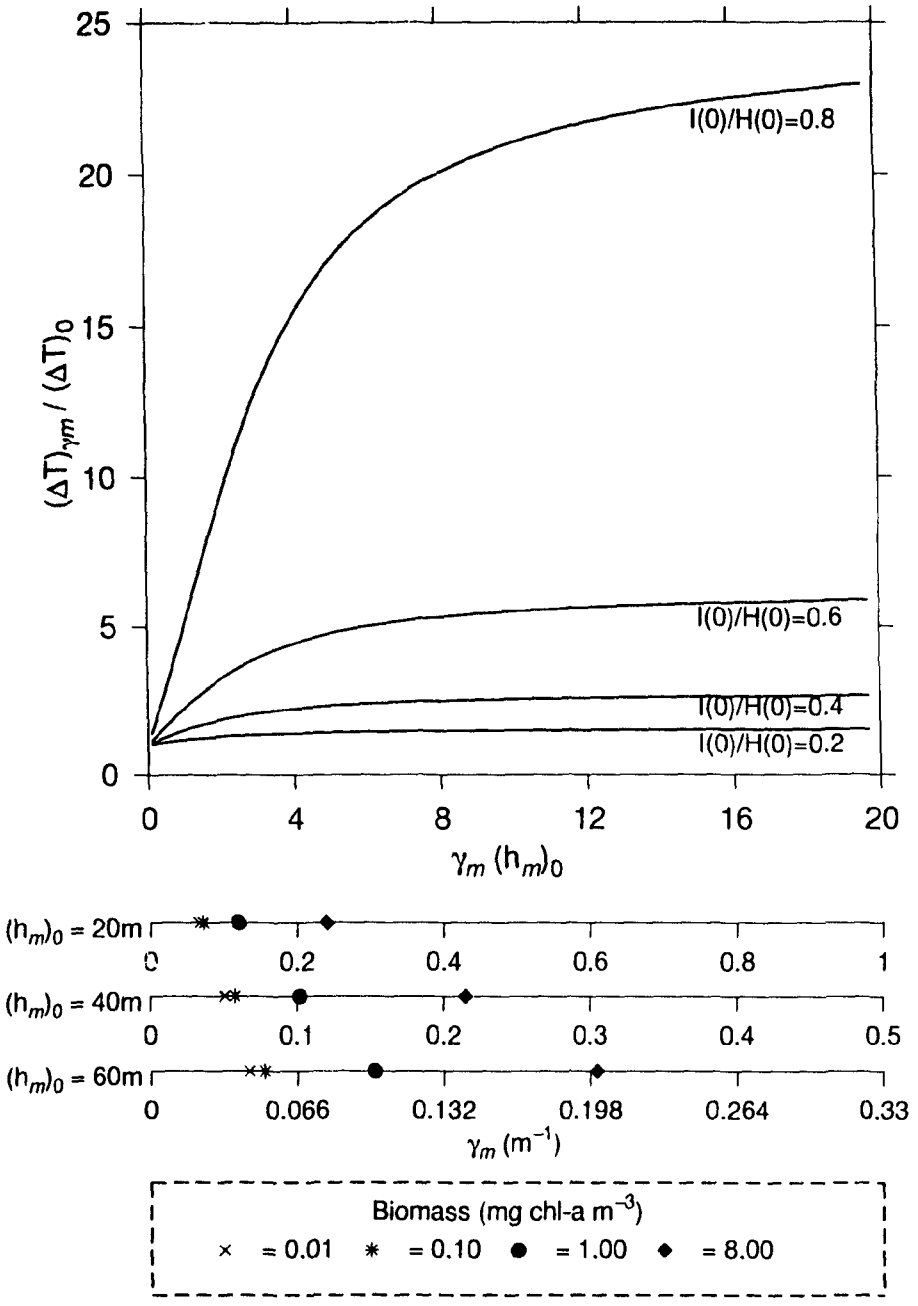

FIGURE 2.2. Dependence of the equilibrium-layer temperature on $\gamma_m(h_m)_0$, based on equation (2.23). In this figure, $(\Delta T)_{\gamma_m}/(\Delta T)_0$ is plotted as a function of $\gamma_m(h_m)_0$ for different values of $I(0)/H(0)$ (dimensionless). The additional axes are used to represent the dependence on the mean attenuation coefficient of the mixed layer and phytoplankton concentration as in the previous figure.

depth further. In turn, such a decrease in the layer depth will tend to increase the layer temperature as mentioned earlier. Comparing ΔT for an arbitrary γ_m with the corresponding value for the limiting case of $\gamma_m \to 0$ gives:

$$\frac{(\Delta T)_{\gamma_m}}{(\Delta T)_0} = \frac{(h_m)_0}{h_m}\left[1 - \frac{I(0)}{H(0)}e^{-\gamma_m h_m}\right]\left[1 - \frac{I(0)}{H(0)}\right]^{-1}. \tag{2.23}$$

In Figure 2.2, the relative changes in temperature $(\Delta T)_{\gamma_m}/(\Delta T)_0$ are plotted as a function of $\gamma_m(h_m)_0$, for different values of $I(0)/H(0)$. Once $(h_m)_0$ is specified, the figure represents the dependence of the relative change in the equilibrium layer temperature on the attenuation coefficient of the medium. Here also I have shown three additional axes to emphasize the dependence of $(\Delta T)_{\gamma_m}/(\Delta T)_0$ on γ_m for different values of $(h_m)_0$. As in the case of Figure 2.1, there is an increased sensitivity to changes in γ_m as $(h_m)_0$ decreases.

Note that equation (2.23) is a function of $(h_m)_0/h_m$ and therefore, the temperature of a shallowing mixed layer is also affected by change in the layer depth h_m. The figure also illustrates how the relative importance of solar radiation in the net heat input across the sea surface modifies the effect of changes in the attenuation coefficient.

Figures 2.1 and 2.2 show that changes in the depth and temperature of a shallowing mixed layer are strongly affected by changes in the attenuation coefficient, when the attenuation coefficient is relatively small. For large values of the attenuation coefficient the changes become saturated. Also, changes in the depth of the mixed layer, resulting from variability in the attenuation coefficient, can play an important role in determining the temperature of the layer.

2.3.3 Deepening Mixed Layer: The Layer Depth

The rate of deepening of the mixed-layer depends on the TKE produced by the action of wind, the buoyancy input to the mixed layer and the density difference across the base of the layer. It is given by equation (2.12) with $\Phi = 1$:

$$\left(w + \frac{dh_m}{dt}\right) =$$

$$\left[\frac{2(G-D)}{\rho\alpha g h_m} + \frac{1}{\rho C_p}\left[\frac{2}{\gamma_m h_m}(I(0) - I(h_m)) - I(h_m)\right] - \frac{1}{\rho C_p}H(0)\right](T_m - T_b)^{-1}. \tag{2.24}$$

Case I: Strong absorption

For high values of the attenuation coefficient, the entrainment velocity $(w + dh_m/dt)$ is determined by the generation of TKE and the net heat flux across the sea surface. The limiting case of $\gamma_m \to \infty$ gives:

$$\left(w + \frac{dh_m}{dt}\right)_{\gamma_m=\infty} = \left[\frac{2(G-D)}{\rho\alpha g h_m} - \frac{H(0)}{\rho C_p}\right](T_m - T_b)^{-1}. \tag{2.25}$$

Note that the case of a deepening mixed layer corresponds to

$$\left(w + \frac{dh_m}{dt}\right)_{\gamma_m=\infty} > 0, \tag{2.26}$$

or

$$\frac{2(G-D)}{\rho\alpha g h_m} > \frac{H(0)}{\rho C_p}. \tag{2.27}$$

Equation (2.25) indicates that as the attenuation coefficient of the medium increases, the entrainment velocity becomes independent of the attenuation coefficient. This is so because, when the attenuation coefficient is high, all the light is absorbed close to the surface, and for a given mixed-layer depth, the amount of TKE required to work against the stratification produced by the absorption of solar radiation approaches a constant.

Case II: Weak absorption

The entrainment velocity corresponding to the limiting case of $\gamma_m \to 0$ can be expressed as:

$$\left(w + \frac{dh_m}{dt}\right)_{\gamma_m=0} = \left[\frac{2(G-D)}{\rho\alpha g h_m} - \frac{Q(0)}{\rho C_p}\right](T_m - T_b)^{-1}. \tag{2.28}$$

Equation (2.28) shows that when the medium is completely transparent to solar radiation, the entrainment velocity becomes independent of the amount of solar radiation entering the ocean. This is because, under the conditions of complete transmission, solar heating is absent, and therefore does not modify either the vertical distribution of density or the buoyancy within the water column. The condition of complete transmission is identical to the night-time condition when $I(0) = \hat{I}(0) = 0$. Equations (2.24), (2.25) and (2.28) can be compared to identify the relative importance of net TKE generation, solar radiation and surface heat input to the water column on the entrainment velocity, for different values of the attenuation coefficient.

From equations (2.25) and (2.28) we have,

$$\left(w+\frac{dh_m}{dt}\right)_{\gamma_m=0}-\left(w+\frac{dh_m}{dt}\right)_{\gamma_m=\infty}=\frac{I(0)}{\rho C_p}(T_m-T_b)^{-1}. \tag{2.29}$$

The right side of equation (2.29) gives the maximum range of variability in the entrainment velocity that can be produced by changes in the attenuation coefficient of the medium. This maximum range of variability is directly proportional to the solar radiation and inversely proportional to the temperature difference between the mixed layer and its base. Note that the result is independent of both the non-penetrative surface heat flux and the wind speed.

Case III: Arbitrary attenuation coefficient

From equation (2.24), the change in the entrainment velocity of a mixed layer caused by a change in the attenuation coefficient of the layer from $\gamma_m = 0$ (complete transmission) to γ_m (arbitrary attenuation coefficient) can be expressed as:

$$\left[\left(w+\frac{dh_m}{dt}\right)_0-\left(w+\frac{dh_m}{dt}\right)_{\gamma_m}\right]=$$
$$\left[\frac{I(0)/(\rho C_p)}{T_m-T_b}\right]\left[1-\frac{2}{\gamma_m h_m}(1-e^{-\gamma_m h_m})+e^{-\gamma_m h_m}\right]. \tag{2.30}$$

2.3.4 Deepening Mixed Layer: The Layer Temperature

The evolution of the temperature of a deepening mixed layer with time is given by equation (2.13). Consider two cases of the equation for arbitrary attenuation coefficients γ_m and $(\gamma_m)_0$. Upon subtracting one from the other we get,

$$\left(\frac{dT_m}{dt}\right)_{\gamma_m} - \left(\frac{dT_m}{dt}\right)_{(\gamma_m)_0} = \frac{2I(0)}{\rho C_p h_m}\left[\frac{1-e^{-(\gamma_m)_0 h_m}}{(\gamma_m)_0 h_m} - \frac{1-e^{-\gamma_m h_m}}{\gamma_m h_m}\right]. \tag{2.31}$$

Taking the limiting case $(\gamma_m)_0 \to 0$, equation (2.31) becomes

$$\left[\left(\frac{dT_m}{dt}\right)_{\gamma_m} - \left(\frac{dT_m}{dt}\right)_0\right] = \left[\frac{2I(0)}{\rho C_p h_m}\right]\left[1 - \frac{1-e^{-\gamma_m h_m}}{\gamma_m h_m}\right]. \tag{2.32}$$

This equation represents the change in the temperature of a deepening mixed layer of arbitrary attenuation coefficient γ_m with respect to the temperature change of the layer when $\gamma_m = 0$.

The functions of $\gamma_m h_m$ in equations (2.30) and (2.32), and their sensitivity to changes in γ_m are addressed in detail in the next section.

2.4 Parametrization of Solar Energy Distribution in the Ocean as a Function of Phytoplankton Biomass

So far I have analyzed the effect of changes in the attenuation coefficient of the mixed layer on the evolution of mixed-layer depth and temperature. As stated earlier, phytoplankton and phytoplankton-derived compounds are among the most important sources of variability in the upper-ocean optical properties. Thus, it is appropriate to examine, explicitly, the effect of changes in the phytoplankton variability on the mixed-layer dynamics. To start with, consider equation (2.12). It can be expressed as

$$\Phi \cdot \left(w + \frac{dh_m}{dt}\right) = \left[\frac{2(G-D)}{\rho\alpha g h_m} - \frac{Q(0)}{\rho C_p} - \frac{I(0)}{\rho C_p} f_{h_m}\right]\left(T_m - T_b\right)^{-1}, \tag{2.33}$$

where

$$f_{h_m} = 1 - \frac{2}{\gamma_m h_m}(1 - e^{-\gamma_m h_m}) + e^{-\gamma_m h_m}. \tag{2.34}$$

Note that, if a depth-independent attenuation coefficient is used to describe the distribution of solar radiation in the ocean (equation (2.11), f_{h_m} is related to the function F (equation (2.5)) given in Section 2.2 through the equation:

$$f_{h_m} = -0.5F/I(0). \tag{2.35}$$

The function f_{h_m} varies between 0 and 1 as $\gamma_m h_m$ changes from 0 to ∞.

When $\gamma_m = 0$, $f_{h_m} = 0$ and therefore equation (2.33) reduces to equation (2.18) in the case of a shallowing mixed layer, and to equation (2.28) in the case of a deepening mixed layer. On the other hand, when $\gamma_m = \infty$, $f_{h_m} = 1$ and equation (2.33) becomes equation (2.17) or equation (2.25) according whether $\Phi = 0$ or 1. The equation describing the evolution of mixed-layer temperature can be written as:

$$\frac{dT_m}{dt} = \frac{2}{h_m}\left[-\frac{(G-D)}{\rho\alpha g h_m} + \frac{Q(0)}{\rho C_p} + \frac{I(0)}{\rho C_p} f_{T_m}\right]. \tag{2.36}$$

Here f_{T_m} is a function defined as:

$$f_{T_m} = 1 - \frac{1 - e^{-\gamma_m h_m}}{\gamma_m h_m}. \tag{2.37}$$

Like f_{h_m}, the function f_{T_m} varies between 0 and 1 as $\gamma_m h_m$ changes from 0 to ∞.

I will next examine the contribution from phytoplankton variability in the upper ocean to the evolution of mixed-layer depth and temperature using the functions f_{h_m} and f_{T_m}. This analysis requires a method for describing the attenuation coefficient of the mixed layer as a function of phytoplankton biomass. I have used a spectral-irradiance model of under-water light transmission (Sathyendranath and Platt, 1988) for this purpose.

The distribution of solar radiation was computed, using the spectral-irradiance model, at 5 nm wavelength intervals from 400 to 700 nm, with a depth resolution of 1 m from the sea surface to the base of the mixed layer. The calculations were repeated for different hours of the day at a time resolution of half an hour, to account for changes in the solar angle. The concentration of phytoplankton biomass was altered from 0 to 10 mg chl-a m^{-3}, covering the range commonly encountered in the open ocean. The calculations were carried out for a hypothetical station at 5°N latitude and for July 15. (These specifications are arbitrary and do not affect the validity of the model results, except for the fact that a different time and place will modify the magnitude of solar-radiation at the sea surface and the angular distribution of the light field under water.) The results are used to estimate the daily solar radiation at the surface, $I_d(0)$, and at the base of the mixed layer, $I_d(h_m)$. The daily mean attenuation coefficient of the mixed layer is then estimated as:

$$\gamma_m = \frac{\ln I_d(0) - \ln I_d(h_m)}{h_m}. \tag{2.38}$$

2.4.1 Contribution From Phytoplankton Variability to the Evolution of Mixed-Layer Depth and Temperature

The functions f_{h_m} and f_{T_m} account for the effect of attenuation of solar radiation within the mixed layer on the evolution of mixed-layer depth and temperature, respectively. The theoretical values of these functions vary between 0 and 1, but the

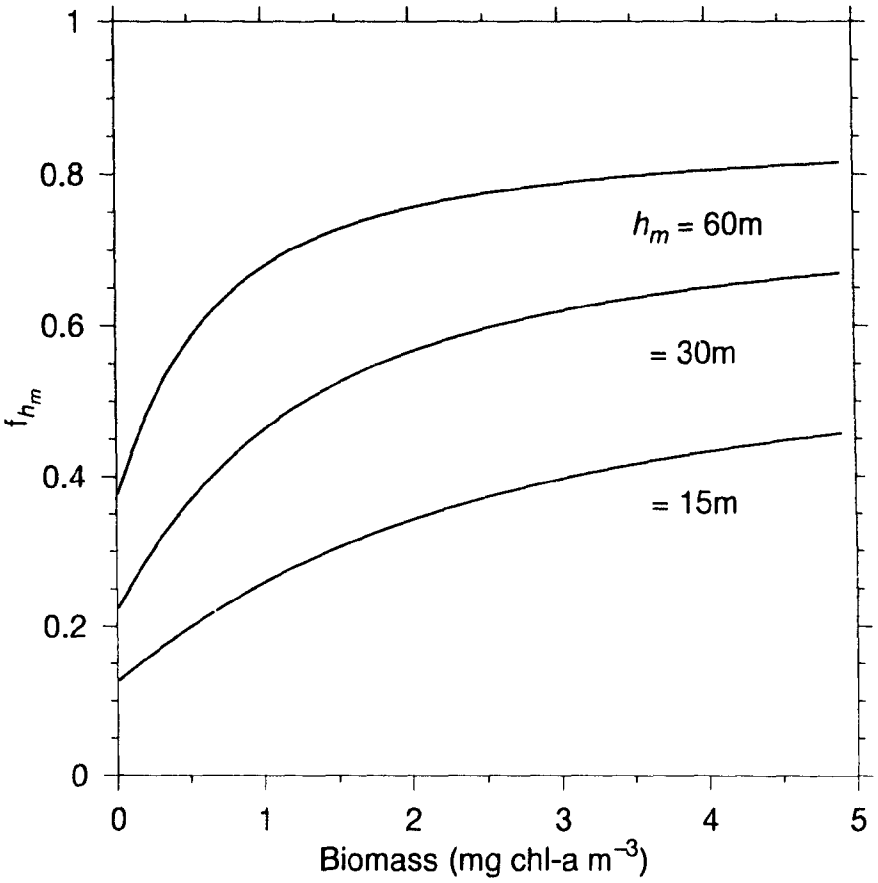

FIGURE 2.3. Dependence of $f_{h_m} = 1 - \frac{2}{\gamma_m h_m}\left(1 - e^{-\gamma_m h_m}\right) + e^{-\gamma_m h_m}$ on phytoplankton biomass for different values of the mixed-layer depth.

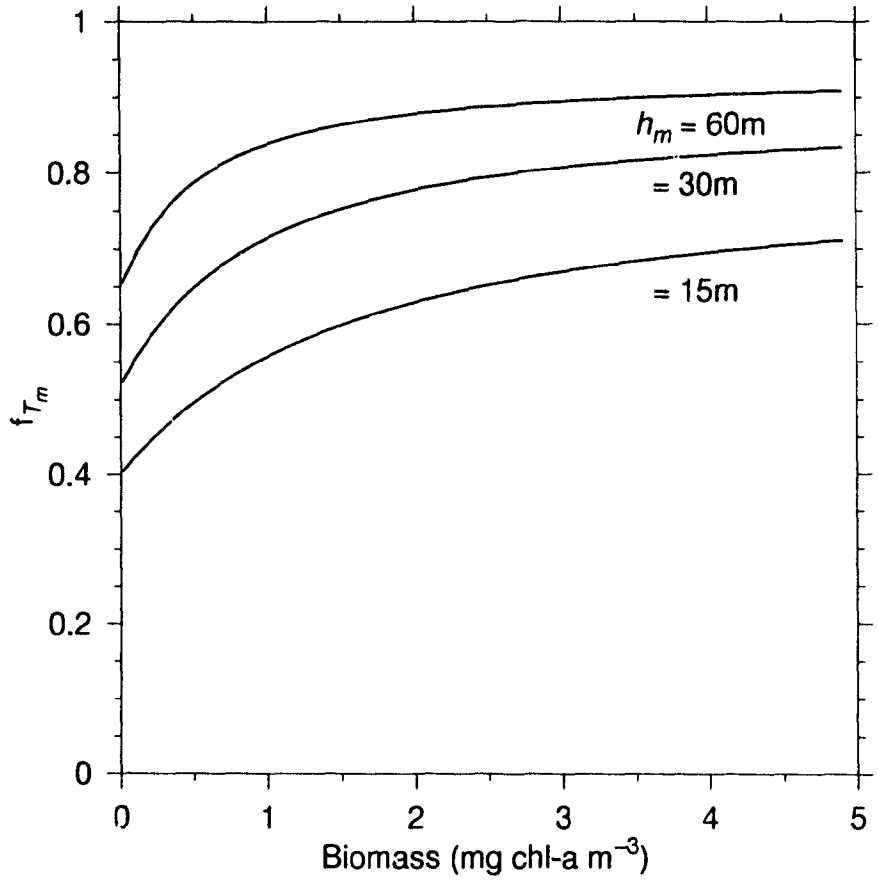

FIGURE 2.4. Dependence of $f_{T_m} = 1 - \frac{1}{\gamma_m h_m}\left(1 - e^{-\gamma_m h_m}\right)$ on phytoplankton biomass for different values of the mixed-layer depth.

lower bound is determined, in practice, by the attenuation coefficient of pure sea water. When the water column is relatively free of phytoplankton, these functions will have a value close to that of pure sea water. With increasing phytoplankton concentration, their value increases. Equations (2.38) and (2.34) are used to estimate f_{h_m} for given concentrations of phytoplankton biomass and mixed-layer depth. Figure 2.3 shows f_{h_m} as a function of biomass concentration for mixed layers of depth 15, 30 and 60 m. The dependence of f_{h_m} on the biomass concentration weakens with increasing biomass. When the layer is relatively shallow, the shape of the curve is also affected by the solar radiation lost below the base of the mixed layer. The value of f_{h_m} increases from 0.15 to 0.45 for a 15 m deep mixed layer, and from 0.37 to 0.82 for a mixed layer of depth 60 m, when the biomass increases from 0 to 5 mg chl-a m^{-3}.

Figure 2.4 shows f_{T_m} as a function of biomass for different mixed-layer depths. The shapes of the curves are similar to those shown in Figure 2.3. As the biomass increases from 0 to 5 mg chl-a m^{-3}, f_{T_m} increases from 0.40 to 0.70 for a mixed-layer depth of 15 m, and from 0.65 to 0.85 for a mixed-layer depth of 60 m.

From equations (2.33) and (2.36) it can be seen that the effect of an increase in f_{h_m} or f_{T_m} is identical to an increase in solar radiation without changing these functions. In other words, the effects of changes in f_{h_m} or f_{T_m} are analogous to changes in the penetrative component of solar radiation. Therefore the effect of phytoplankton variability on the evolution of mixed-layer depth and temperature can be expressed in terms of changes in the penetrative component of solar radiation. In other words, a given change in f_{h_m} or f_{T_m} can be achieved by a corresponding change in $I(0)$. The effect of changes in the solar radiation on the evolution of mixed-layer depth and temperature has been studied (see for example, Niiler and Kraus, 1977) and therefore, the effect of phytoplankton variability on f_{h_m} and f_{T_m}, and thus on the mixed-layer dynamics can also be easily understood once the problem is recast in terms of the changes in the solar radiation. However, such

recasting would neglect the depth-dependent and time-dependent changes in the optical characteristics of phytoplankton.

In general, an increase in cloud cover decreases the solar radiation at the sea surface, and therefore, affects the evolution of mixed-layer depth and temperature. From equations (2.33) and (2.36), it can be observed that a similar effect can be achieved by reductions in f_{h_m} and f_{T_m} due to a decrease in the phytoplankton concentration in the mixed layer.

2.5 The Depth Dependence of the Optical Attenuation Coefficient: Consequences for Mixed-Layer Models

Many bulk models approximate the distribution of solar radiation in the ocean using a depth-independent attenuation coefficient (see for example, Kraus and Turner, 1967; Denman, 1973; Kim, 1976; Niiler and Kraus, 1977). Because the attenuation of solar radiation in the ocean is a depth-, and wavelength-dependent process, such an approximation can lead to inaccurate representations of total solar energy absorbed by the mixed layer and of the vertical distribution of the energy absorbed in the layer. Here I consider the problem of parameterizing the wavelength-dependent distribution of solar radiation in the mixed layer as a function of phytoplankton biomass, with special reference to bulk models of the mixed layer. To address this problem, I have used a spectral-irradiance model of underwater light transmission (Sathyendranath and Platt, 1988) to develop a piece-wise profile of the attenuation coefficient by dividing the layer into a number of sub-layers and calculating the irradiance at the base of each sub-layer. Within each of these sub-layers the penetrative component of solar radiation is assumed to decay exponentially with depth. Daily integrated solar radiation is estimated at one meter intervals. Once the total solar radiation available at the top ($I_d(z_i)$) and at the

bottom ($I_d(z_{i+1})$) of the i^{th} sub-layer are obtained, the mean attenuation coefficient of the sub-layer is estimated as

$$(\gamma_m)_i = \frac{\ln I_d(z_i) - \ln I_d(z_{i+1})}{(z_{i+1} - z_i)}. \tag{2.39}$$

Figure 2.5 shows a comparison between the depth distributions of total solar radiation between 400 and 700 nm in a mixed layer of 30 m deep, estimated using equations (2.38) and (2.39), for sub-layers of thickness 1 m.

Necessarily (by the definition of γ_m in equation (2.38)) , the methods yield the same amount of solar radiation at the base of the mixed layer. However, the two parametrization schemes give very different distributions of solar radiation within the mixed layer. The difference between the two schemes is greater when the mixed layer is relatively transparent.

2.5.1 Generalization of Bulk Model Equations to Account for Depth-Dependent Changes in the Attenuation of Solar Radiation

Attenuation of solar radiation in the ocean is wavelength-dependent. Once we take into account this wavelength-dependence, we are automatically introducing depth-dependence of attenuation coefficient into equations describing the distribution of solar radiation in the ocean. Note that the depth-dependence of the attenuation coefficient, caused by its wavelength dependence, exists even in the case of a mixed-layer in which the light attenuating substances, such as phytoplanktons, are distributed uniformly with depth. So far these complications have been ignored, for simplicity, through use of a depth-independent attenuation coefficient γ_m. From Figure 2.5, we see that the effect of using an exponential profile with a single attenuation coefficient for the mixed layer is that we predict that more energy is transmitted to the lower levels of the mixed layer compared with the light transmission associated with the multi-layer calculations. Thus, the TKE required in the

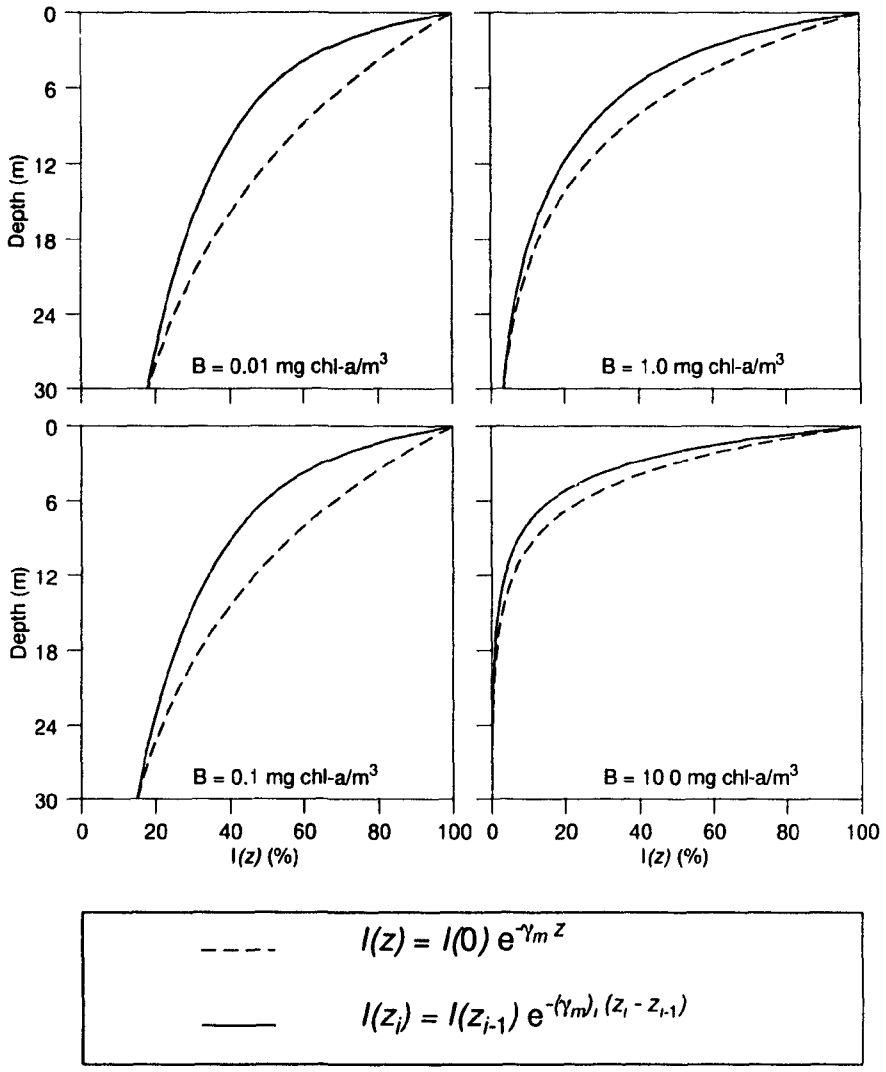

FIGURE 2.5. A comparison between the distribution of solar radiation predicted by depth dependent (solid curves), and depth independent (broken curves), attenuation coefficients for different values of phytoplankton biomass, based on equations (2.38) and (2.39).

Denman (1973) model for balancing the effect of the depth-dependent distribution of solar radiation is less than what would be required if equation (2.39) were used. This also has the consequence that the residual TKE (after the buoyancy input to the mixed layer is overcome) would be overestimated. Therefore, the depth of the mixed layer estimated by the conventional, depth-independent parameterization of attenuation coefficient would be greater than that estimated using a multi-layer parametrization of solar radiation in the mixed layer. This also implies that the mixed-layer temperature estimated using the single attenuation coefficient would be less than that predicted by a multi-layer parametrization scheme.

The Denman (1973) model can be modified to account for the depth dependence in the attenuation coefficient resulting from the wavelength dependent-attenuation of solar radiation in the mixed layer as follows: The term containing solar radiation in the depth-integrated equation for conservation of heat that is used to derive equation (2.1) (see Denman (1973)) can be expressed as:

$$\int_0^{h_m} \frac{-1}{\rho C_p} \frac{dI}{dz} dz = \frac{I(0) - I(h_m)}{\rho C_p}. \tag{2.40}$$

Let the mixed layer be subdivided into n layers of thickness Δz_i and let the mean attenuation coefficient for the i^{th} layer be $(\gamma_m)_i$. The solar radiation available at the base of the i^{th} layer is

$$I(z_i) = I(z_{i-1}) e^{-(\gamma_m)_i \Delta z_i}. \tag{2.41}$$

Therefore, the solar radiation at the base of the mixed layer can be expressed as

$$I(h_m) = I(0) \exp[-\sum_{i=1}^{n} (\gamma_m)_i \Delta z_i]. \tag{2.42}$$

Then,

$$\frac{I(0)-I(h_m)}{\rho C_p}=\frac{I(0)-I(0)\exp[-\sum_{i=1}^{n}(\gamma_m)_i\Delta z_i]}{\rho C_p}. \tag{2.43}$$

Similarly, the integral in equation (2.2), containing solar radiation, becomes:

$$\int_0^{h_m}\int_0^{z}\frac{-1}{\rho C_p}\frac{dI}{dz'}dz'dz=\int_0^{h_m}\frac{\big(I(0)-I(z)\big)}{\rho C_p}dz \tag{2.44}$$

$$=\frac{I(0)}{\rho C_p}\Big\{h_m+\sum_{i=1}^{n}\exp\Big[-\sum_{j=1}^{i-1}(\gamma_m)_j\Delta z_j\Big]\Big[\frac{1-\exp[-(\gamma_m)_i\Delta z_i]}{(\gamma_m)_i}\Big]\Big\}. \tag{2.45}$$

By substituting equations (2.43) and (2.45) into the conservation equations for heat and TKE of Denman (1973), the model equations predicting the evolution of mixed-layer temperature and depth can be expressed as

$$\frac{dT_m}{dt}=\frac{2}{h_m}\Big[-\frac{(G-D)}{\rho\alpha g h_m}+\frac{Q(0)}{\rho C_p}+\frac{I(0)}{\rho C_p}f_{T_m}^{n}\Big] \tag{2.46}$$

and

$$\Phi\cdot\big(w+\frac{dh_m}{dt}\big)=\Big[\frac{2(G-D)}{\rho\alpha g h_m}-\frac{Q(0)}{\rho C_p}-\frac{I(0)}{\rho C_p}f_{h_m}^{n}\Big](T-T_b)^{-1}, \tag{2.47}$$

where

$$f_{h_m}^{n}=\Big\{1+\exp\Big[-\sum_{i=1}^{n}(\gamma_m)_i\Delta z_i\Big]-$$

$$\frac{2}{h_m}\sum_{i=1}^{n}\exp\Big[-\sum_{j=1}^{i-1}(\gamma_m)_j\Delta z_j\Big]\Big[\frac{1-\exp[-(\gamma_m)_i\Delta z_i]}{(\gamma_m)_i}\Big]\Big\}, \tag{2.48}$$

and

$$f^n_{T_m} = \Big\{1-\frac{1}{h_m}\sum_{i=1}^{n}\exp\Big[-\sum_{j=1}^{i-1}(\gamma_m)_j\Delta z_j\Big]\Big[\frac{1-\exp[-(\gamma_m)_i\Delta z_i]}{(\gamma_m)_i}\Big]\Big\} \tag{2.49}$$

In Figure 2.6, $f^n_{h_m}$ is plotted as a function of phytoplankton biomass, for mixed layers of depth 15, 30 and 60 m. The rate of change of $f^n_{h_m}$ is maximum towards low concentrations of biomass. The flatness of the curve increases as the layer depth decreases.

A similar plot of $f^n_{T_m}$ is shown in Figure 2.7. The effect of changes in the phytoplankton concentration on $f^n_{T_m}$ is also maximum towards lower concentrations of phytoplankton.

Figures 2.6 and 2.7 show that the maximum range of variability in the mixed-layer depth and temperature produced by phytoplankton-induced changes in the attenuation coefficient of the mixed layer is equivalent to a change of approximately 30% in the input of penetrating solar radiation. The effect of these changes on the mixed-layer depth and temperature is determined by the TKE available for mixing and by the relative importance of solar radiation in the net heat input across the sea surface.

The functions $f^n_{h_m}$ and $f^n_{T_m}$ are similar to f_{h_m} and f_{T_m} shown in Figures 2.3 and 2.4 respectively. However, the curvature at low biomass concentration is decreased and the overall range of variability is reduced compared with those given in figure 2.3 and 2.4. When the mixed layer is very transparent, the effect of depth-dependency may be equivalent to about a 20% change in the penetrative component of solar

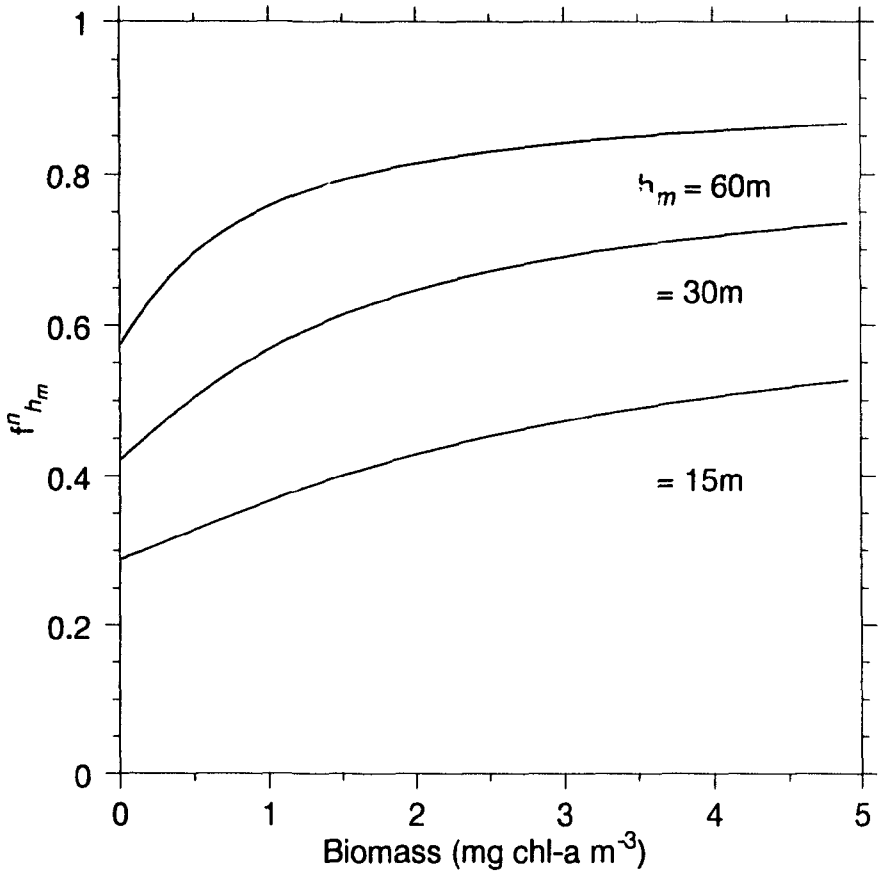

FIGURE 2.6. Dependence of $f^n_{h_m}$ on phytoplankton biomass for different values of the mixed-layer depth, based on equation (2.48).

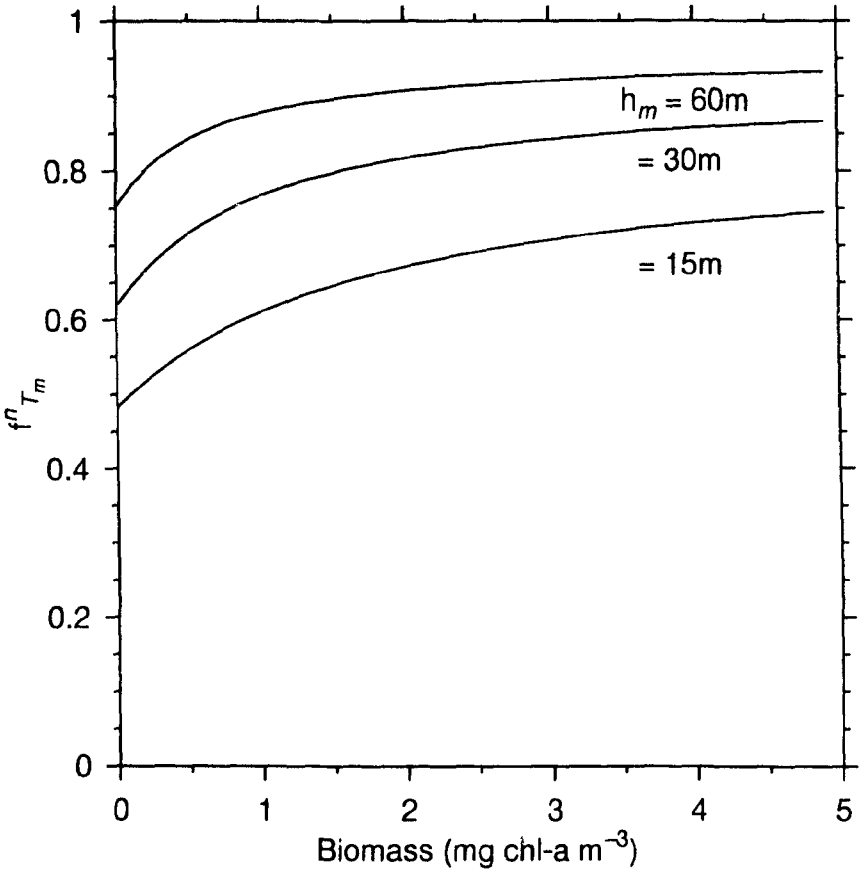

FIGURE 2.7. Dependence of $f^n_{T_m}$ on phytoplankton biomass for different values of the mixed-layer depth, based on equation (2.49).

radiation. However, for moderately deep and phytoplankton-rich mixed layers, the difference in the estimated mixed-layer depth would be small. Under such conditions the use of $f^n_{h_m}$ and $f^n_{T_m}$ is not justified because of the complexity involved in their estimation.

Equations (2.48) and (2.49) are extensions of the general parameterization scheme of solar heating in bulk models to take into account the depth-dependent attenuation of solar radiation in the ocean. These equations can be used for bulk mixed-layer model simulations in conjunction with a high-resolution, spectral, irradiance model of under-water light transmission.

2.6 Discussion

In the present study I have examined the effect of changes in the attenuation coefficient of the mixed layer on the evolution of mixed-layer depth and temperature. Various factors that make thermodynamic models of the upper ocean sensitive to changes in attenuation coefficient are explained. Such information is expected to be useful for incorporating the effects of phytoplankton-induced changes in the attenuation of solar radiation into large-scale models of upper-ocean thermodynamics and air-sea interactions.

The contribution from solar heating to the evolution of mixed-layer depth is determined by the magnitude and the depth distribution of solar radiation entering the ocean. Changes in the attenuation coefficient of the layer modify the stratification within the layer, as well as the amount of solar radiation penetrating the base of the mixed layer. The latter, in turn, affects the stratification at the base of the layer and therefore the rate of entrainment during mixed-layer deepening.

The sensitivity analysis examines the conditions under which the effect of optical variability on the upper-ocean thermodynamics can be expected to be significant

and under what conditions it can be ignored. The analysis shows that the effect of optical variability on the mixed-layer depth can be expected to be maximum when the attenuation coefficient is low. Also, in the presence of a strong heat input to the ocean from the non-penetrative components, the effect of optical variability on mixed-layer depth becomes weak. Thus, we can identify a region of the parameter space, characterized by low attenuation coefficient and high contribution from solar radiation to the total heat input to the ocean, within which the effect of changes in the attenuation coefficient on the evolution of mixed-layer depth can be expected to be significant. The analysis is used to explain how the phytoplankton-induced optical variability in the high-latitude seas can influence the onset of stratification in the Spring.

The sensitivity analysis also revealed that the dependence of mixed-layer depth and temperature on the optical depth of the mixed layer saturates with increasing values of the optical depth. In the presence of strong winds, the mixed layer tends to be deeper or the optical depth of the mixed layer tends to be larger. Therefore, the sensitivity of mixed-layer depth to phytoplankton-induced changes in the attenuation coefficient of the layer will be less than it would be in the presence of weak winds.

Absorption of solar radiation is parameterized in bulk models as an exponential function of depth. In section 2.5, I have attempted to improve this parameterization by accounting for the depth-dependent changes in the attenuation coefficient of the mixed layer resulting from the spectral variations in light transmission in the ocean. Equations (2.48) and (2.49) are extensions of the Kraus-Turner type mixed-layer models that incorporate the effects of depth-dependency in the attenuation coefficient of the mixed layer. Note that these equations can be easily adapted to deal with absorption by substances other than phytoplankton.

To study the effect of changes in the attenuation coefficient on the depth of a shallowing mixed layer, only the changes in the stratification within the layer need be considered. This is because the new layer depth is determined in such a way

that the net TKE input is exactly sufficient to remove the stratification within the new layer. In the case of a deepening mixed layer, we should also take into account the temperature distribution beneath the mixed layer. In both cases, however, the way in which the changes in the stratification within the mixed layer, resulting from optical variability, affect the layer depth depends on the details of the energy budget of the mixed layer. To further illustrate this point, let us consider equation (2.33), which describes the evolution of mixed-layer depth. From this equation, a measure of the relative importance of the penetrative component of solar radiation in the energy budget can be obtained as the ratio of the energy input from the penetrative component, $\left(\frac{I(0)}{\rho C_p} f_{h_m}\right)$, to the algebraic sum of the energy inputs that are independent of the penetrative component, $\left(\frac{2(G-D)}{\rho g \alpha h_m} - \frac{Q(0)}{\rho C_p}\right)$. The contours of this (dimensionless) ratio are plotted in Figure 2.8 as functions of the wind stress, $\tau = \rho_a C_d U^2$, and the layer depth h_m. The TKE input to the water column is calculated as: $(G - D) = 0.0012 \rho_a C_d U^3$ (Denman, 1973) and the penetrative component of solar radiation at the sea surface is specified as: $I(0) = 200$ W/m^2. Three cases of non-penetrative energy input across the sea surface are shown in the figure: (a) $Q(0) = -150$ W/m^2, (b) $Q(0) = 0$ W/m^2 and (c) $Q(0) = 150$ W/m^2. The solid lines represent conditions when the phytoplankton concentration is 8 mg chl-a m^{-3} and the dashed lines represent conditions when the concentration is 0.01 mg chl-a m^{-3}. The contours of 1.5 represent the case in which $\left(\frac{2(G-D)}{\rho g \alpha h_m} - \frac{Q(0)}{\rho C_p}\right)$ exceeds $\left(\frac{I(0)}{\rho C_p} f_{h_m}\right)$ by 50% (deepening mixed layer). Similarly, the contours of 0.5 represent the condition when $\left(\frac{2(G-D)}{\rho g \alpha h_m} - \frac{Q(0)}{\rho C_p}\right)$ is only 50% of $\left(\frac{I(0)}{\rho C_p} f_{h_m}\right)$ (shallowing mixed layer) and the contours of 1.0 represent the case when these two quantities are equal.

When the non-penetrative heat input to the ocean is negative, $Q(0) < 0$, as shown in case (a), the penetrative component of solar radiation is the only source of buoyancy input to the mixed layer. Under this condition, the effect of changing the attenuation coefficient is more pronounced than that in the presence of a buoyancy

input from non-penetrative heat components, as shown in case (c). This is because in case (c), a given change in the attenuation coefficient will affect only a portion of the total buoyancy input to the mixed layer, whereas in case (a), a change of the same magnitude will affect the entire buoyancy input. Case (b), in which the non-penetrative heat input to the ocean is zero, represents an intermediate stage between case (a) and case (c).

So far I have avoided any discussion of alternative parametrizations of the term $(G - D)$: it has been assumed that the generation and dissipation of TKE are not functions of buoyancy input to the mixed layer. The models of Kraus and Turner (1967), Denman (1973) and Kim (1976) make this assumption. Some other models have incorporated an extra term to account for the TKE generation at the base of a deepening mixed layer, typically from shear (Niiler, 1975; Niiler and Kraus, 1977; Garwood, 1977). In such models the generation of TKE has an additional dependence on the entrainment velocity that can be modified by changes in the attenuation coefficient of the medium. Garwood (1977) incorporated a separate budget for the vertical component of TKE based on the argument that turbulent processes in the mixed layer are nonisotropic. This vertical component of the TKE budget is affected by the buoyancy input to the mixed layer and therefore would be sensitive to changes in the attenuation coefficient, an effect not accounted for in the present analysis.

Another path through which optical variability may affect the evolution of mixed-layer depth and temperature, which is not considered in the present study, is through the dissipation of TKE. Garwood (1977) and Gaspar (1988) have parametrized the dissipation of TKE as a function of the ratio of mixed-layer depth to the bulk Monin-Obukhov depth. Changes in the attenuation coefficient can modify the specification of bulk Monin-Obukhov depth in Garwood (1977) and Gaspar (1988) and therefore the rate of dissipation in these models.

FIGURE 2.8. An example of the effect of changes in the attenuation coefficient on the energy balance in the mixed layer. The figure shows the contours of the ratio of the term containing the penetrative component of solar radiation, $\left(\frac{I(0)}{\rho C_p} f_{h_m}\right)$, to the algebraic sum of the terms that are independent of the penetrative component, $\left(\frac{2(G-D)}{\rho g \alpha h_m} - \frac{Q(0)}{\rho C_p}\right)$ in equation (2.33). Three different cases of non-penetrative energy input across the sea surface are considered as $Q(0) = -150$ W m^{-2}, $Q(0) = 0$ W m^{-2} and $Q(0) = 150$ W m^{-2}. The solid lines represent the conditions when the phytoplankton concentration is 8 mg chl-a m^{-3} and the dashed lines represent the condition when the concentration is 0.01 mg chl-a m^{-3}. When $Q(0) < 0$ (case (a)) the effect of change in the attenuation coefficient is more pronounced than when $Q(0) > 0$ (case (c)). Case (b) represents an intermediate stage between case (a) and case (c).

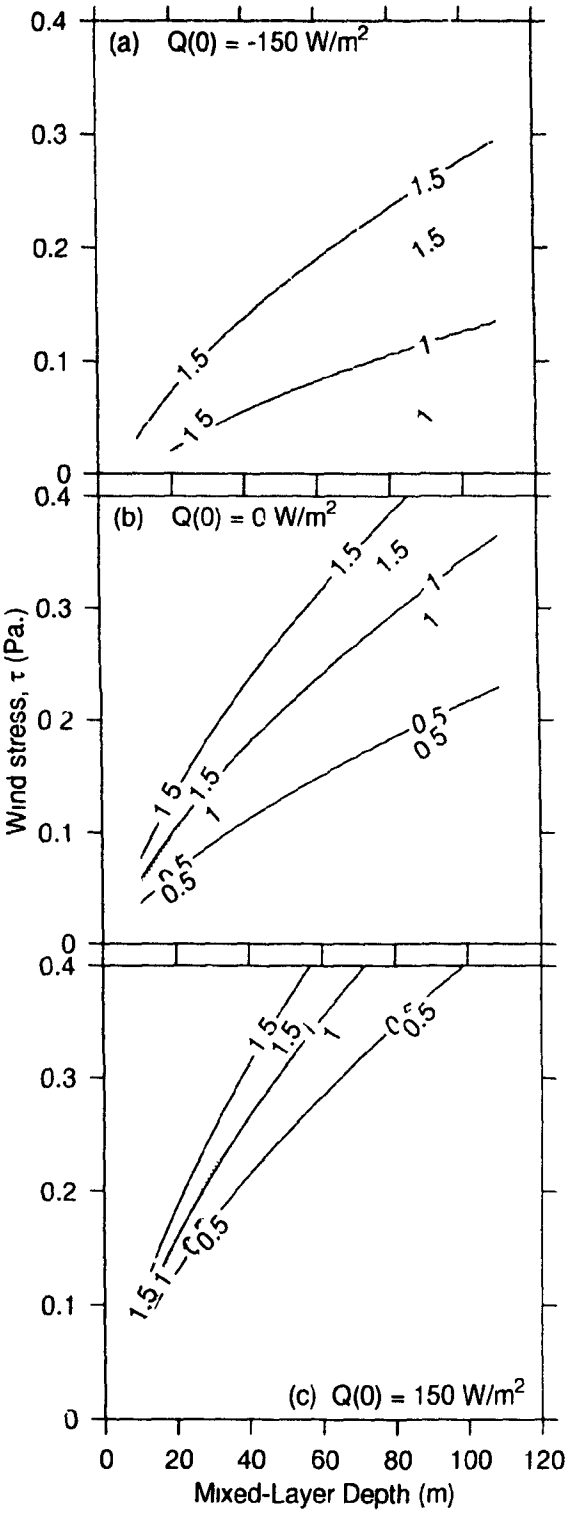
(a) Q(0) = -150 W/m²
(b) Q(0) = 0 W/m²
(c) Q(0) = 150 W/m²
Wind stress, τ (Pa.)
Mixed-Layer Depth (m)
0
0.1
0.2
0.3
0.4
0
20
40
60
80
100
120
1.5
1
0.5

Figure 2.8

Even though the parameterization of the $(G-D)$ term in the bulk mixed-layer models has been steadily improved in the past two decades, these models do not yet fully explain the variability in observed SST (see for example Martin, 1985; McCormick, 1988; and Gaspar, 1988). Some of the differences between models and observations may of course be caused by the neglect of the three-dimensional dynamics. However, some of the differences may also be caused by phytoplankton-induced variability in the light attenuation, an effect that is seldom considered. Even though this view has been put forward in a variety of studies in the past (Dickey and Simpson, 1983; Lewis *et al.*, 1983; Kirk, 1988; Simonot, *et al.*, 1988, Sathyendranath *et al.*, 1991; Ramp *et al.*, 1991; Stramska and Dickey, 1993; Platt *et al.*, 1994; Sathyendranath and Platt, 1994), serious attempts to incorporate the biological contribution into *large-scale* models of upper-ocean dynamics and air-sea interactions have yet to be presented.

Mixed-layer models are included in *large-scale* models to incorporate thermodynamic processes. Therefore, attempts to incorporate the effect of phytoplankton variability into *large-scale* models should begin by modifying mixed-layer models. Information on phytoplankton distribution can be obtained from satellite data on ocean color such as that provided by Coastal Zone Color Scanner (CZCS). The functions f_{h_m} and f_{T_m} derived in Section 2.5 or the functions $f^n_{h_m}$ and $f^n_{T_m}$ derived in Section 2.6, can be used to account for the effect of phytoplankton variability in mixed-layer models. These functions can be modified easily to study the effect of yellow substances or atmospheric dust inputs on the evolution of mixed-layer depth and temperature, if information on the variability of these components is available.

With respect to spectral effects on light transmission under water, these have also been incorporated into Kraus-Turner type models of upper-ocean thermodynamics (see for example, Woods *et al.*, 1984; Woods and Barkmann, 1986). The method presented in this chapter differs from many previous methods in the sense that it does not depend on any specific classification of the optical water type. It

can be used in conjunction with any spectral-irradiance model of under-water light transmission, irrespective of the structural details of the model. For such applications, the only requirement is that the spectral-irradiance model should provide the mean attenuation coefficient of different sub-layers within the mixed layer.

The effect of phytoplankton on the evolution of mixed-layer depth and temperature is also significant in the sense that it represents a feedback between oceanic microscopic biota and its environment. According to the critical mixing-depth theory introduced by Sverdrup (1953), a decrease in mixed-layer depth favours an increase in phytoplankton biomass. Such an increase in phytoplankton will alter the optical properties of the mixed-layer such that the layer depth will decrease further (Platt *et al.*, 1994; Sathyendranath and Platt, 1994). Thus, the dependence of phytoplankton growth on mixed-layer depth and the sensitivity of mixed-layer depth to phytoplankton concentration together represent a feedback loop between physical and biological processes in the mixed layer. Incorporation of this feedback loop into models of mixed-layer physics and biology may be expected to improve the performance of such models, a problem that will be examined in Chapter 4.

2.7 Concluding Remarks

Changes in the attenuation coefficient of the mixed layer influence the evolution of the depth and temperature of the surface layer of the ocean by modifying the magnitude and the depth-distribution of solar radiation absorbed in the layer. The depth and temperature of a mixed layer characterized by a small value of the optical depth are more sensitive to changes in the attenuation coefficient than the corresponding properties of a mixed layer characterized by a high value of the optical depth. The sensitivity of mixed-layer depth and temperature to changes in the attenuation coefficient increases with increasing contributions from solar radiation

to the total heat input to the ocean. Because phytoplankton and phytoplankton-derived products are the major sources of variability in the attenuation coefficient in open ocean waters, mixed-layer models should include a parameterization of the attenuation coefficient of the mixed layer as a function of phytoplankton biomass. Besides, the equations used in conventional, bulk, mixed-layer models can be modified to take into account the depth-dependent changes in the attenuation of solar radiation in the ocean.

In addition to change in the layer depth, modulations in phytoplankton concentration will change the layer temperature. An increase in the layer temperature will, in turn, modify the heat flux across the sea surface, the moisture content in the atmospheric boundary layer, and the drag coefficient at the sea surface. All these modifications can, in theory, affect the energy input to the mixed layer and therefore initiate a feedback from the atmosphere to the ocean.

Are the time scales associated with these oceanic and atmospheric feedback mechanisms compatible? What are the characteristics and magnitudes of these feedbacks? Does the atmospheric feedback mechanism amplify or diminish (counteract) the positive feedback mechanism that is identified in the ocean? Some of these questions will be addressed in Chapter 4 of this thesis, through simulation experiments using a coupled model of mixed-layer thermodynamics, phytoplankton growth and air-sea interaction. As a step in the development of such a coupled model of physical-biological interaction, a general, bulk, mixed-layer model with improved treatment of the energy budget is presented in the next chapter.

CHAPTER 3

A Generalized, Bulk Model of the Oceanic Mixed Layer

3.1 Introduction

Physical and biogeochemical processes in the surface mixed layer of the ocean are sensitive to the seasonal evolution of the layer depth and temperature. By regulating the transfer of mass and energy across the sea surface, the mixed layer influences various atmospheric processes. By acting as a buffer between the deep ocean and the atmosphere, it also regulates the global biogeochemical cycles. Understanding of the processes responsible for the formation and the evolution of the mixed layer provides an essential background to studies of upper-ocean dynamics, air-sea interaction and biogeochemical cycles.

To this end, numerous attempts have been made to model the surface layer of the ocean. In general, such models can be classified into two groups: depth-dependent models and bulk (depth-integrated) models. Some of the commonly-used, depth-dependent models share the theoretical foundation introduced by Mellor and Yamada (1974). One of the characteristics of these models, that restricts their wider acceptance, is their substantial computational requirement. In this respect, bulk models have a definite advantage over depth-dependent models. Bulk models (such as Denman, 1973; Niiler and Kraus, 1977; Garwood, 1977 and Gaspar, 1988) share a common origin in Kraus and Turner (1967). These models are developed by integrating the heat and energy conservation equations over the mixed layer: they are computationally faster than depth-dependent models. However, their simplicity and computational advantage are overshadowed by two of the assumptions used in the model formulation. These are (i) the assumption of *a priori* existence of a

well-mixed layer; and (ii) the requirement of a density discontinuity at the base of the mixed layer.

As a contribution to the provision of a more generally useful model, I present here a conceptually-simple, bulk model of the upper ocean with realistic physical foundations and reduced computational requirements. The change in the potential energy of the upper ocean associated with stratification is balanced against the kinetic energy input from wind, to describe the evolution of the mixed-layer depth. The heat budget of the upper ocean is used to determine the mixed-layer temperature. The requirement of a density discontinuity at the base of the mixed layer, common to all conventional bulk models, is eliminated in the present model. Further, the model is capable of describing the evolution of the mixed layer even in cases where a surface mixed layer is lacking initially. Also, the model equations are simple and computationally efficient. The model is expected to be useful in a wide variety of applications involving the thermodynamics of the upper ocean, and as an element of models of general circulation of the ocean, air-sea interactions and biogeochemical cycles in the ocean-atmosphere system.

The general features of the model ocean and the basic theory are presented in Section 3.2. Mathematical expressions for the energetics of various physical processes considered in the model formulation are derived in Section 3.3. An equation describing the deepening of the mixed layer is derived in Section 3.4, and it is simplified to obtain an analytical expression for the depth of an entraining mixed layer. A similar expression describing the depth of a detraining mixed layer is derived in Section 3.5, which is then simplified to formulate the corresponding analytical expression. The temperature of deepening and shallowing mixed layers are considered in Sections 3.6 and 3.7, respectively. A general discussion of model features is presented in Section 3.8.

3.2 The Model Ocean

The basic features of the model ocean are shown in Figure 3.1. At the beginning of each discrete time step, Δt, the surface layer is characterized by a uniform density ρ_m, temperature T_m and depth h_m. During the interval Δt (chosen to be sufficiently small that, during the interval, the energy inputs to the ocean from wind and Sun can be considered to remain constant), the absorption of solar radiation within the water column and the input of heat at the sea surface tend to stratify the layer. However, the turbulent-kinetic energy (TKE) input to the water column works against the stratifying tendency. The erosion of stratification by TKE is considered to occur instantaneously at the end of each discrete time step. If the TKE input during the time step exceeds that required to remove the stratification caused by the heat input, the surface layer will deepen through entrainment. On the other hand, if the TKE input is not sufficient to remove the stratification in the surface layer, the layer will retreat to a shallower depth within which the TKE input is exactly sufficient to effect complete mixing.

During the deepening phase of mixed-layer evolution, water is entrained into the layer from below. To account for this, we specify an entrainment layer of thickness h_e (of initially-unknown magnitude), defined as that portion of the thermocline through which the mixed layer will extend at the end of the time step. Then, we seek an expression for h_e as a function of the density distribution in the ocean at the beginning of the time step and the energy input across the sea surface during the time step. For the shallowing phase, there is no entrainment: our aim in this case is to calculate the new mixed-layer depth as that of the equilibrium layer within which the depth-integrated TKE input by the action of wind balances the stratification produced by the heat input.

The total heat input $H(0)$ across the sea surface is divided into a penetrative component $I(0)$ and a non-penetrative component $Q(0)$. The depth distribution of

FIGURE 3.1. The model ocean. The upper panel shows the conditions at the beginning of a time step that are characterized by a surface layer overlying an entrainment layer. The lower middle panel shows the conditions at the end of the time step in which the density distributions in the mixed layer and the entrainment layer are modified by the absorption of heat. The panels on the left and right show two possible paths (deepening, given by equation (3.25) and shallowing, given by equation (3.32)) of mixed-layer evolution depending upon the balance between the TKE input and the change in the potential energy associated with vertical mixing.

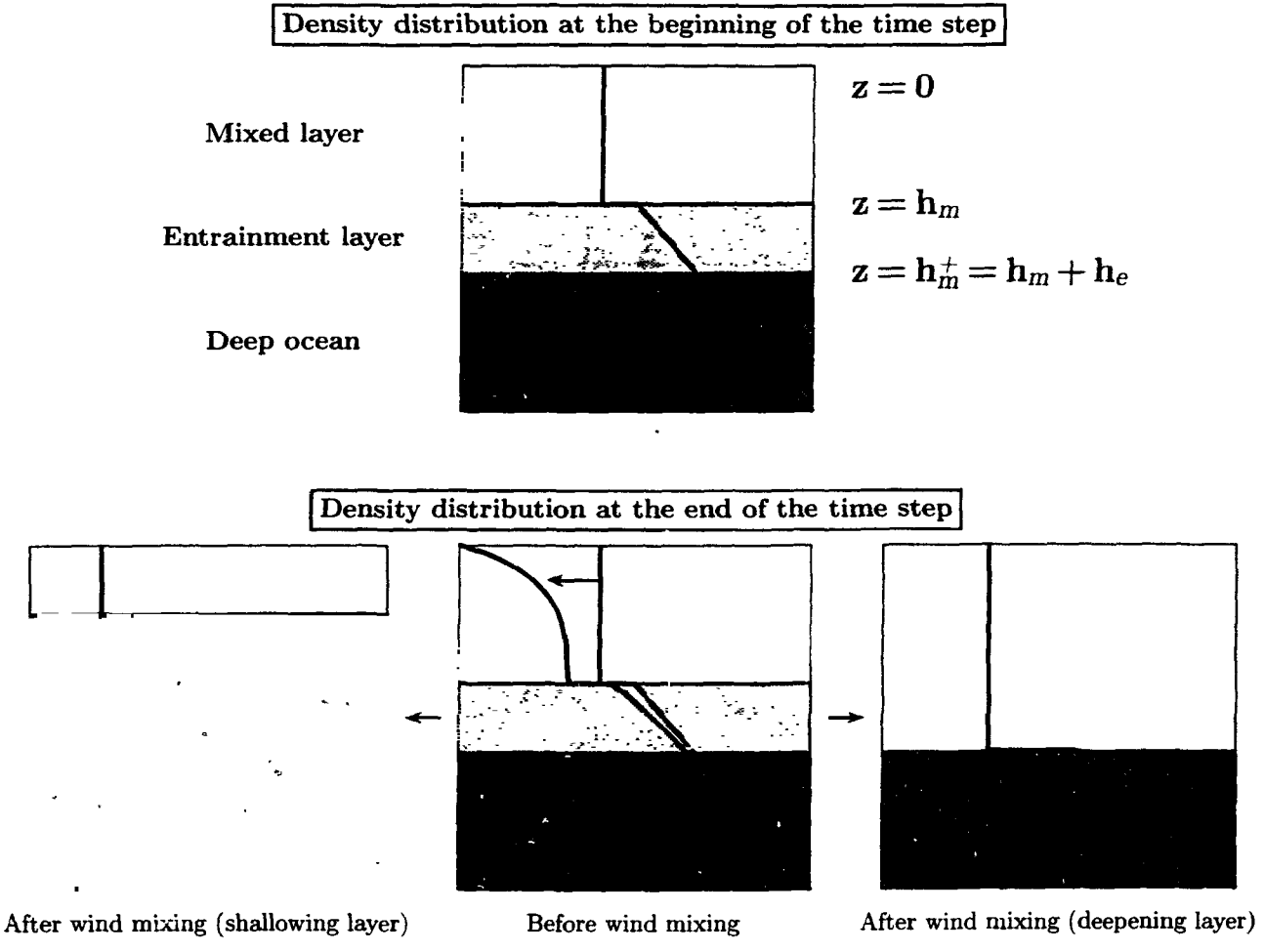
Density distribution at the beginning of the time step
Mixed layer
Entrainment layer
Deep ocean
z = 0
z = h_m
z = h_m^+ = h_m + h_e
Density distribution at the end of the time step
After wind mixing (shallowing layer)
Before wind mixing
After wind mixing (deepening layer)

Figure 3.1

the penetrative component is given by

$$I(z) = I(0)e^{-\int_0^z \gamma(z)dz}, \tag{3.1}$$

where $\gamma(z)$ is the diffuse vertical attenuation coefficient. We assume that $\gamma(z) = \gamma_m$ in the mixed layer and $\gamma(z) = \gamma_e$ in the entrainment layer where γ_m and γ_e are constants. The non-penetrative component consists of the net heat flux resulting from the remaining portion of the solar radiation, $\hat{I}(0)$, the fluxes of sensible heat $S(0)$ and latent heat $E(0)$, and the net longwave radiation at the sea surface $L(0)$ such that

$$Q(0) = \hat{I}(0) + S(0) + E(0) + L(0). \tag{3.2}$$

The sign convention I have used for $Q(0)$, $S(0)$, $E(0)$ and $L(0)$ is that when they are directed into the ocean their sign will be positive.

The equation of state is given by $\rho = \rho(T)$, neglecting the effect of salinity changes on the density distribution. The density distribution in the entrainment layer is assumed to be a linear function of depth z of the form

$$\rho_e(z) = \rho_b + a(z - h_m), \tag{3.3}$$

where ρ_b is the density immediately below the mixed layer. Nonlinear forms of $\rho_e(z)$ can easily be considered, but for clarity of exposition, I have restricted the treatment to the simpler form given here.

If the rate of input of TKE to the layer exceeds the rate of change of potential energy arising from stratification of the layer, the excess energy will be used to entrain water across the base of the surface layer, resulting in the deepening of the layer. The mixed-layer depth at the end of the time step is then calculated by equating the depth-integrated change in the potential energy of the layer associated with vertical mixing during the interval Δt, to the net TKE input during the same time interval (cf. Turner, 1969; Denman, 1972; Simpson *et al.*, 1978). Once the new

mixed-layer depth is known, the corresponding layer temperature is determined by considering the heat budget of the layer

The change in the potential energy (ϕ) resulting from vertical mixing of a layer of arbitrary thickness $z_2 - z_1$ can be written as

$$\phi(z_1, z_2) = \int_{z=z_1}^{z_2} [\rho(z) - \overline{\rho}] g z dz, \tag{3.4}$$

where $\overline{\rho}$ is the mean density of the layer, given by

$$\overline{\rho} = \left(\frac{1}{z_2 - z_1}\right) \int_{z=z_1}^{z_2} \rho(z) dz, \tag{3.5}$$

and $\rho(z)$ is the density of water at depth z, before mixing.

Let $h_m^+ = h_m + h_e$ be the depth of the final mixed layer, during the deepening phase of the layer evolution. In the model that is now to be developed, the total change in the potential energy, $\phi(0, h_m^+)$, associated with mixing at the end of the time interval Δt, is decomposed into three parts:

1. The change in the potential energy associated with the internal mixing in the surface layer $[\phi(0, h_m)]$. This accounts for the TKE required to remove the stratification developed in the surface layer during the time step.

2. The change in the potential energy associated with internal mixing of the entrainment layer, resulting in the removal of the stratification associated with the linear density distribution and the additional stratification caused by the absorption of solar radiation beneath the mixed layer $[\varphi(h_m, h_m^+)]$

3. The change in potential energy associated with complete mixing between the surface layer and the entrainment layer, each of which is internally well-mixed through processes described in (1) and (2) $[\tilde{\phi}(0, h_m^+)]$.

FIGURE 3.2. Changes in the potential energy of the water column associated with wind mixing. The density distribution at the beginning of the time step is shown in Panel (1). The modification to the density distribution at the end of the time step (before vertical mixing), resulting from the absorption of heat is shown in Panel (2). Changes in the density distribution in the surface layer and in the entrainment layer, resulting from internal mixing of the layers are shown in Panels (3) and (4), respectively. The contributions from these processes to the total change in the potential energy of the water column are denoted by $\phi(0, h_m)$ and $\phi(h_m, h_m^+)$, respectively. The effect of mixing between the surface layer and the entrainment layer on the density distribution is shown in Panel (5). The corresponding change in the potential energy is denoted by $\tilde{\phi}(0, h_m^+)$. The density distribution in the newly-formed mixed layer is shown in Panel (6). The total change in the potential energy associated with the formation of the new mixed layer is denoted by $\phi(0, h_m^+)$, which is given by: $\phi(0, h_m^+) = \phi(0, h_m) + \phi(h_m, h_m^+) + \tilde{\phi}(0, h_m^+)$. The straight arrows indicate the change in the density distribution and the curved arrows indicate the vertical extent of mixing considered in each panel.

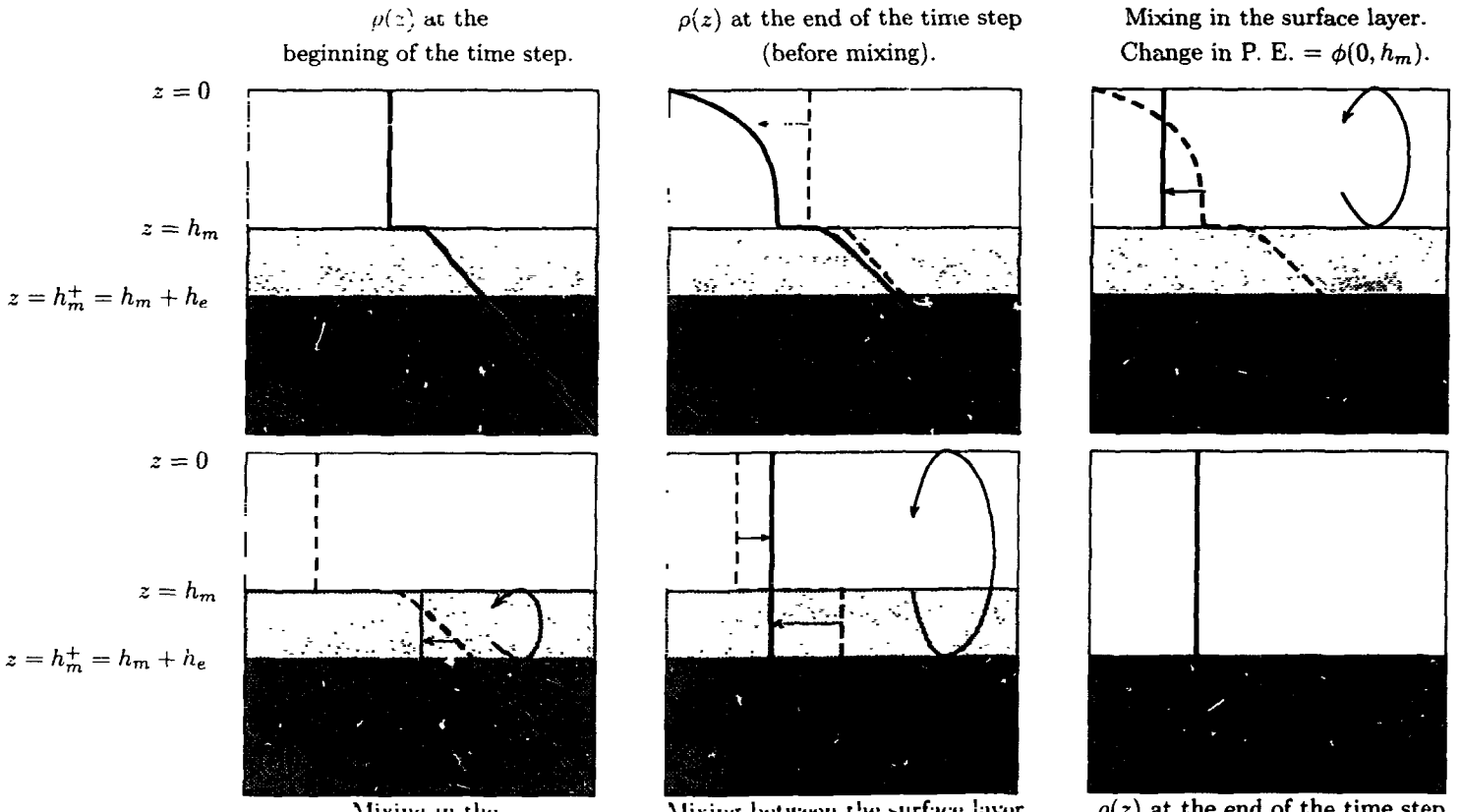
$\rho(z)$ at the beginning of the time step.
$\rho(z)$ at the end of the time step (before mixing).
Mixing in the surface layer. Change in P. E. = $\phi(0, h_m)$.
$z = 0$
$z = h_m$
$z = h_m^+ = h_m + h_e$
$z = 0$
$z = h_m$
$z = h_m^+ = h_m + h_e$
Mixing in the entrainment layer. Change in P. E. = $\phi(h_m, h_m^+)$.
Mixing between the surface layer and the entrainment layer. Change in P. E. = $\tilde{\phi}(0, h_m^+)$.
$\rho(z)$ at the end of the time step (after mixing) Net change in P. E. = $\phi(0, h_m^+)$.

Figure 3.2

The total change in potential energy of a deepening mixed layer $\phi(0, h_m^+)$ can be expressed as

$$\phi(0, h_m^+) = \phi(0, h_m) + \phi(h_m, h_m^+) + \tilde{\phi}(0, h_m^+), \tag{3.6}$$

which follows from the identity

$$\int_0^{h_m^+} [\rho(z) - \overline{\rho}] g z dz = \int_0^{h_m} [\rho(z) - \overline{\rho}^m] g z dz + \int_{h_m}^{h_m^+} [\rho(z) - \overline{\rho}^e] g z dz + \int_0^{h_m^+} [\rho'(z) - \overline{\rho}] g z dz. \tag{3.7}$$

In equation (3.7), $\overline{\rho}^m$ and $\overline{\rho}^e$ are the mean density of the initial mixed layer and the entrainment layer, respectively, at the end of the time step after internal mixing. Also, in equation (3.7)

$$\rho'(z) = \overline{\rho}^m \quad \text{for} \quad 0 \leq z \leq h_m$$

and

$$\rho'(z) = \overline{\rho}^e \quad \text{for} \quad h_m \leq z \leq h_m^+. \tag{3.8}$$

See Figure 3.2 for a pictorial representation of the mixing processes described above.

In the following section, analytical expressions for each of these components are derived, which are then used to develop the equations describing the depth and the temperature of the layer, after time Δt.

3.3 The Change in the Potential Energy Associated With Wind Mixing

3.3.1 The Change in the Potential Energy Associated With Mixing in the Surface Layer

Applying equation (3.4) to the surface layer, the change in the potential energy associated with vertical mixing in the layer at the end of the time step can be

expressed as

$$\phi(0, h_m) = \int_0^{h_m} \left[\rho(z) - \overline{\rho}^m\right] g z dz. \tag{3.9}$$

Here, $\rho(z)$ is the density profile at the end of the time step in the surface layer, given by

$$\rho(z) = \rho_m - \Delta t \frac{\alpha}{C_p}\left[\gamma_m I(0) e^{-\gamma_m z} + \delta(z) Q(0)\right], \text{ for } 0 \leq z \leq h_m. \tag{3.10}$$

In equation (3.10), $\delta(z)$ is the Dirac-delta function, with properties $\delta(z) = 0$ for $z > 0$ and $\int_0^z \delta(z')dz' = 1$.

The depth-average of equation (3.10) for $0 \leq z \leq h_m$ is

$$\overline{\rho}^m = \rho_m - \frac{1}{h_m}\int_0^{h_m} \rho(z)dz = \rho_m - \Delta t \frac{\alpha}{C_p h_m}\left[I(0)(1 - e^{-\gamma_m h_m}) + Q(0)\right]. \tag{3.11}$$

Substituting equations (3.10) and (3.11) into equation (3.9) and solving gives

$$\phi(0, h_m) = \frac{\Delta t\, g \alpha h_m}{2C_p}\left[I(0) f_{h_m} + Q(0)\right], \tag{3.12}$$

where

$$f_{h_m} = 1 - \frac{2}{\gamma_m h_m}\left(1 - e^{-\gamma_m h_m}\right) + e^{-\gamma_m h_m}, \tag{3.13}$$

is a function that accounts for the depth distribution of heat input to the mixed layer by the penetrative component of solar radiation. The numerical value of the function f_{h_m} varies between 0 and 1; $f_{h_m} = 1$ when all the radiation is absorbed at the sea surface.

3.3.2 The Change in the Potential Energy Associated With Mixing in the Entrainment Layer

Applying equation (3.4) to the entrainment layer gives

$$\phi(h_m, h_m^+) = \int_{h_m}^{h_m^+} \left[\rho(z) - \overline{\rho}^e\right] g z dz, \tag{3.14}$$

where $\rho(z)$ is now the density profile in the entrainment layer at the end of the time interval Δt, given by

$$\rho(z) = \rho_b + a(z - h_m) - \Delta t \frac{\alpha\gamma_e I(h_m) e^{-\gamma_e(z-h_m)}}{C_p}, \text{ for } h_m \leq z \leq h_m^+, \quad (3.15)$$

and $\overline{\rho}$ is now the depth-averaged density of the entrainment layer which can be written using equation (3.15) as

$$\overline{\rho}^e = \frac{1}{h_e}\int_{h_m}^{h_m^+} \rho(z)dz = \rho_b + \frac{ah_e}{2} - \frac{\Delta t\,\alpha I(h_m)}{C_p h_e}\left[1 - e^{-\gamma_e h_e}\right]. \quad (3.16)$$

Substituting equations (3.15) and (3.16) into equation (3.14) and simplifying gives

$$\phi(h_m, h_m^+) = \frac{agh_e^3}{12} + \Delta t \frac{g\alpha h_e}{2C_p}\left[I(h_m) f_{h_e}\right], \quad (3.17)$$

where

$$f_{h_e} = \left[1 - \frac{2}{\gamma_e h_e}\left(1 - e^{-\gamma_e h_e}\right) + e^{-\gamma_e h_e}\right]. \quad (3.18)$$

Equation (3.17) represents the change in the potential energy associated with the removal of stratification within the entrainment layer. The first term on the right denotes the contribution from the linear density gradient within the entrainment layer and the second term represents that from the additional stratification produced by the absorption of solar radiation.

3.3.3 The Change in the Potential Energy Associated With Mixing Between the Surface Layer and the Entrainment Layer

The mixing between the surface layer and the entrainment layer is considered next, assuming that each of these layers is already, internally well-mixed. From equation (3.4), the change in potential energy associated with the removal of the density difference between these layers can be expressed as

$$\tilde{\phi}(0, h_m) = \int_0^{h_m^+} \left[\rho'(z) - \overline{\rho}\right] gz dz, \quad (3.19)$$

where $\rho'(z)$ is the density profile after the internal mixing of the surface layer and the entrainment layer. From equation (3.11), $\rho'(z) = \overline{\rho}^m$ in the surface layer and from equation (3.16), $\rho'(z) = \overline{\rho}^e$ in the entrainment layer.

The depth-averaged density of the mixed layer and the entrainment layer together, $\overline{\rho}$ can be written as,

$$\overline{\rho} = \frac{1}{h_m^+}\int_0^{h_m^+} \rho'(z)dz = \frac{1}{h_m^+}\left[\overline{\rho}^m h_m + \overline{\rho}^e h_e\right]. \tag{3.20}$$

Substituting equation (3.20) into equation (3.19) and simplifying gives

$$\tilde{\phi}(0, h_m^+) = \frac{g h_m h_e}{2}\left[\overline{\rho}^e - \overline{\rho}^m\right]. \tag{3.21}$$

3.3.4 The Total Change in the Potential Energy of an Entraining Mixed Layer

From equations (3.6), (3.12), (3.17) and (3.21), the depth-integrated change in potential energy of a entraining mixed layer can be expressed as

$$\phi(0, h_m^+) = \Delta t \frac{g\alpha h_m}{2C_p}\left[I(0)f_{h_m} + Q(0)\right] +$$

$$\Delta t \frac{g\alpha h_e}{2C_p}\left[I(h_m)f_{h_e}\right] + \frac{agh_e^3}{12} + \frac{gh_m h_e}{2}\left[\overline{\rho}^e - \overline{\rho}^m\right]. \tag{3.22}$$

Substituting the expressions for $\overline{\rho}^m$ and $\overline{\rho^e}$ from equations (3.11) and (3.16) into equation (3.22) we get

$$\phi(0, h_m^+) = \Delta t \frac{g\alpha h_m}{2C_p}\left[I(0)f_{h_m} + Q(0)\right] + \frac{agh_e^3}{12} +$$

$$\Delta t \frac{g\alpha h_e}{2C_p}\left[I(h_m)f_{h_e}\right] + \frac{gh_m h_e}{2}\left\{\rho_b - \rho_m + \frac{ah_e}{2} + \Delta t \frac{\alpha}{C_p h_m}\left[I(0)\left(1 - e^{-\gamma_m h_m}\right) + Q(0)\right] -\right.$$

$$\left.\Delta t \frac{\alpha I(h_m)}{C_p h_c}\left[1 - e^{-\gamma_e h_e}\right]\right\}, \tag{3.23}$$

which is the total change in potential energy associated with the buoyancy redistribution through vertical mixing in the entraining mixed layer.

3.4 The Depth of an Entraining Mixed Layer

The change in potential energy associated with the formation of a new mixed layer through entrainment is determined from the equation

$$\phi(0, h_m^+) - \Delta t\,(G - D) = 0, \tag{3.24}$$

where G and D represent, respectively, the rates of generation and dissipation of TKE, in the water column. Substituting for $\phi(0, h_m^+)$ from equation (3.23) into equation (3.24) we have an expression for h_e, the increase in the depth of the mixed layer after time Δt:

$$\underbrace{\frac{agh_e^3}{12}}_{1} + \underbrace{\frac{agh_m h_e^2}{4}}_{2} + \underbrace{\Delta t\,\frac{\alpha g h_e}{2C_p}\left[I(0)\left(1 - e^{-\gamma_m h_m}\right) + Q(0)\right]}_{3} -$$

$$\underbrace{\Delta t\,\frac{\alpha g h_m}{2C_p} I(h_m)\left[1 - e^{-\gamma_e h_e}\right]}_{4} + \underbrace{\Delta t\,\frac{\alpha g h_e}{2C_p}\left[I(h_m) f_{h_e}\right]}_{5} +$$

$$\underbrace{\frac{g h_m h_e}{2}\left(\rho_b - \rho_m\right)}_{6} + \underbrace{\Delta t\,\frac{\alpha g h_m}{2C_p}\left[I(0) f_{h_m} + Q(0)\right]}_{7} - \underbrace{\Delta t\,(G - D)}_{8} = 0. \tag{3.25}$$

Equation (3.25) represents the energy budget of the upper ocean associated with the evolution of the mixed layer, under the influence of solar heating, surface heat exchange and wind forcing. The first term represents the TKE required to remove the linear density gradient in the entrainment layer. The second term denotes the TKE required to work against the increase in the density at the base of the

surface layer, resulting from the removal of the linear density gradient in the entrainment layer. The effects of heat input to the surface layer and the entrainment layer on the TKE required for mixing between these two layers are given by terms three and four, respectively. The TKE required to work against the stratification in the entrainment layer resulting from solar heating is given by term five. If a density discontinuity is present at the base of the mixed layer ($\rho_b \neq \rho_m$) at the beginning of the time step, the TKE required to remove this discontinuity is given by the sixth term. The energy required to remove the stratification in the surface layer produced by the heat input during the time interval Δt is represented by the seventh term. The last term on the left represents the net TKE input to the water column.

Equation (3.25) can be solved numerically, using standard routines for finding the roots of a continuous function, such as ZEROIN (Morris, Jr., 1993).

When the density gradient in the entrainment layer is absent, terms 1 and 2 of equation (3.25) will vanish. If we assume that the effect of solar heating does not contribute to the stratification in the entrainment layer, term 5 can be neglected. Again, if the input of heat during the time step does not modify the mean density of the mixed layer and the entrainment layer, terms 3 and 4 can also be neglected. Dropping these terms is equivalent to taking the limiting case of equation (3.25) as $\Delta t \rightarrow 0$:

$$\lim_{\Delta t \rightarrow 0} \frac{h_e}{\Delta t} = \frac{(G-D) - \alpha g h_m (2C_p)^{-1} \left[I(0) f_{h_m} + Q(0) \right]}{\frac{1}{2} g h_m \left(\rho_b - \rho_m \right)}, \tag{3.26}$$

Note that equation (3.26) has the general form of the equation for $h_e/\Delta t$ used in conventional bulk models for the deepening of mixed layer. In other words, the equation used to describe the evolution of mixed-layer depth by conventional bulk models represents a limiting case of equation (3.25). Thus the mixed-layer depth predicted by equations (3.25) and (3.26) will be the same when the time step of integration is small. However, with increasing time step, the mixed-layer depth predicted by equation (3.26) will deviate from its true value as the condition

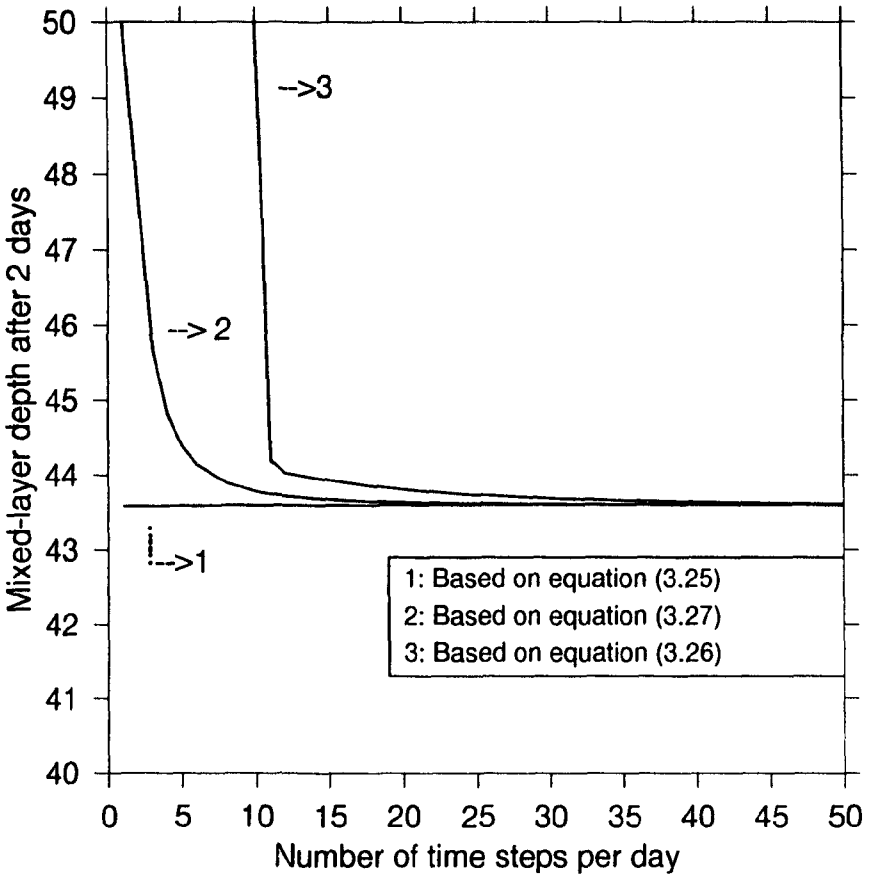

FIGURE 3.3. A comparison between the mixed-layer depths calculated using the complete equation (3.25), the quadratic approximation (3.27) and the conventional bulk-model equation (3.26). The mixed-layer depths, after two days of simulated time, are plotted as a function of the number of time steps used in the calculation. For large time steps the solutions to the conventional bulk-model equation and the quadratic approximation deviate from the solution to the complete equation (3.25). In this typical example, the TKE input is estimated as $(G - D) = 0.0012\rho_a C_d U^3$ (Denman, 1973). The depth and temperature of the initial mixed layer are 5m and 8.5°C, respectively. The temperature at the base of the initial mixed layer is 8°C and the temperature gradient in the entrainment layer is 0.0385°C m^{-1}. Also, the attenuation coefficients of the mixed layer and the entrainment layer are chosen to be $\gamma_m = \gamma_e = 0.2\,m^{-1}$. The forcing fields used in the model simulation are: wind speed = 12.5m s^{-1}, $Q(0)$ = - 19.45 W m^{-2} and $I(0)$ = 194.5 W m^{-2}.

$\Delta t \rightarrow 0$ is violated. Thus, conventional models fail in predicting the mixed-layer depth correctly if the time step is taken excessively large.

Another approach to simplification of equation (3.25) leads to an analytical approximation for the increase in depth of an entraining mixed layer. We proceed as follows. When h_e is very small, terms 1 and 5 of equation (3.25), which are of the order of h_e^3, can be neglected. Also, under such conditions, term 4 of the equation can be simplified by neglecting third and higher order terms in the Taylor series expansion of $e^{-\gamma_e h_e}$. The resulting quadratic equation can then be solved for h_e:

$$h_e = \frac{-X_1 + \sqrt{X_1^2 - 4X_0X_2}}{2X_2} \tag{3.27}$$

where

$$X_2 = \frac{agh_m}{4} + \Delta t \frac{\alpha g h_m \gamma_e}{4C_p}, \tag{3.28}$$

$$X_1 = \frac{gh_m}{2}(\rho_b - \rho_m) + \Delta t \frac{\alpha g}{2C_p}\left[I(0)(1 - e^{-\gamma_m h_m}) + Q(0)\right] - \Delta t \frac{\alpha g h_m}{2C_p}\left[I(h_m)\gamma_e\right], \tag{3.29}$$

and

$$X_0 = \Delta t \frac{\alpha g h_m}{2C_p}\left[I(0) f_{h_m} + Q(0)\right] - \Delta t \left(G - D\right). \tag{3.30}$$

Once the increase in the layer depth, h_e, after time Δt is known, the depth of the newly-formed mixed layer h_m^+ is given by

$$h_m^+ = h_m + h_e. \tag{3.31}$$

A comparison between mixed-layer depths calculated using equations (3.25), (3.26) and (3.27) is shown in Figure 3.3. The initial depth and temperature of the surface mixed layer are 5 m and 8.5°C, respectively. The initial temperature at the base of the layer is 8.0 °C and the initial temperature gradient in the entrainment layer is 0.0385°C m^{-1}. Using the Denman (1973) parameterization of the net TKE input to the water column, $(G - D)$ is estimated as: $(G - D) = 0.0012\rho_a C_d U^3$, where $U = 12.5$ m s^{-1} is the wind speed, $C_d = 0.0013$ is the drag coefficient and

$\rho_a = 1.2$ Kg m^{-3} is the air density. In this figure, the depth of the mixed layer at the end of 2 days of simulated time is plotted as a function of the number of time steps used. The figure shows that, for fixed forcing conditions, the solution based on equation (3.25) is independent of the time step used in the calculation, whereas the errors in the solutions based on equations (3.26) and (3.27) increase with increasing step size or decreasing number of steps per day.

3.5 The Depth of a Detraining Mixed Layer

When the TKE input to the mixed layer is not sufficient to counter the stratification produced by the input of heat, the surface layer will retreat to a shallower level within which the TKE balances the buoyancy input. In such instances, the depth of the newly-formed layer (h_m^+) is less than or equal to h_m, such that entrainment cannot occur. None of the terms in equation (3.25) that are functions of h_e contribute to the change in depth of the surface layer. Also, in equation (3.25), h_m can be replaced by h_m^+ since the layer depth is determined by the energy balance within the newly-formed layer of depth h_m^+, which is independent of the surface-layer depth h_m at the beginning of the time step. The resulting equation is

$$\frac{\alpha h_m^+}{C_p}\left[I(0) f_{h_m^+} + Q(0)\right] - \frac{2(G-D)}{g} = 0, \tag{3.32}$$

where

$$f_{h_m^+} = 1 - \frac{2}{\gamma_m h_m^+}(1 - e^{-\gamma_m h_m^+}) + e^{-\gamma_m h_m^+}. \tag{3.33}$$

Equation (3.32) is identical to the equation used in conventional bulk mixed-layer models to describe the shallowing of a mixed layer. An analytical solution for equation (3.32) can be obtained by using a rational-polynomial approximation of $f_{h_m^+}$ of the form

$$f_{h_m^+} = \frac{p_1 + p_2\theta + p_3\theta^2}{p_4 + p_5\theta} \quad \text{for} \quad \theta_1 \le \theta < \theta_2, \tag{3.34}$$

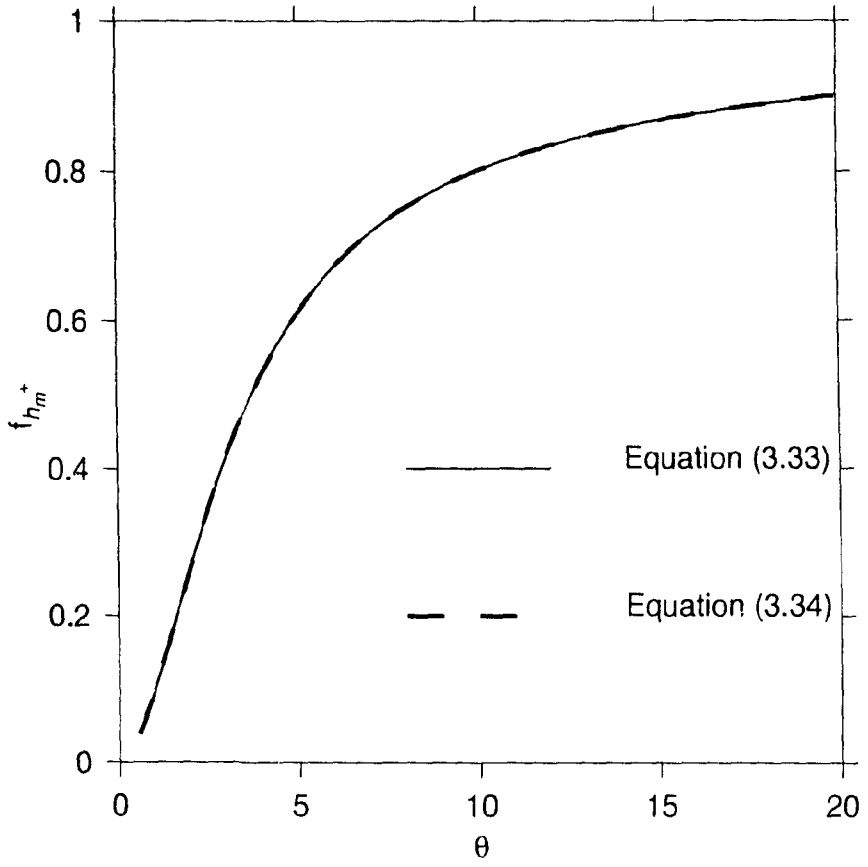

FIGURE 3.4. The rational-polynomial approximation to $f_{h_m^+}$ is plotted as a function of θ. The solid curve represents the original equation and the broken curve represents the approximation.

Table 3.1 The coefficients used in the rational polynomial approximation to $f_{h_m^+}$ are given in this table. Three ranges of variation $\theta_1 < \theta \leq \theta_2$ are considered. They are: $0.6 < \theta \leq 1.25$, $1.25 < \theta \leq 4.5$, $4.5 < \theta \leq 20$.

$\theta_1 - \theta_2$	0.6 - 1.25	1.25 - 4.5	4.5 - 20.0
p_1	0.08608	0.68290	6.44400
p_2	-0.42370	-1.37100	-5.00600
p_3	0.79830	1.02800	0.92850
p_4	-0.01420	0.86830	0.92710
p_5	4.45100	2.05100	3.11700

where $\theta = \gamma_m h_m^+$ and θ_1 and θ_2 are the lower and upper bounds of the range of θ for which the equation is valid. Note that this particular form of the rational polynomial is selected only for the convenience of obtaining an analytical approximation. Equation (3.34) gives good results if the range of θ generally observed in the ocean is divided into three intervals. Coefficients for a typical example using three sub-intervals are given in Table 3.1. Note that the coefficients need be calculated only once. The validity of this approximation is shown in Figure 3.4 by comparing $f_{h_m^+}$ estimated using equations (3.33) and (3.34). Using equation (3.34), equation (3.32) can be written in the form

$$Y_2\theta^2 + Y_1\theta + Y_0 = 0, \tag{3.35}$$

where

$$Y_2 = p_3 I(0) + p_5 Q(0), \tag{3.36}$$

$$Y_1 = \left[p_2 I(0) + p_4 Q(0) - p_5 \frac{2(G-D)\gamma_m C_p}{\alpha g}\right], \tag{3.37}$$

and

$$Y_0 = \left[p_1 I(0) - p_4 \frac{2(G-D)\gamma_m C_p}{\alpha g}\right]. \tag{3.38}$$

To determine the mixed-layer depth, first, the positive real roots of equation (3.35), for each of the sub-ranges of θ are computed as

$$\theta = \frac{-Y_1 + \sqrt{Y_1^2 - 4Y_2Y_0}}{2Y_2}. \tag{3.39}$$

Among these roots, the appropriate value of θ is the one that satisfies the condition $\theta_1 \leq \theta < \theta_2$. Once the appropriate θ is identified, the layer depth can be determined by specifying γ_m.

3.6 The Temperature of an Entraining Mixed Layer

Once the new layer depth (h_m^+) is known, the temperature of the new mixed layer (T_m^+) can be calculated from the surface-layer temperature at the beginning

of the time step, the effects of the absorption of solar radiation, exchange of heat across the sea surface and the entrainment of water across the base of the mixed layer. That is,

$$T_m^+ = \frac{1}{h_m^+}\Big\{T_m h_m + \frac{\Delta t}{\rho_m C_p}\Big[I(0)\big(1-e^{-\gamma_m h_m^+}\big) + Q(0)\Big] - h_e\big(T_m - T_b + \frac{bh_e}{2}\big)\Big\}, \tag{3.40}$$

where the first term on the right denotes the heat content of the surface layer at the beginning of the time step, the second term takes into account the heat input from the non-penetrative heat flux and the absorption of solar radiation, and the last term denotes the change in the layer temperature associated with the water entrained across the base of the surface layer.

3.7 The Temperature of a Detraining Mixed Layer

Given the depth of a detraining mixed layer, the layer temperature, T_m^+, is calculated as the sum of the surface layer temperature at the beginning of the time step and the increase in the layer temperature produced by the heat absorption in the new mixed layer

$$T_m^+ = T_m + \frac{\Delta t}{\rho_m C_p h_m^+}\Big[I(0)\big(1-e^{-\gamma_m h_m^+}\big) + Q(0)\Big]. \tag{3.41}$$

3.8 Discussion

Equation (3.25) can be non-dimensionalised by dividing throughout by term 6 of the equation. This gives

$$\underbrace{\frac{agh_e^3}{12\Lambda}}_{(i)} + \underbrace{\frac{agh_m h_e^2}{4\Lambda}}_{(ii)} + \underbrace{\frac{\Delta t\, \alpha g h_e\Big[I(0)\big(1-e^{-\gamma_m h_m}\big) + Q(0)\Big]}{2C_p\Lambda}}_{(iii)} -$$

$$\underbrace{\frac{\Delta t\,\alpha g h_m I(h_m)\left[1-e^{-\gamma_e h_e}\right]}{2C_p\Lambda}}_{(iv)}+\underbrace{\frac{\Delta t\,\alpha g h_e\left[I(h_m)f_{h_e}\right]}{2C_p\Lambda}}_{(v)}+$$

$$\underbrace{1+\frac{\Delta t\;\alpha g h_m\left[I(0)f_{h_m}+Q(0)\right]-2\Delta t\;C_p(G-D)}{2C_p\Lambda}}_{(vi)}=0, \tag{3.42}$$

where

$$\Lambda=\frac{1}{2}g h_m h_e\left(\rho_b-\rho_m\right). \tag{3.43}$$

If we assume that terms $(i)-(v)$ of equation (3.42) are negligible, then the equation reduces to equation (3.26), which is the general equation employed in conventional bulk models to describe the deepening of the mixed layer. However, neglecting terms $(i)-(v)$ implies stringent conditions on the maximum time step that can be used in the model simulation. The conditions that would have to be satisfied are:

$$\Delta t \ll \frac{C_p h_m(\rho_b-\rho_m)}{\alpha[I(0)(1-e^{-\gamma_m h_m})+Q(0)]} \quad \text{from} \quad \text{term} \quad (iii), \tag{3.44}$$

$$\Delta t \ll \frac{C_p(\rho_b-\rho_m)}{\alpha\gamma_e I(h_m)} \quad \text{from} \quad \text{term} \quad (iv), \tag{3.45}$$

$$\Delta t \ll \frac{C_p h_m(\rho_b-\rho_m)}{\alpha I(h_m)f_{h_e}} \quad \text{from} \quad \text{term} \quad (v), \tag{3.46}$$

$$h_e \ll \sqrt{6h_m\left(\frac{\rho_b-\rho_m}{a}\right)} \quad \text{from} \quad \text{term} \quad (i), \tag{3.47}$$

and

$$h_e \ll 2\left(\frac{\rho_b-\rho_m}{a}\right) \quad \text{from} \quad \text{term} \quad (ii). \tag{3.48}$$

Note that the last two conditions on h_e are equivalent to conditions on Δt, because the increase in the layer depth during any given time step is a function of the time step itself. Inequalities (3.44) - (3.48) limit the accuracy of conventional models (for example, equation (3.26)) when the time step is chosen to be too large. If they are not satisfied, either the time step must be reduced, or the complete equation (3.42) must be used.

Another issue relevant to the choice of time step is that of numerical stability. Figure 3.3 shows that the mixed-layer depth predicted by conventional bulk models becomes unstable with increasing time step. As a consequence, during model simulations using observed data, the time step of integration is determined by the stability of the model rather than the frequency of observations. On the other hand, the depth of the mixed layer predicted by the general bulk model is not sensitive to the size of the time step used provided temporal variation in the forcing are resolved. Therefore, model simulation using the general model can be optimized for computational efficiency by choosing the time interval between observations (or between significant changes in the observations) as the time step for model simulation.

Bulk models of the oceanic mixed layer are conceptually simple and computationally efficient. They have also proven to be successful in reproducing the observed fields of mixed-layer depth and temperature (Martin, 1985, Gaspar, 1988). However, their wider usage as a modelling tool is diminished by the requirements of the *a priori* existence of a well-mixed layer and a positive density discontinuity at the base of the layer.

The model developed in this chapter does not require the *a priori* existence of a well-mixed layer. In the absence of a surface mixed layer ($h_m = 0$), the entrainment layer will extend from the sea surface, and therefore $I(h_m) = I(0)$. With this modification equation (3.25) becomes

$$\frac{agh_e^3}{12} + \Delta t \frac{\alpha g h_e}{2C_p}\Big[I(0)f_{h_e} + Q(0)\Big] - \Delta t\,(G - D) = 0. \tag{3.49}$$

This equation describes the development of a mixed layer in a linearly-stratified water column in the presence of TKE input, absorption of solar radiation and the exchange of heat across the sea surface. The assumption of a linearly-stratified medium can be modified easily to incorporate any other type of stratification. On the other hand, linearity is only required over the depth interval $h_m \leq z \leq h_m^+$ so by selecting small time steps for model integration, non-linear density profiles can be approximated very well using linear profiles.

There have been several attempts to incorporate thermodynamic processes into models of the upper-ocean dynamics (Schopf and Cane, 1983; McCreary and Kundu, 1989; McCreary *et al.,* 1993). One of the major problems faced by researchers in incorporating bulk thermodynamic models into dynamic models of the upper ocean is the requirement, common to all conventional bulk models, of a positive density discontinuity at the base of the mixed layer. In the presence of strong surface cooling or advection of cold water, the density discontinuity at the base of the layer may disappear ($\rho_b = \rho_m$). This introduces a mathematical singularity in the equation used by conventional bulk models to describe the evolution of the mixed-layer depth (equation (3.26)). Attempts to overcome this difficulty by specifying a constant temperature difference at the base of the mixed layer (McCreary and Kundu, 1989) or by estimating the temperature difference from the temperature distribution in the thermocline (Schopf and Cane, 1983) can introduce errors in the heat and energy budget of the mixed layer. This is because the evolution of the temperature at the base of the mixed layer is a time-dependent process that is influenced more by the evolution of the mixed layer than that of the thermocline. The bulk model developed in this chapter eliminates this potential problem and therefore it is well suited for incorporating mixed-layer thermodynamics into three-dimensional circulation models of the upper ocean.

A significant portion of research associated with the modelling of the upper-ocean thermodynamics, during the past two decades, has focused on the parameterization of the TKE budget. As a result, a number of schemes, with different

degrees of complexity and different physical foundations, are available for describing the generation and dissipation of TKE (Zilitinkevich *et al.*, 1979; Garwood, 1979; Gaspar, 1988). Equation (3.25) is not based on any particular parametrization scheme for representing the TKE input to the ocean, and it can be easily adapted to any scheme one may select. The exact form of the equation is determined by the parametrization of the generation and dissipation of TKE in the mixed layer and the equation can be solved in a straight-forward manner for many of these parameterization schemes. However, incorporation of some of the recent parameterization schemes such as that of Gaspar (1988) may result in a complex system of algebraic equations and the solution will become much more time consuming.

The model developed in this chapter provides a solid foundation for the depth-integrated approach of mixed-layer modelling as it is free from two of the major limitations of conventional bulk mixed-layer models. The model's ability to incorporate larger time steps than would be allowed by conventional bulk models will be exploited in the next chapter, to develop a coupled model of physical-biological interactions with a time step of one day.

CHAPTER 4

A Model of Physical-Biological Interactions in the Mixed Layer

4.1 Introduction

The analysis presented in Chapter 2 shows that changes in the attenuation of solar radiation in the mixed layer, produced by modulations in phytoplankton concentration, will affect the evolution of the layer depth and temperature. It is also well known that changes in the layer depth regulate the accumulation of phytoplankton biomass in the mixed layer (Sverdrup, 1953; Platt *et al.*, 1991). Together, these two processes constitute a physical-biological interaction that influences the evolution of mixed layer and phytoplankton biomass in the ocean (Platt *et al.*, 1994; Sathyendranath and Platt, 1994).

Figure 4.1 provides additional insight into the nature of this interaction. In Panel (a) of the figure, the daily, depth-integrated, net production of phytoplankton biomass in the mixed layer is plotted as a function of the layer depth, following the Platt *et al.* (1991) model (see Section 4.2). The net production is calculated as the difference between the gross production of phytoplankton and the loss of phytoplankton, which are also plotted in the panel as functions of the layer depth. We see that the gross production increases with increasing layer depth when the mixed layer is relatively shallow but becomes constant for deeper layers. The loss of biomass shows a quasi-linear increase with increasing layer depth. Consequently, the net production shows an initial increase at small values of the mixed-layer depth, followed by a gradual decrease at larger values of the layer depth. The broken

FIGURE 4.1. Physical-biological interactions in the mixed layer associated with phytoplanktor variability: In Panel (a), the daily, depth-integrated, net production of phytoplankton biomass in the mixed layer are plotted as functions of the layer depth, following the Platt *et al.* (1991) model. The net production is calculated as the difference between the gross production of phytoplankton and the loss of phytoplankton, which are also plotted in the panel as functions of the layer depth. The broken line indicates the layer depth within which the net production is zero, defined by Sverdrup (1953) as the critical depth. Given the mixed-layer depth, the daily change in the mean attenuation coefficient of the mixed layer, resulting from daily changes in depth-averaged phytoplankton biomass in the mixed layer, is shown in Panel (b) as a percentage of the mean attenuation coefficient at the end of the day. Similarly, Panel (c) shows a measure of the change in the stratifying tendency resulting from phytoplankton-induced changes in the attenuation of solar radiation in the mixed layer. In this panel the change in f_{h_m} (see equation (2.33)) is plotted as a function of the layer depth.

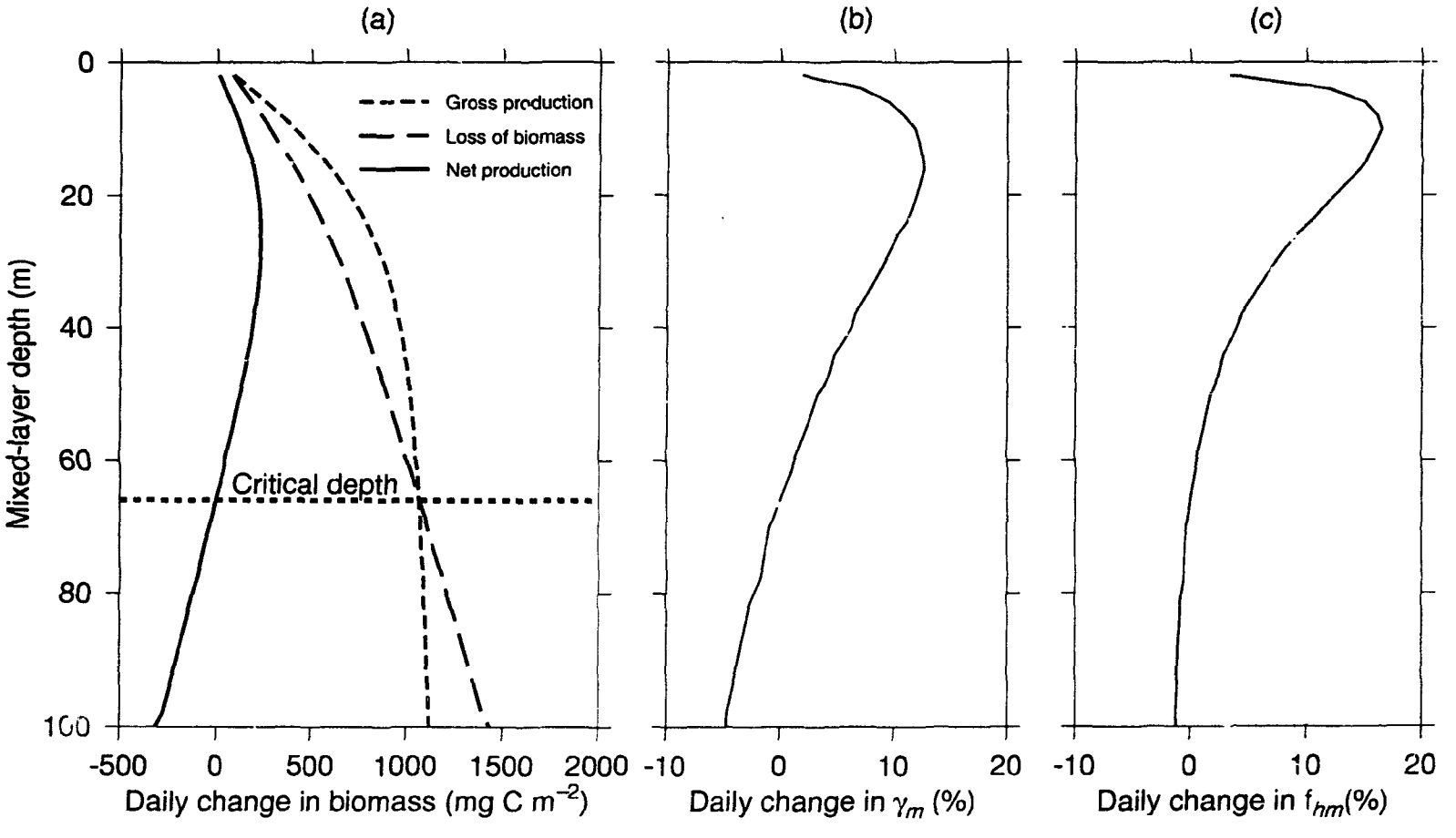
(a)
(b)
(c)
Gross production
Loss of biomass
Net production
Critical depth
Mixed-layer depth (m)
0
20
40
60
80
100
-500
0
500
1000
1500
2000
Daily change in biomass (mg C m^{-2})
-10
0
10
20
Daily change in γ_m (%)
-10
0
10
20
Daily change in f_{hm}(%)

Figure 4.1

horizontal line indicates the layer depth within which the net production is zero, defined by Sverdrup (1953) as the critical depth. When the depth of the mixed layer is less than the critical depth, net growth and accumulation of phytoplankton in the mixed layer is possible. This dependence of net production of phytoplankton biomass in the mixed layer on the depth of the layer is one component of the physical-biological interaction that is the central theme of this chapter.

The response of mixed-layer physics to changes in the phytoplankton concentration in the mixed layer is the second component of the interaction that is considered in this study. This response is caused by the fact that the evolution of the mixed-layer depth depends on the attenuation of solar radiation in the mixed layer which, in turn, depends on the phytoplankton concentration. Given the mixed layer depth, the daily change in the mean attenuation coefficient of the mixed-layer, resulting from daily changes in depth-integrated phytoplankton biomass in the mixed layer, is shown in Panel (b) of Figure 4.1 as a percentage of the mean attenuation coefficient. Modifications to the attenuation of solar radiation in the ocean will change the depth-distribution of solar radiation and therefore the tendency for stratification within the layer. The evolution of the mixed-layer depth during the subsequent time step will be affected by the change in the stratifying tendency of the layer. Panel (c) of the figure shows a measure of the change in the stratifying tendency resulting from phytoplankton-induced optical variability. In this panel the change in f_{h_m} (see equation (2.31)) is plotted as a function of the layer depth. The dependence of f_{h_m} on phytoplankton concentration in the layer is accounted for by specifying the attenuation coefficient of the mixed layer as a function of the biomass using the spectral-irradiance model of under-water light transmission (see Section 2.4). This panel shows that the net production of biomass in the mixed layer (shown in the Panel (a) of the figure) can account for more than 15% of variations in f_{h_m}. Thus, changes in f_{h_m} may significantly modify the layer depth. As suggested by Panel (a), such changes will further modify the net production in the layer, establishing

a feedback loop between the evolution of mixed-layer depth, evolution of the mean attenuation coefficient of the layer and the phytoplankton biomass in the layer.

The depth of the mixed layer determines the vertical extent over which the solar energy absorbed by the mixed layer is being distributed and therefore the layer temperature. The mixed-layer temperature affects the exchange of heat across the ocean-atmosphere interface. The heat exchange, in turn, affects the subsequent evolution of the layer depth and temperature. Thus, as suggested in Chapter 2, physical-biological interactions in the mixed layer might modify the feedback between the air-sea heat exchange and mixed-layer thermodynamics. This is the third component of the interaction considered in this chapter. A schematic representation of the physical-biological interactions associated with the evolution of mixed-layer biology, mixed-layer physics and air-sea heat exchange is shown in Figure 4.2.

To examine the nature of such feedback loops, a numerical analysis of the interactions between physical and biological processes in the ocean-atmosphere system is presented. This analysis is carried out using an oceanic model coupled to an atmospheric model. The atmospheric component is used specifically to examine the contributions from physical-biological interactions to the air-sea heat exchange.

The chapter is divided into six sections. An overview of the coupled model used in the analysis is presented in Section 4.2 followed, in Section 4.3, by a general description of the physical-biological interactions in the ocean-atmosphere system based on the results of model simulations. The effects of air-sea heat exchange on the physical-biological interactions in the mixed layer are examined in Section 4.4 and the implications of the results for modelling of upper ocean processes are addressed in Section 4.5. Some concluding remarks are presented in Section 4.6.

FIGURE 4.2. A schematic representation of the physical-biological interactions associated with the evolution of mixed-layer biology, mixed-layer physics and air-sea heat exchange. The evolution of mixed-layer depth influences the evolution of phytoplankton biomass in the layer, which in turn, modifies the attenuation of solar radiation in the ocean and therefore the mixed-layer physics. Evolution of the layer temperature will modify the heat exchange and the air temperature, which will influence the evolution of the mixed layer during the subsequent time step.

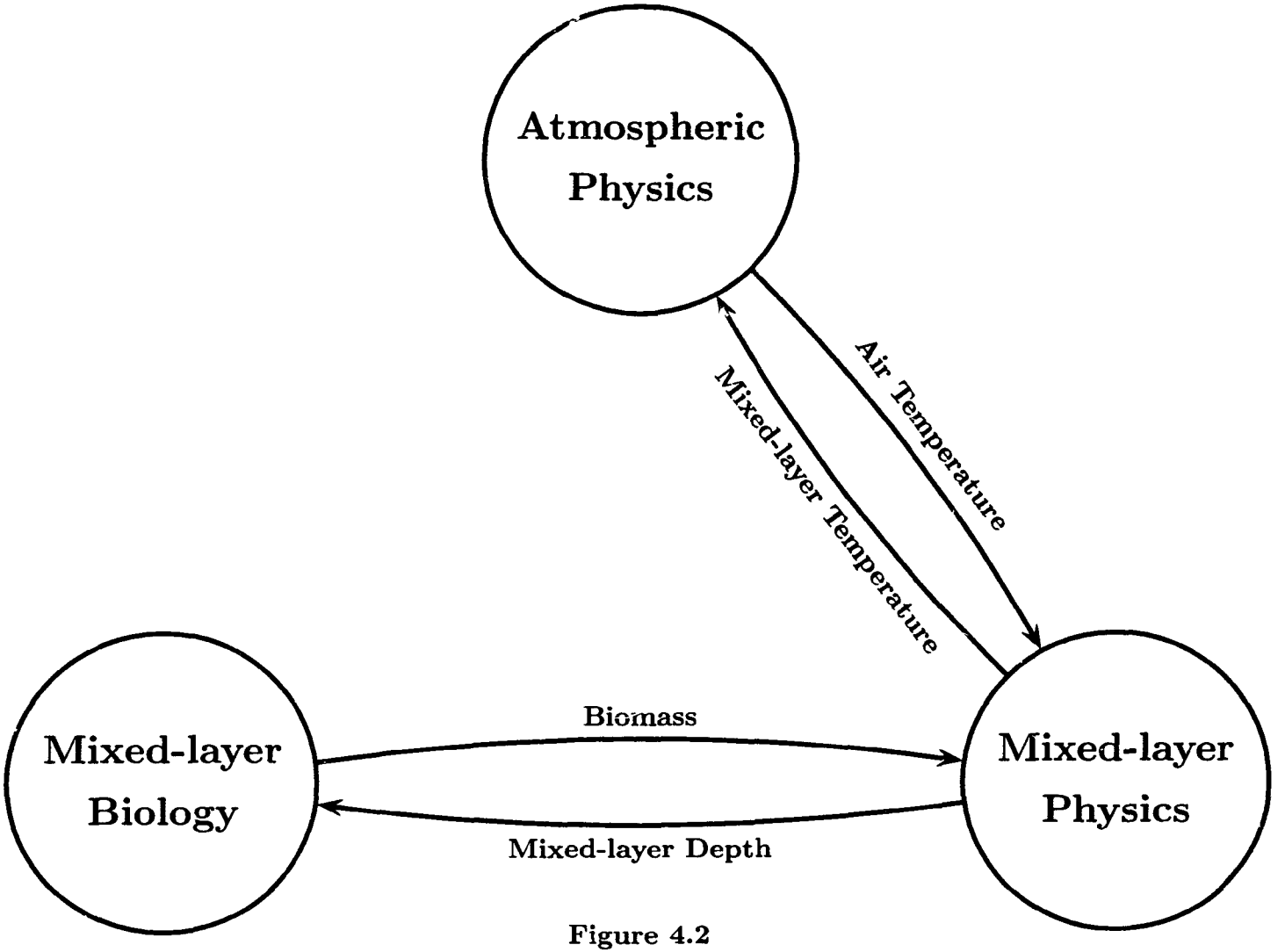
Atmospheric Physics
Air Temperature
Mixed-layer Temperature
Mixed-layer Biology
Biomass
Mixed-layer Physics
Mixed-layer Depth

Figure 4.2

4.2 A Coupled Model of Physical-Biological Interactions in the Mixed Layer

To simulate the interactions between physical and biological processes in the mixed layer in the presence of air-sea heat exchange, a coupled model is developed. In this model, the evolution of the mixed-layer is simulated by the general bulk model developed in Chapter 3, the biological processes are described by the Platt *et al.* (1991) model of the net production of organic material in the mixed layer by phytoplankton, and the heat exchange between the ocean and the atmosphere is incorporated using an energy-balance atmospheric model (Stocker *et al.*, 1992). All three components of the coupled model use a daily (24 h) time step. The evolution of mixed-layer depth, under the influence of seasonally-modulated solar radiation is the physical factor in the model that modifies the biological processes. Through its effect on the attenuation of solar radiation in the water column, variability in the biomass field is the biological factor that contributes to the evolution of mixed-layer depth, temperature and the heat exchange between the ocean and the atmosphere. The coupling between the ocean and the atmosphere depends on the air-sea heat exchange. Structural details of the atmospheric and biological components of the model are presented below.

4.2.1 The Atmospheric Component

The seasonal evolution of the surface layer of the ocean is strongly affected by the heat exchange between the ocean and the atmosphere. Therefore, a complete description of physical-biological interactions in the mixed layer should take this exchange into account. In this study it is described by a one-dimensional adaptation of the energy-balance model of the atmosphere as used by Stocker *et al.* (1992). The model parameters are selected to represent the mean state of the atmosphere

rather than its time-dependent behaviour: solar radiation is the only independent variable that is allowed to vary with season. The model is one dimensional, and the effects of horizontal advection of properties are therefore neglected.

The change in the air temperature, ΔT_a, during a time interval Δt is

$$\Delta T_a = \frac{\Delta t}{\rho_a C_a h_a}(H(-h_a) - H(0)), \tag{4.1}$$

where ρ_a is the air density, C_a is the specific heat capacity of the dry air, h_a is the height of the model atmosphere $H(0)$ is the net heat flux across the sea surface, and $H(-h_a)$ is the net heat flux across the top of the atmosphere, equal to the difference between the incoming solar radiation, $R(-h_a)$, and the outgoing longwave radiation $L(-h_a)$. That is,

$$H(-h_a) = R(-h_a) - L(-h_a). \tag{4.2}$$

The present model deviates from the Stocker *et al.* (1992) model in its specification of the solar radiation. In the absence of clouds, the daily solar radiation at the top of the atmosphere, $R(-h_a)$, is

$$R(-h_a) = \frac{2d}{\pi} R^m(-h_a). \tag{4.3}$$

In equation (4.3), $R^m(-h_o)$ is the daily-maximum value of the extra-terrestrial solar radiation as given by (Iqbal, 1983)

$$R^m(-h_a) = R_s(\sin\beta \sin\psi + \cos\beta \cos\psi), \tag{4.4}$$

where

$$R_s = 1367 \ \mathrm{Wm}^{-2} \tag{4.5}$$

is the solar constant (Foukal and Lean, 1990),

$$\beta = 0.006918 - 0.399912\cos\Gamma + 0.070257\sin\Gamma - 0.006758\cos(2\Gamma) +$$

$$0.000907\sin(2\Gamma) - 0.002697\cos(3\Gamma) + 0.00148\sin(3\Gamma) \tag{4.6}$$

is the solar declination (Paltridge and Platt, 1976), Γ is a function of the day number J defined as: $\Gamma = 2\pi(J-1)/365$, and d is the day length (i.e. the period during which the solar radiation is non-zero) in hours, calculated as a function of the latitude ψ and the solar declination β using the equation (Kirk, 1983),

$$d = 0.133(180/\pi)\cos^{-1}(\tan\psi\tan\beta). \tag{4.7}$$

Note that equation (4.3) is derived by assuming a sinusoidal distribution of solar radiation with time t between the dawn ($t = 0$) and the dusk ($t = d$)

$$R(-h_a, t) = R^m(-h_a)\sin\Big(\frac{\pi t}{d}\Big), \quad \text{for} \quad 0 \le t \le d$$

and

$$R(-h_a, t) = 0 \qquad \text{for} \quad d < t. \tag{4.8}$$

The back radiation to outer space is

$$L(-h_a) = \sigma e_p T_a^4, \tag{4.9}$$

where σ is the Stefan-Boltzmann constant and e_p is the planetary emissivity.

The total solar radiation at the sea surface ($R(0)$) is

$$R(0) = (1-\kappa)R(-h_a), \tag{4.10}$$

which is subdivided into the penetrative component $I(0)$ and the non-penetrative component $\hat{I}(0)$. In equation (4.10) κ is the absorptivity of shortwave radiation in the atmosphere. Here, it is assumed that $I(0)$ accounts for 50% of $R(0)$.

The net heat flux across the ocean-atmosphere interface, $H(0)$, is the sum of a penetrative component $I(0)$ and a non-penetrative component $Q(0)$. As in previous chapters, the non-penetrative component $Q(0)$ is given by:

$$Q(0) = \hat{I}(0) + S(0) + E(0) + L(0). \tag{4.11}$$

The sign convention used for $Q(0)$, $S(0)$, $E(0)$ and $L(0)$ is that these quantities are positive when the heat transfer is from the atmosphere to the ocean. The net longwave radiation at the sea surface $L(0)$ is parameterized by

$$L(0) = \sigma e_a T_a^4 - \sigma e_o T_m^4, \tag{4.12}$$

where e_o and e_a are the emissivity of the ocean and the downwelling emissivity of the atmosphere respectively. The sensible heat flux across the ocean-atmosphere interface is parameterized by

$$S(0) = \zeta(T_a - T_m), \tag{4.13}$$

ζ being the transfer coefficient of sensible heat. The latent heat flux is estimated as a function of the mixed-layer temperature and the air temperature using the Haney (1971) parameterization scheme

$$E(0) = -c_E e^{(14.7-5418/T_a)}\left\{0.2 + 5418\frac{T_m - T_a}{T_o^2}\right\}, \tag{4.14}$$

where c_E is a local bulk coefficient for evaporation. In reality, c_E and ζ depend on factors such as wind speed and atmospheric stability. Here we take both c_E and ζ to be constants.

Note that the effect of buoyancy fluxes associated with net air-sea exchange of moisture is not considered here. However, the air-sea heat exchange associated with locally-balanced evaporation and precipitation is accounted for. The numerical values of the atmospheric-model parameters used in this section are given in Table 4.1.

4.2.2 The Biological Component

The biological component of the model is intended to simulate the seasonal evolution of phytoplankton biomass in the mixed layer. The change in the phytoplankton biomass in the layer is calculated as the difference between the production

Table 4.1 Numerical values of parameters used in the model simulation. Values of κ, ρ_a, σ, ζ, C_a, C_E, e_a, e_o, e_p and h_a are taken from Stocker *et al.* (1992).

Parameters	Value	Units
α	1.3×10^{-4}	$^{\circ}C^{-1}$
α^B	0.11	mg C h^{-1}(W m^{-2})$^{-1}$(mg Chl)$^{-1}$
χ	30	Dimensionless
$\hbar$	1.0	m
κ	0.2857	Dimensionless
ψ	+50	°Latitude
ρ_a	1.225	Kg m^{-3}
ρ_w	1026.0	Kg m^{-3}
σ	5.67×10^{-8}	W m^{-2} K^{-4}
ζ	10	W m^{-2} $^{\circ}C^{-1}$
C_a	1004	J kg^{-1} $^{\circ}C^{-1}$
C_d	0.0013	Dimensionless
C_p	4000	J kg^{-1} $^{\circ}C^{-1}$
C_E	5×10^4	W m^{-2}
e_a	0.78	Dimensionless
e_o	0.96	Dimensionless
e_p	0.63	Dimensionless
g	9.8	m s^{-2}
h_a	8320	m
K_m	0.05	mmol N m^{-3}
P_m^B	3	mg C (mg Chl-a)$^{-1}$ h^{-1}
R_0^B	0.09	mg C (mg Chl-a)$^{-1}$ h^{-1}
R_D	0.15	Dimensionless
R_L	0.15	Dimensionless
R_s	1367	W m^{-2}

of biomass by photosynthesis and the loss of biomass through respiration, sedimentation, excretion and zooplankton grazing. In the mixed layer, the phytoplankton distribution is depth-independent. The water column below the mixed layer is assumed to be biologically inactive, with a constant phytoplankton concentration of 0.01 mg chl-a m^{-3}. Because the phytoplankton production and loss below the mixed layer are not taken into account this assumption may result in the underestimation of the biomass entering the mixed layer during the deepening phase.

The change in depth-averaged phytoplankton biomass (ΔB) in the mixed layer during a 24 hour period is modelled by

$$\Delta B = \frac{1}{\chi h_m}\left[P_{h_m,d} - l_{h_m,24}\right]. \tag{4.15}$$

Here, χ is the carbon-chlorophyll ratio, $P_{h_m,d}$ is the daily (integrated over the day length) total production of organic carbon by phytoplankton photosynthesis in the mixed layer and $l_{h_m,24}$ is the total loss of organic carbon from the phytoplankton community from the layer during a 24h period. Procedures for calculating $P_{h_m,d}$ and $l_{h_m,24}$ are described below.

a) The gross production of organic carbon by phytoplankton in the mixed layer

The daily primary production in the mixed layer can be expressed as (Platt *et al.*, 1990; Platt *et al.*, 1991)

$$P_{h_m,d} = B \cdot P_m^B \int_0^d \int_0^{h_m} \left[1 - e^{-\alpha^B I^m(0)\sin(\pi t/d)e^{-\gamma_m z}/P_m^B}\right] dz dt. \tag{4.16}$$

In the above equation P_m^B is the biomass-specific maximum photosynthetic rate (mg C (mg chl-a)$^{-1}$ h^{-1}), B is the phytoplankton biomass (mg chl-a m^{-3}), and α^B is the biomass-specific initial slope of the photosynthesis-irradiance curve (mg C h^{-1} (W

$m^{-2})^{-1}$ (mg chl-a)$^{-1}$). The superscript B represents normalization with respect to biomass. Also, $I^m(0)$ is the daily maximum (noon) value of the penetrative component of solar radiation at the sea surface. The attenuation coefficient γ_m is assumed to be depth-independent. Note the difference between α^B used in this section and the α (coefficient of thermal expansion) used in the previous chapter.

An analytical expression for the daily gross primary production in the mixed layer can be obtained by evaluating the integrals in equation (4.16) (Platt *et al.*, 1990, Platt *et al*, 1991; Platt and Sathyendranath, 1993) giving

$$P_{h_m,d} = \frac{2A}{\pi} \sum_{n=1}^{\infty} \frac{(I_*^m)^{2n-1}(1 - M^{2n-1})(2n-2)!!}{(2n-1)(2n-1)!(2n-1)!!}$$

$$A \sum_{n=1}^{\infty} \frac{(I_*^m)^{2n}(1 - M^{2n})(2n-1)!!}{2n(2n)!(2n)!!}, \tag{4.17}$$

where

$$A = \frac{P_m^B B d}{\gamma_m} \tag{4.18}$$

is the scale factor determining the magnitude of production (mg C m^{-2}),

$$I_*^m = \frac{\alpha^B I^m(0)}{P_m^B} \tag{4.19}$$

is the dimensionless form of daily-maximum (noon) solar radiation at the sea-surface, and

$$M = e^{-\gamma_m h_m} \tag{4.20}$$

is the optical transmittance for the layer.

b) The loss of organic carbon from the mixed layer

The loss of phytoplankton biomass from the mixed layer during a 24 hour period is represented following Platt *et al.* (1991). According to this scheme, the

daily loss of phytoplankton biomass from the mixed layer ($l_{h_m,24}$) can be expressed as

$$l_{h_m,24} = 24 h_m B l_T^B, \tag{4.21}$$

where l_T^B is the generalized, biomass-specific, loss rate of phytoplankton from the layer, averaged over a day and over the layer depth, given by

$$l_T^B = l_R^B + l_E^B + l_G^B + l_S^B. \tag{4.22}$$

In the above equation, l_R^B is the loss rate of phytoplankton resulting from respiration, l_E^B is the excretion rate of phytoplankton, l_G^B is the zooplankton grazing rate and l_S^B is the loss rate of phytoplankton resulting from sedimentation. In equation (4.22) all these terms have units of mg C (mg chl-a)$^{-1}$ h^{-1}.

Assuming that the biomass-specific dark respiration depends on the growth rate in the light, the loss of organic material from the mixed layer resulting from respiration is

$$l_R^B = R_0^B + (R_D + R_L)\frac{P_{h_m,d}}{24 B h_m}. \tag{4.23}$$

Here, $R_0^B = 0.09$ mg C (mg chl-a)$^{-1}$ h^{-1} represents respiration in the absence of growth, R_D is a nondimensional coefficient representing the change in the dark respiration of phytoplankton per unit change in growth rate, and R_L is a nondimensional coefficient representing the increase in respiration of phytoplankton in the presence of light. Numerical values of R_D and R_L are chosen to be 0.15.

Based on the conventional view that about 5% of the organic carbon produced by phytoplankton is lost through excretion (Platt *et al.*, 1991), l_E^B is parameterized by

$$l_E^B = 0.05\frac{P_{h_m,d}}{24 B h_m}. \tag{4.24}$$

The biomass-specific zooplankton grazing rate, l_G^B, is determined by

$$l_G^B = \frac{0.25\chi}{24}. \tag{4.25}$$

The implied removal of 25% of the phytoplankton standing stock per day by grazing is consistent with the conclusions in recent reviews of the significance of grazing in the pelagic ecosystem (eg. Banse, 1992).

The loss of biomass through sedimentation is parameterized by

$$l_S^B = \frac{\chi \hbar}{24 h_m}. \tag{4.26}$$

Here, $\hbar$ is the depth over which a phytoplankton cell sinks during one day. I have used $\hbar = 1$ m, which is suitable for describing the sedimentation of diatoms (Smayda, 1970; Platt *et al.*, 1991).

c) Effect of nutrient limitation

The general procedure used to account for the effect of nutrient limitation on phytoplankton growth rate is similar to that used by Wroblewski (1976), Fasham *et al.* (1990) and Taylor *et al.* (1991). It is assumed that dissolved nitrogen is the limiting nutrient, without considering the specific forms of nitrogen available. The daily primary production in the mixed layer in the presence of nutrient limitation, $P^N_{h_m,d}$, is estimated by scaling the corresponding quantity in the absence of nutrient limitation ($P_{h_m,d}$) with a Michaelis-Menten function:

$$P^N_{h_m,d} = \frac{N_m}{K_m + N_m} P_{h_m,d}. \tag{4.27}$$

In equation (4.27), N_m is the dissolved nitrogen concentration in the mixed layer and K_m is the half saturation constant for nitrogen uptake. I have specified K_m as 0.05 mmol N m^{-3}, which is consistent with the recommendation of Harrison *et al.* (1996).

Implementation of equation (4.27) requires information on the dissolved nitrogen concentration, N_m, in the mixed layer. It is calculated from the nitrogen

budget of the mixed layer as described below, ensuring that runaway growth of phytoplankton cannot occur and that the conservation of mass is not violated. Two further checks on the phytoplankton model are that the nitrogen content of the total biomass produced at any given time step cannot exceed the dissolved nitrogen available in the layer during that time step, and that the nitrogen content of the total biomass produced in the mixed layer during the model simulation should not exceed the sum of the initial dissolved nitrogen content of the mixed layer and the net input of dissolved nitrogen through various processes considered by the model.

d) Parameterization of the Nutrient Budget

The dissolved-nitrogen content of the mixed layer at the end of a time step can be written as the sum of the initial, dissolved, nitrogen content and the change in the dissolved, nitrogen content during the time step. That is,

$$h_m^+ N_m^+ = h_m\Big(N_m + \Delta N_m\Big) + \Phi h_e\Big(N_e + \Delta N_e\Big). \tag{4.28}$$

In equation (4.28), the concentrations of dissolved nitrogen in the mixed layer and in the entrainment layer are denoted by N_m and N_e, respectively. The superscript '+' is used to denote the conditions at the end of the time step and Φ is the Heaviside step function defined by equation (2.3) and (2.4) as $\Phi = 1$ for a deepening mixed layer and $\Phi = 0$ for a shallowing mixed layer. Also, the changes in the dissolved nitrogen concentration in the mixed layer and in the entrainment layer are denoted by ΔN_m and ΔN_e, respectively.

In the mixed layer, primary production by phytoplankton decreases the concentration of dissolved nitrogen, whereas respiration and excretion increase the concentration through conversion of particulate nitrogen into dissolved form. The change in the dissolved nitrogen content of the mixed layer is calculated as,

$$\Delta N_m = \frac{1}{h_m}\frac{1}{12}\frac{16}{106}24h_m Bl_R^B + \frac{1}{h_m}\frac{1}{12}\frac{16}{106}24h_m Bl_E^B -$$

$$\frac{1}{h_m}\frac{1}{12}\frac{16}{106}P_{h_m,d}. \tag{4.29}$$

Because it is assumed that the water column below the mixed layer is biologically inactive we have,

$$h_e \Delta N_e = 0. \tag{4.30}$$

Therefore,

$$h_m^+ N_m^+ = h_m N_m + \Phi h_e N_e + \frac{1}{12}\frac{16}{106}24 h_m B l_R^B + \frac{1}{12}\frac{16}{106}24 h_m B l_E^B - \frac{1}{12}\frac{16}{106}P_{h_m,d}. \tag{4.31}$$

It is assumed that the nitrogen produced by respiration and excretion is readily available as a substrate for primary production.

The average nitrogen concentration in the entrained water during the deepening phase of mixed layer evolution, N_e, is calculated from the vertical profile of nitrogen, $N(z)$, using the equation

$$N_e = \frac{1}{h_e}\int_{h_m}^{h_m^+} N(z)dz. \tag{4.32}$$

4.3 A General Description of Physical-Biological Interactions in the Ocean-Atmosphere System

Even though several models have been developed in the past to describe the seasonal evolution of phytoplankton in the ocean, such models seldom consider the feedback from phytoplankton to the evolution of the mixed-layer physics. Simonot *et al.* (1988) and Antoine and Morel (1995) are examples of exceptions to this general trend. The model developed in this chapter is similar to the models of Simonot *et al.* (1988) and Antoine and Morel (1995) in that it accounts for physical-biological interactions resulting from the feedback from phytoplankton variability to mixed-layer evolution. However, it differs significantly from them in the specification of

the air-sea heat exchange. This is because the models of Simonot *et al.* (1988) and Antoine and Morel (1995) calculate air-sea heat fluxes as a function of the prescribed air temperature whereas, in the present study, the surface heat flux components are calculated using an atmospheric model. Note that incorporation of the atmospheric component makes it possible in the present study to examine the effect of air-sea heat exchange on the physical-biological interactions in the mixed layer, an aspect that has not been considered before.

After specifying the initial conditions (see Table 4.2), the model is integrated for a simulated period of 720 days starting from January 1^{st}. The specific values of the model parameters used are given in Table 4.1. The wind field is held constant during the model simulation and therefore seasonal change in the solar-radiation is the only variable external forcing responsible for the cycle of mixed-layer depth and of the biological fields within the layer. As in the previous chapters, the TKE input from wind is determined, following Denman (1973), by $(G - D) = 0.0012\rho_a C_d U^3$. The forcing field of solar radiation is calculated for 50°N latitude. The seasonal evolution of the day length d, and the daily-averaged values of the total solar radiation at the top of the atmosphere, $R(-h_a)$, are shown in Figure 4.3.

Figure 4.4 shows the relative errors in the heat content of the model atmosphere, the model ocean and the coupled model of the ocean-atmosphere system as a function of the day number. The relative error in each panel shows the daily change in the heat content of the respective medium that is not accounted for by the model calculations as a percentage of the total heat content of that medium at the end of the day. The figure shows that the coupled model accurately accounts for the heat exchanges within the ocean-atmosphere system.

The evolution of the mixed-layer depth during a 720-day simulation of the coupled model of the ocean and the atmosphere in the absence of biological feedback is shown in Figure 4.5. The figure shows that, in the early stages of the evolution, the layer depth is influenced by the initial depth of the mixed layer. Therefore,

Table 4.2 The initial conditions used in the model simulation.

Variable	Value	Units
h_m	250	m
T_m	4.5	°C
T_a	4.5	°C
T_b	4.0	°C
a	0.0385	Kg m^{-4}
B	0.01	mg Chl-a m^{-3}
U	8.0	m s^{-1}

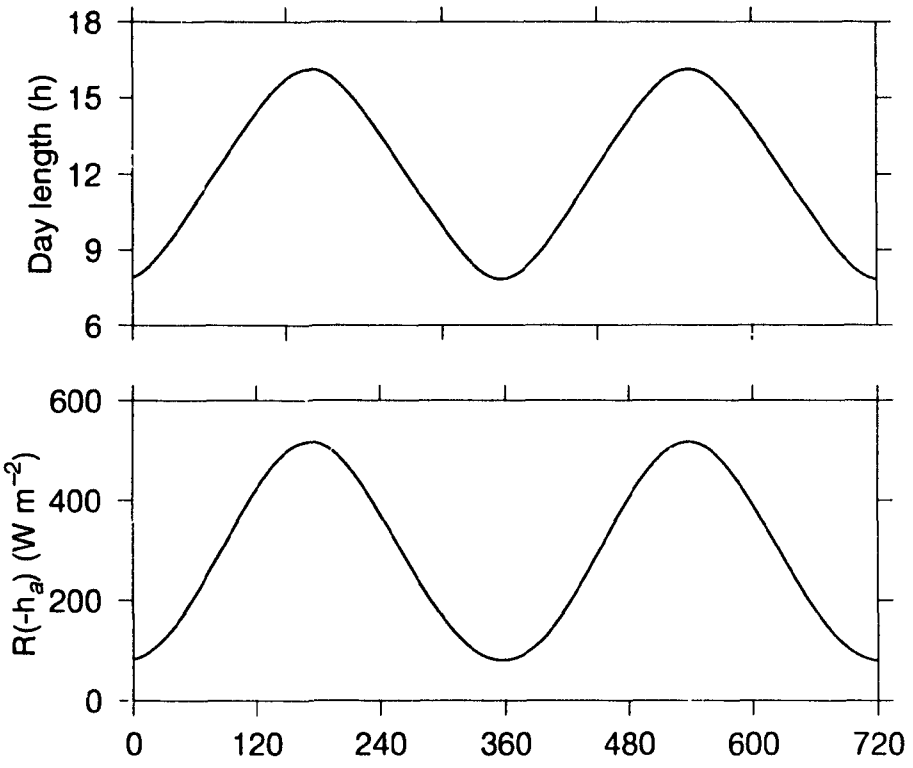

FIGURE 4.3. The seasonal evolution of the day length and the total solar radiation at the top of the atmosphere. These are the independent variables responsible for the evolution of physical and biological processes in the model ocean and the atmosphere.

FIGURE 4.4. Relative errors in the heat content of the model atmosphere, the model ocean and the coupled model of the ocean-atmosphere system as functions of the day number: The relative error in each panel shows the daily change in the heat content of the respective medium that is not accounted for by the model calculations, as a percentage of the total heat content of the medium at the end of the day. The daily change in the heat content is calculated as the difference between the heat content at the end of the day and the sum of the initial heat content and the change in the heat content resulting from net heat input. Zero relative error would indicate perfect heat conservation in the model.

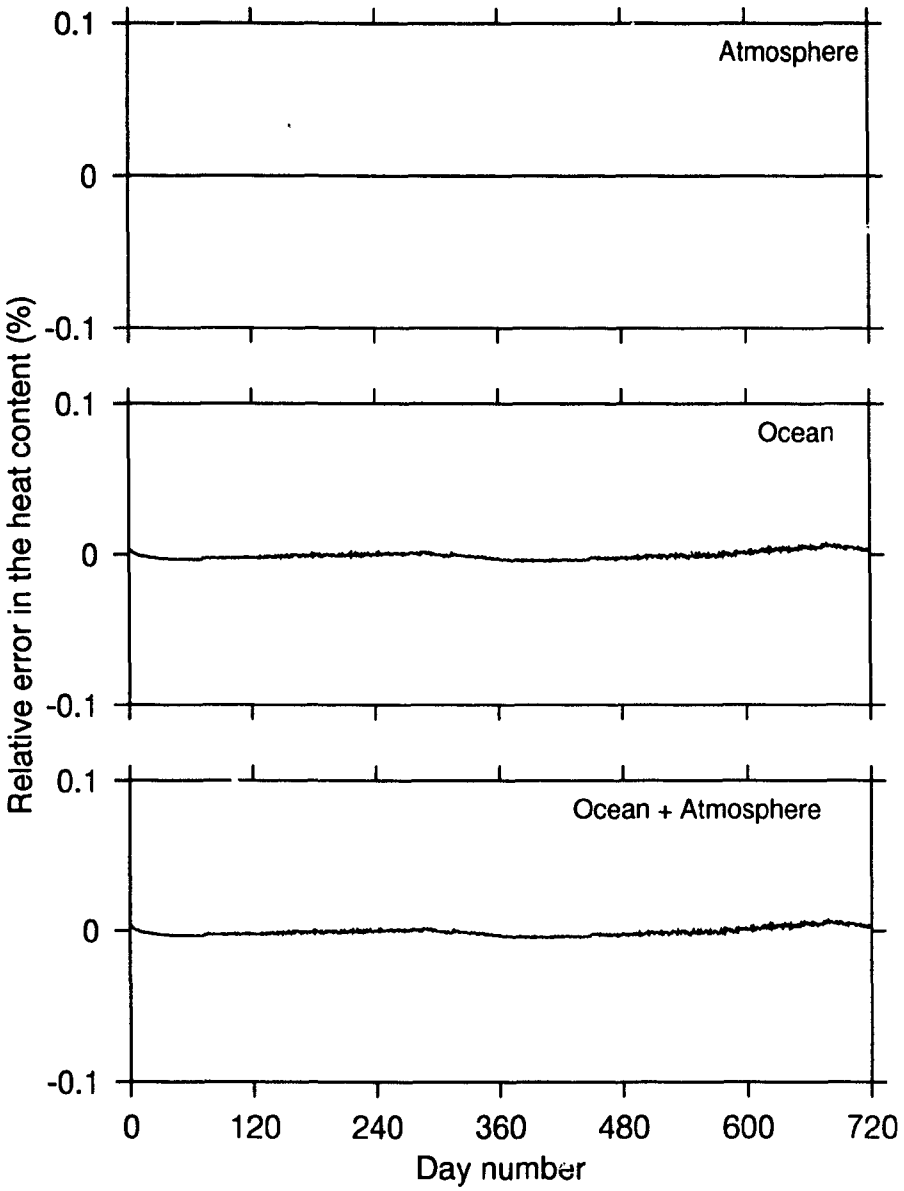
0.1
0
-0.1
Atmosphere
0.1
0
-0.1
Ocean
0.1
0
-0.1
Ocean + Atmosphere
Relative error in the heat content (%)
0
120
240
360
480
600
720
Day number

Figure 4.4

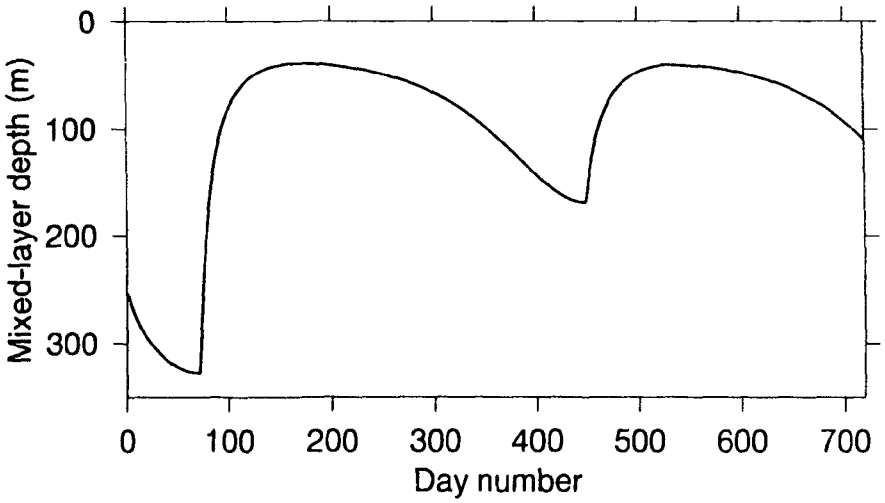

FIGURE 4.5. The evolution of mixed-layer depth during a 720-day simulation of the coupled model of the ocean and the atmosphere in the absence of biological feedback.

to minimize the dependence of the model results on the arbitrarily-specified initial conditions, I have used the hydrographic conditions that prevailed at the end of the first seasonal cycle (day 365) as the initial conditions for all other model simulations throughout the rest of this chapter.

Nitrogen limitation depresses phytoplankton growth and therefore affects the net production of biomass in the mixed layer by altering the balance between the gross production and loss of biomass. Changes in the net production, in turn, affect the biological feedback to the mixed-layer physics by modifying the attenuation coefficient of the layer. To examine the effect of nitrogen limitation on the evolution of the model variables, I have compared the results of three simulations. In the first simulation, the daily primary production in the mixed layer is estimated using equation (4.17). In the second and third simulations the effect of nitrogen limitation is taken into account by using equation (4.27) and by assuming arbitrary initial nitrogen concentrations of 18 and 4 mmol N m^{-3}, respectively. The nitrogen concentration of 18 mmol N m^{-3} is selected to represent the nitrate concentration in the North Atlantic during the winter (Takahashi *et al.*, 1993).

The seasonal evolution of phytoplankton biomass associated with these experiments is shown in Figure 4.6. In the absence of nitrogen limitation, the time series of biomass (Panel (a)) shows a single bloom with maximum biomass of about 25 mg chl-a m^{-3}. In the presence of nitrogen limitation the time series (Panels (b) and (c)) shows a rapid increase in the biomass associated with the shallowing mixed layer, followed by a sharp decline resulting from nutrient depletion, and a secondary maximum caused by the input of nitrogen through entrainment and regeneration. These are typical features of the seasonal evolution of biomass in mid-latitude seas (Heinrich, 1962). In other words, this simple model reproduces the principal features of the seasonal evolution of phytoplankton biomass in the mid-latitude oceans. Seasonal evolution of mixed-layer depth, mixed-layer temperature, air temperature

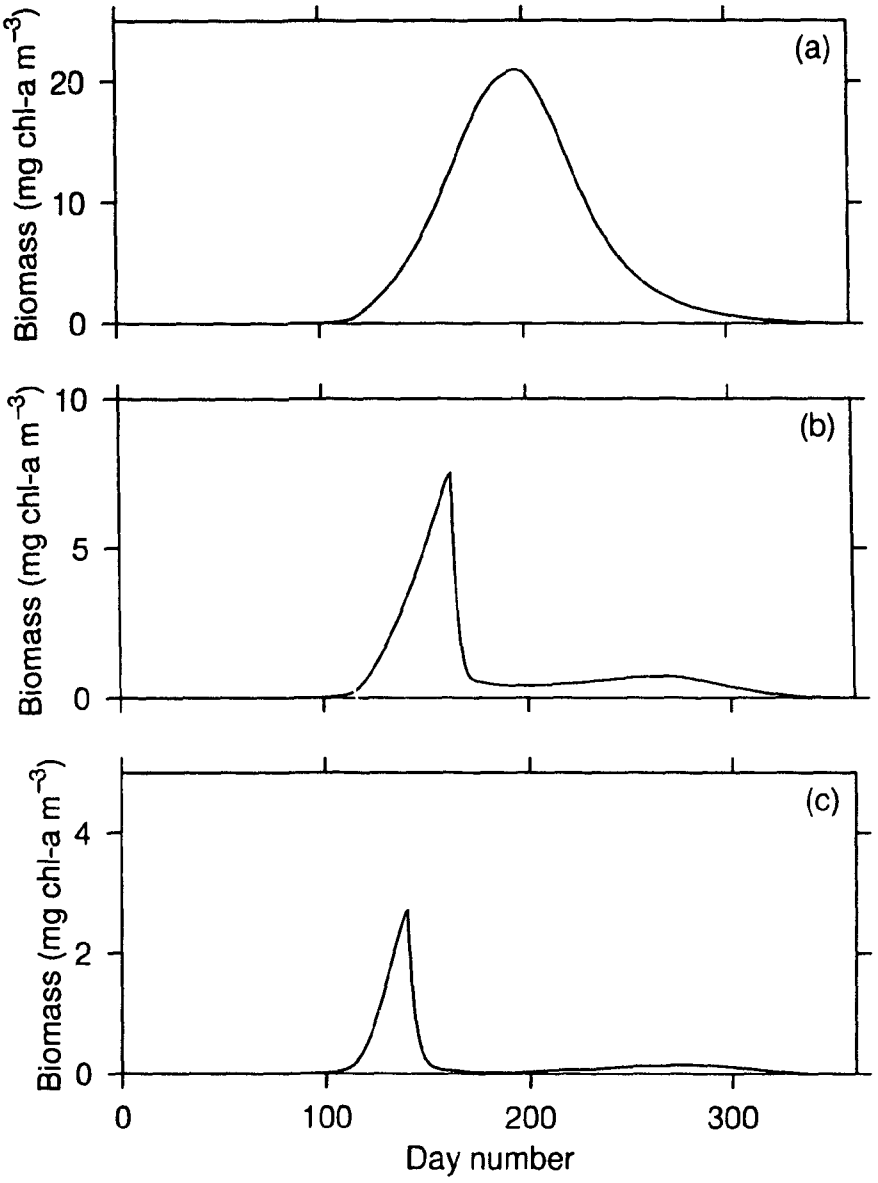

FIGURE 4.6. The seasonal evolution of phytoplankton biomass. The upper Panel (a) shows the time series of biomass in the absence of nutrient limitation. Panels (b) and (c) show the time series in the presence of nutrient limitation, when initial nutrient concentrations of 18 and 4 mmol N m^{-3} are assumed, respectively. Note the change in scale between the panels.

and the non-penetrative heat flux corresponding to the three cases of biomass evolution given in Figure 4.6 is shown in Figure 4.7 by the solid and broken curves respectively. Corresponding results from a reference ocean are also shown in the figure as dotted curves. The reference ocean is chosen to be the model ocean in the absence of biological feedback, characterized by a constant biomass concentration of 0.01 mg chl-a m^3.

Figure 4.7 also shows the seasonal evolution of mixed-layer depth, mixed-layer temperature, air temperature and heat flux across the sea surface, when the effect of nutrient limitation is taken into account (broken curves). The lower bounds of these variables are given by corresponding values from the reference ocean (dotted curves). Similarly the upper bounds of these variables are given by corresponding values from the nutrient-unlimited ocean (solid curves). Thus, the range of variability in the model variables in the presence of nutrient limitation is a subset of the range of variability in the model variables in a nutrient-unlimited ocean. Therefore, for simplicity, I have neglected the effect of nutrient limitation throughout the rest of this chapter. Note that this maximizes the biological influence in all the results presented here in the sense that the results are representative of a nutrient-unlimited ocean.

Under the forcing conditions upon which Figure 4.6(a) is based, the peak biomass attained, $\approx$ 22 mg chl-a m^{-3}, is not atypical of the biomass observed during phytoplankton blooms. If we take the daily difference in the time series of air temperature, surface heat flux, mixed-layer depth and temperature developed under this forcing with the corresponding time series that would be observed under the same forcing but with a constant biomass of 0.01 mg chl-a m^{-3} we have an indication of the scope of variation in the physical fields that can be attributed to the feedback from pelagic ecology as plotted in Figure 4.8. The figure shows that The time-dependent biomass field can account for about 30 meters difference in the mixed-layer depth, about 5°C difference in the mixed-layer and air temperature

FIGURE 4.7. The evolution of mixed-layer depth, mixed-layer temperature, air temperature and surface heat flux corresponding to the time series of biomass shown in figure 4.6. The solid curves in each of these panels represent the evolution of the respective fields in the absence of nutrient limitation. The dashed curves represent the evolution in nutrient limited oceans with initial nitrogen concentrations of 18 and 4 mmol m^{-3}, respectively. The initial nitrogen concentration of 18 mmol m^{-3} is selected to represent the nitrate concentration in the North Atlantic during the winter. The dotted curves represent corresponding values for a reference ocean. The reference ocean is chosen to be the model ocean in the absence of biological feedback, characterized by a constant biomass concentration of 0.01 mg chl-a m^{-3}.

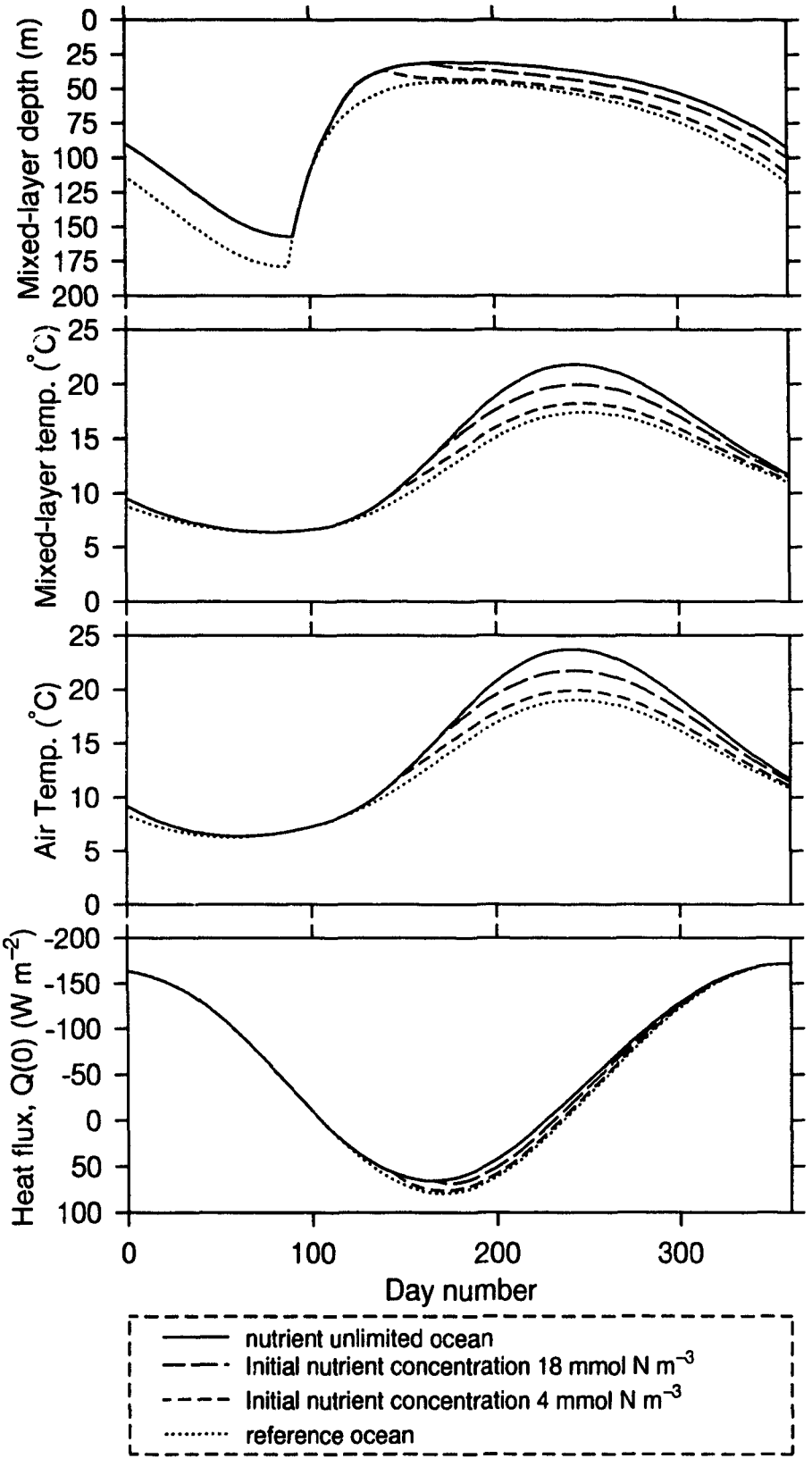
Mixed-layer depth (m)
0
25
50
75
100
125
150
175
200
Mixed-layer temp. (°C)
25
20
15
10
5
0
Air Temp. (°C)
25
20
15
10
5
0
Heat flux, Q(0) (W m^{-2})
-200
-150
-100
-50
0
50
100
0
100
200
300
Day number
nutrient unlimited ocean
Initial nutrient concentration 18 mmol N m^{-3}
Initial nutrient concentration 4 mmol N m^{-3}
reference ocean

Figure 4.7

and about 15 W m^{-2} difference in the non-penetrative heat flux across the sea surface. The differences in the layer depth and temperature are caused by the direct effect of phytoplankton variability on the solar heating of the mixed layer. The air temperature and the heat flux across the sea surface are sensitive to phytoplankton variability as these variables are functions of the mixed-layer temperature and air-sea temperature difference. Note that these results correspond to the model ocean that is assumed to be nutrient unlimited.

The sensitivity of the mixed-layer temperature to changes in the phytoplankton concentration shown in the figure is consistent with the results of the sensitivity analysis reported by Martin (1985). He examined the sensitivity of mixed-layer temperature predicted by several mixed-layer models at stations Papa and November to changes in the optical properties of the water column. Table 3 of Martin (1985) shows that when the optical water type is changed from type I to type III of the Jerlov (1976) classification scheme (roughly corresponding to an increase in attenuation coefficient of 0.138 m^{-1} at $\lambda = 425$ nm, according to Table XXVII of Jerlov (1976)), the maximum, monthly-mean layer temperature at station November increased by 2.9 to 6.2 °C depending upon the mixed-layer model. The same experiment carried out with data collected from station Papa shows changes between 1.0 and 1.2 °C in the layer temperature.

The consequence of any further increase in the phytoplankton concentration in the mixed layer, with respect to Figure 4.6(a), on the physical-biological interactions is examined next. The time series of biomass obtained by reducing the grazing rate by 8% (from 25% to 23% of the daily phytoplankton standing stock) is given in Figure 4.9, which shows more than a 100% increase in the peak biomass with respect to that shown in Figure 4.6(a). The high sensitivity of the biomass in the mixed layer to small changes in the grazing rate is due to the fact that the rate of accumulation of biomass in the mixed-layer depends on the biomass available for primary production at the beginning of the day. A decrease in the grazing rate

FIGURE 4.8. The differences in mixed-layer depth, mixed-layer temperature, air-temperature and surface heat flux between the reference ocean (constant phytoplankton concentration of 0.01 mg chl-a m^{-3}) and the model ocean characterized by the phytoplankton concentrations show in Figure 4.6(a).

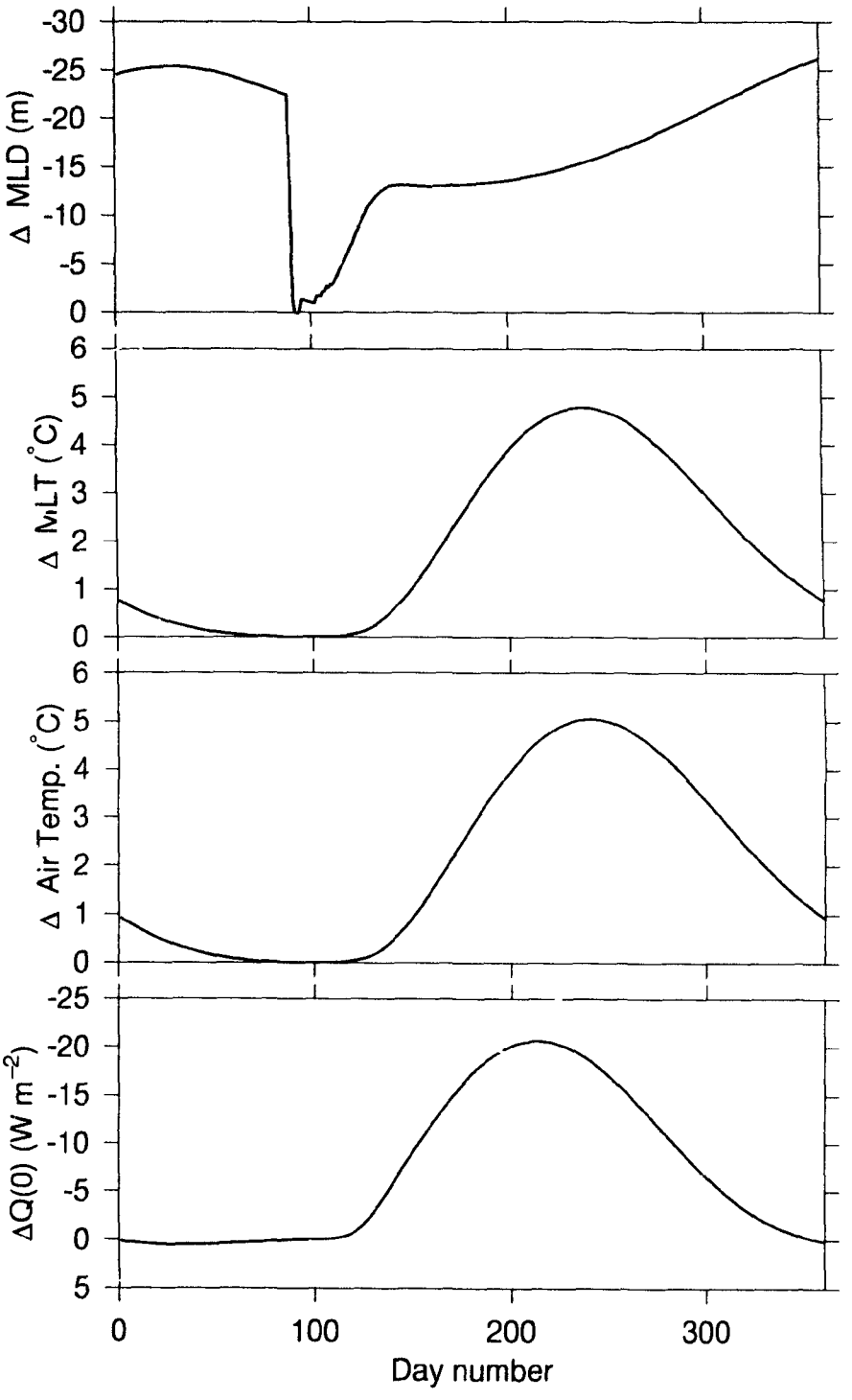
Δ MLD (m)
-30
-25
-20
-15
-10
-5
0
Δ MLT (°C)
6
5
4
3
2
1
0
Δ Air Temp. (°C)
6
5
4
3
2
1
0
ΔQ(0) (W m⁻²)
-25
-20
-15
-10
-5
0
5
0
100
200
300
Day number

Figure 4.8

retains more biomass in the mixed layer. Further, the higher peak biomass ($\approx$ 50 mg chl-a m^{-3}) in Figure 4.9 takes longer to accumulate than the lower one ($\approx$ 22 mg chl-a m^{-3}) in Figure 4.6(a). Similarly, in the model simulation corresponding to Figure 4.6(a), the maximum daily rate of biomass production, 0.412 mg chl-a m^{-3}, was reached on day 167, whereas in the simulation corresponding to Figure 4.9, the maximum daily rate, 1.12 mg chl-a m^{-3}, was reached on day 187.

The mixed-layer depth, mixed-layer temperature, air temperature and the non-penetrative heat flux corresponding to the two cases of phytoplankton evolution considered in Figure 4.6(a) and 4.9 are shown in Figure 4.10. It shows that, even though the amplitude of two time series of biomass differ significantly from each other, the time series of physical variables are identical. These results re-affirm that the sensitivity of physical processes to phytoplankton variability is not a linear function of phytoplankton biomass. Rather, at high values of phytoplankton biomass, further increase in biomass has no effect.

This point is further illustrated in Figure 4.11 where I have plotted the maximum values of mixed-layer depth, mixed-layer temperature, air temperature and the surface heat flux for different rates of net production (obtained by varying the grazing rate between 23 and 95% of the daily phytoplankton standing stock) as a function of the maximum phytoplankton biomass during the simulation. This figure shows that when the biomass is low, the maximum values of the physical variables considered increases sharply with increasing biomass. However, as the biomass increases above about 10 mg chl-a m^{-3}, the maximum values tend to saturate. These results are consistent with the results of the analysis presented in Chapter 2. Figure 2.3 shows that the function f_{h_m} increases with increasing phytoplankton concentration at low values of biomass. However, for higher values of biomass, the sensitivity decreases in such a way that eventually f_{h_m} tends to become insensitive to further changes in the biomass. As the amount of solar radiation penetrating the base of

the mixed layer becomes negligibly small, the mixed-layer temperature also becomes insensitive to further increase in the biomass.

The wind has been held constant in these simulations. But we can speculate on the consequence of fluctuations in the wind speed for conditions in the mixed layer. The vertical mixing associated with wind bursts causes the mixed layer to deepen and thus decreases the growth rate (Platt *et al.,* 1991). Also, if the biomass below the mixed layer is low, such a deepening results in a decrease in phytoplankton concentration in the mixed layer. The intensity of a bloom depends on the initial biomass and on the rate of increase in biomass (Platt *et al.,* 1991). Therefore, changes in the frequency of wind bursts affect the accumulation of biomass in the mixed layer. However, Figures 4.7 and 4.10 indicate that the effect of changes in the phytoplankton biomass in the mixed layer on the evolution of the layer depth and temperature is a function of the biomass itself. That is, when the biomass in the mixed-layer is very high, a given change in biomass may have no significant effect on mixed-layer depth and temperature. On the other hand, when the mixed layer is relatively transparent, a change of the same magnitude in phytoplankton concentration can have a significant impact on the evolution of the layer depth and temperature.

The principal results of this study, in so far as they concern the air temperature, surface heat flux and the depth and temperature of the mixed-layer, are sensitive to the biomass itself, rather than to the particular combinations of model parameters that prescribe it. The physical model of the mixed layer feels the effect of the biological model only through the biomass it produces. It has no memory of, and no information on, the parameter set that underlies the time series of biomass. In other words, to ensure that the model reproduces realistic characteristics of the seasonal evolution of biological processes in the mixed layer, the biological parameters used in the simulation must also be realistic. However, the evolution of mixed-layer

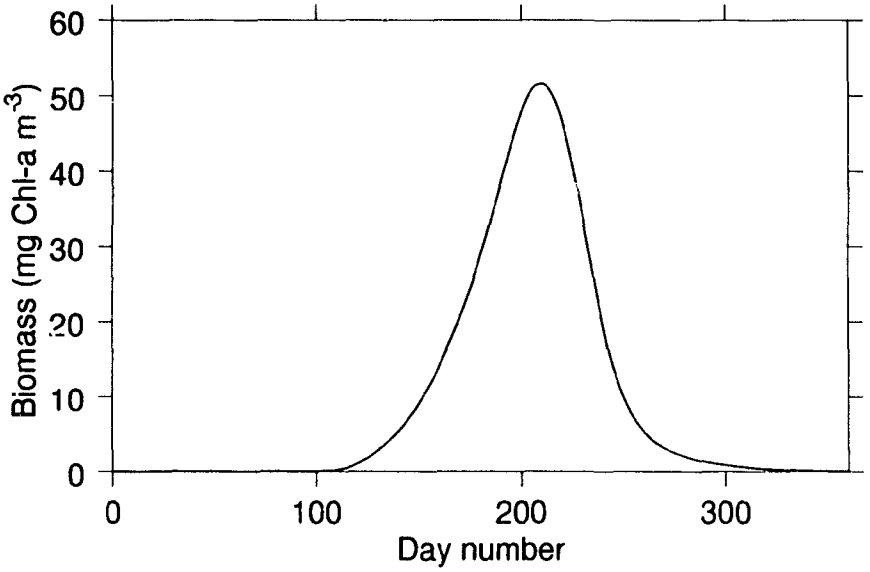

FIGURE 4.9. The time series of biomass used as an example of an intense phytoplankton bloom. Compared with the time series shown in Figure 4.6(a), this figure shows more than 100% increase in the peak phytoplankton concentration.

FIGURE 4.10. A comparison of mixed-layer depth, mixed-layer temperature, air-temperature and surface heat flux between model oceans characterized by the biomass distributions shown in Figure 4.6(a) (solid curves) and Figure 4.9 (broken curves).

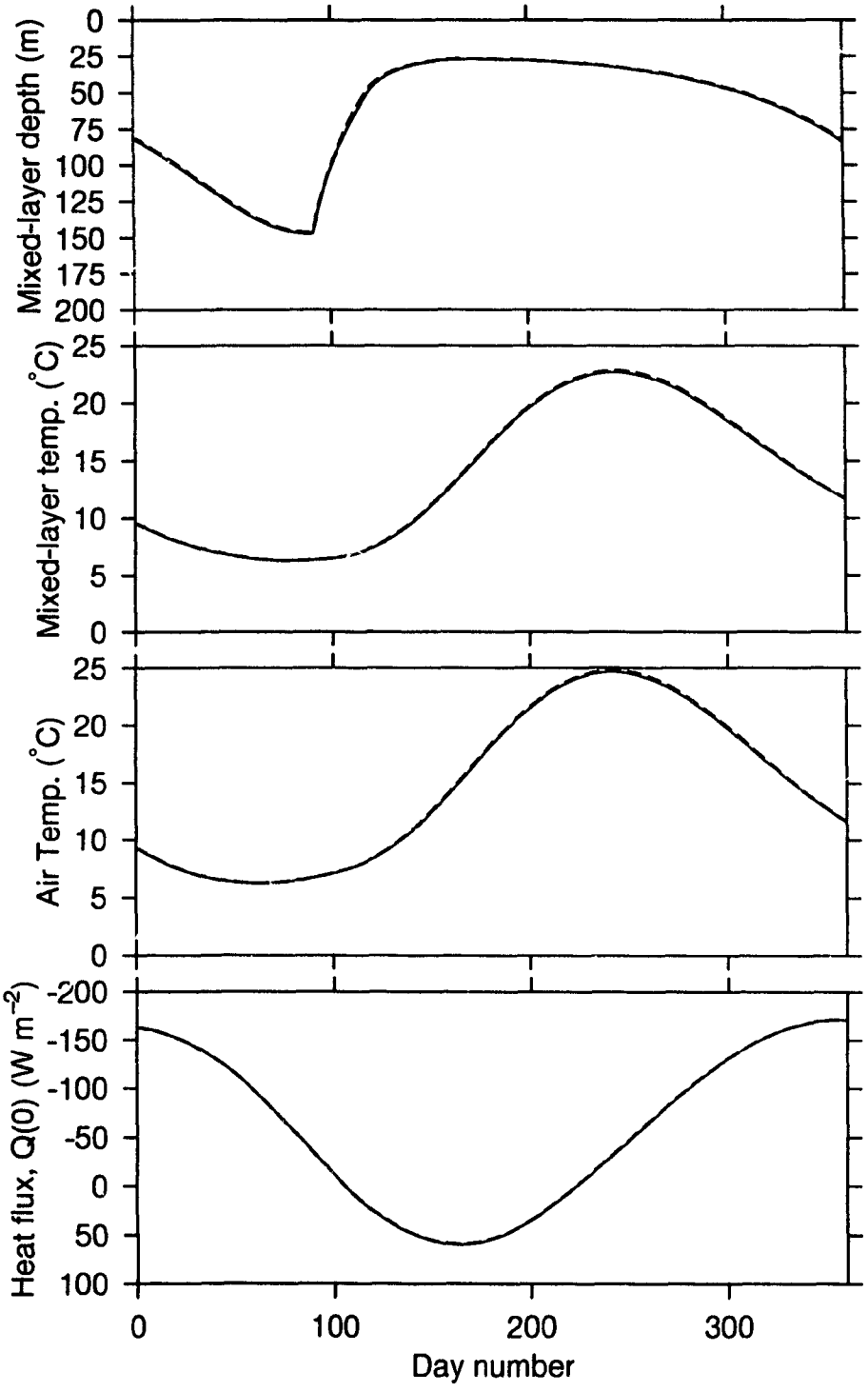
Mixed-layer depth (m)
0
25
50
75
100
125
150
175
200
Mixed-layer temp. (°C)
25
20
15
10
5
0
Air Temp. (°C)
25
20
15
10
5
0
Heat flux, Q(0) (W m^{-2})
-200
-150
-100
-50
0
50
100
0
100
200
300
Day number

Figure 4.10

FIGURE 4.11. The maximum values of mixed-layer depth, mixed-layer temperature, air-temperature and the heat flux across the sea surface are plotted as functions of the maximum biomass encountered during the simulation to illustrate the effect of increasing biomass on the evolution of the physical variables in the model. The experiments are analogous to those corresponding to Figures 4.6 (a) and 4.9 and the maximum biomass is controlled by varying the grazing rate.

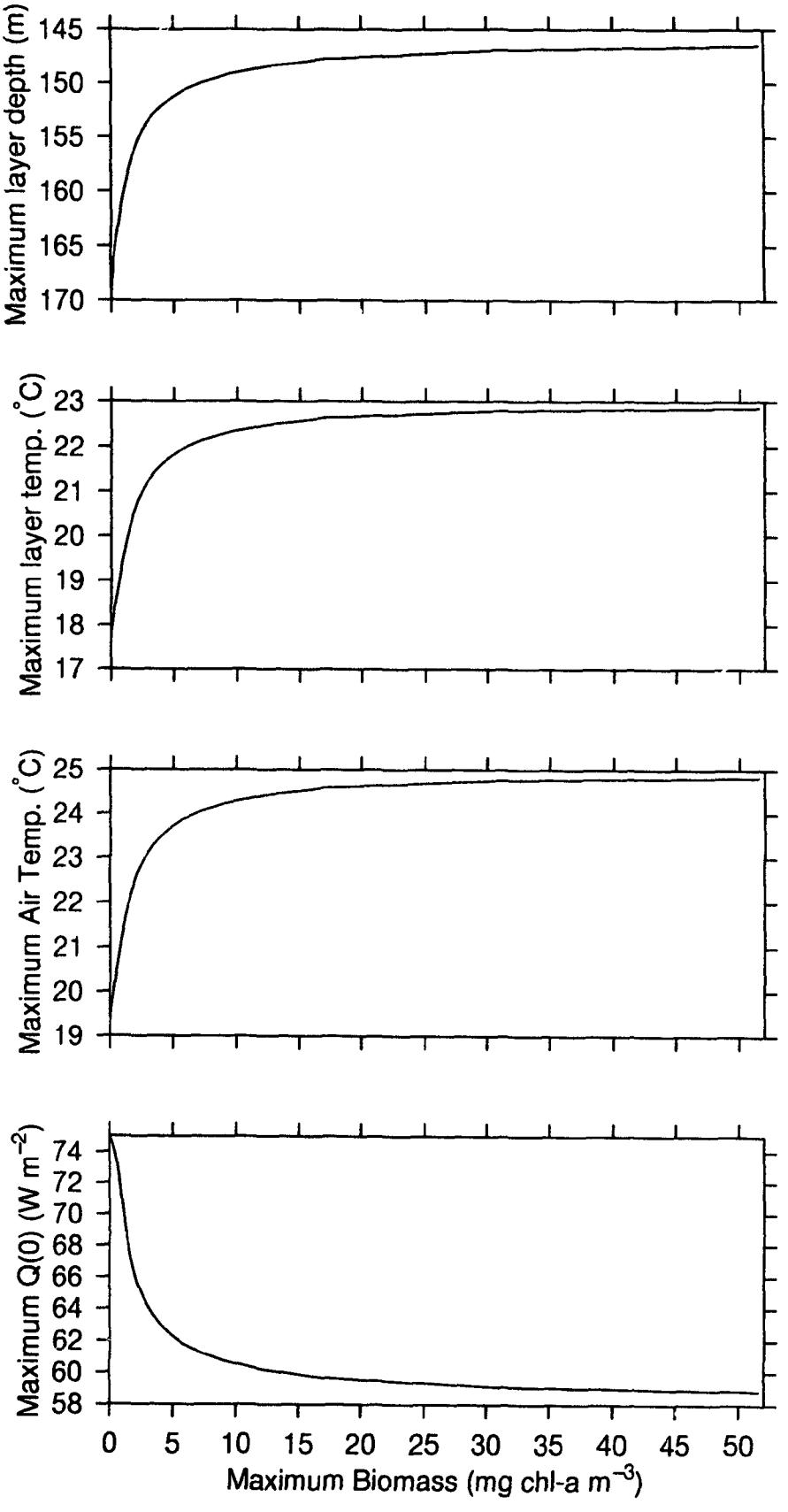
Maximum layer depth (m)
145
150
155
160
165
170
Maximum layer temp. (°C)
23
22
21
20
19
18
17
Maximum Air Temp. (°C)
25
24
23
22
21
20
19
Maximum Q(0) (W m-2)
74
72
70
68
66
64
62
60
58
0
5
10
15
20
25
30
35
40
45
50
Maximum Biomass (mg chl-a m-3)

Figure 4.11

physics and atmospheric physics is sensitive only to the phytoplankton biomass, irrespective of whether the biological parameters used are realistic or not.

To examine the sensitivity of the mixed-layer physics and the atmospheric physics to the choice of biological parameters let us consider the parameterization of sedimentation in the model as an example. Throughout the model simulation, following Smayda (1970), the rate of sinking of phytoplankton is taken as 1 meter per day. However, it is known that the rate of sinking of phytoplankton varies with season and can reach values as high as 100 - 150 meters per day (Lampitt, 1985). An increase in the sinking rate (say to 100 meters per day) will decrease the rate of accumulation of phytoplankton in the mixed layer. Thus, the seasonal changes in the sinking rate of phytoplankton will cause modulations in the phytoplankton growth rate in the mixed layer. The limiting case of a decrease in growth rate is that the biomass concentration in the mixed layer will remain at its initial value of 0.01 mg chl-a m^{-3} throughout the model simulation. On the other hand, if the rate of sedimentation is very low, phytoplankton biomass may accumulate in the mixed layer. But, Figures 4.10 and 4.11 show that when the phytoplankton concentration in the mixed layer increases beyond a certain limit, the evolution of mixed-layer physics and atmospheric physics would become insensitive to further changes in the biomass. Under the initial conditions and the forcing considered in this study, the effects of modulations in phytoplankton biomass on mixed-layer physics and atmospheric physics are bounded. The upper bound is given by the seasonal evolution of properties in a nutrient-unlimited ocean, characterized by very high concentration of phytoplankton, and the lower bound by their evolution in a reference ocean, which is practically free of phytoplankton. These two cases are shown by the solid and dotted curves in Figure 4.7.

Hence we can be confident that, provided our simulation covers the full range of biomass trajectories that might be encountered in the ocean, we are able to describe the full scope of the effect of feedback from pelagic biology to mixed-layer

physics. We need not be afraid that the entire argument depends on a fortuitous combination of parameters used in the biological model.

The effect of biological feedback on the evolution of mixed-layer physics and atmospheric physics shown in Figure 4.8 should be considered as an upper limit of the effect with respect to the given set of initial conditions and the forcing used in the model simulations, for the following reasons.

The specific heat of air, C_a, used in the model simulation (1004 J Kg^{-1} $°C^{-1}$) corresponds to that of dry air (Wallace and Hobbs, 1977). The heat capacity of moist air is greater than that of dry air, and the temperature of moist air is therefore less sensitive to changes in the mixed-layer temperature than that of dry air. Through a model simulation, I have examined the potential reduction in the response of air temperature, resulting from increased moisture content of the atmosphere, to the increased mixed-layer temperature associated with phytoplankton growth. In this simulation, following Gill (1982), C_a is specified as $C_a = 1004.6(1 + 0.837v)$ J Kg^{-1} $°C^{-1}$, where v is the relative humidity of the atmosphere. The effect of water vapor in the atmosphere in reducing the heating of the air by the sea will be maximal when $v = 1$, corresponding to an atmosphere saturated with respect to its moisture content. When v was so specified at this extreme value, the model simulation showed that the contribution from biological variability to the seasonal evolution of of air temperature depicted in Figure 4.8 would be reduced by up to 1°C. This is a significant reduction, but it is not enough to nullify the increment ($\approx$ 5°C) calculated as an upper bound to the effect of phytoplankton variability on the seasonal evolution of air temperature, under the specific initial conditions and forcing used in the model simulation.

Another reason to use caution when interpreting the results of the present study is that the effects of biological feedback are shown in Figure 4.8 as the changes in the model variables between two extreme cases of the nutrient-unlimited ocean, one

characterized by high phytoplankton biomass and the other, reference ocean that is relatively free of phytoplankton. Consequently, the effect of biological variability on the physics of the ocean and the atmosphere estimated as the contrast between these two extreme simulations should be considered as an upper limit demonstrating the full range of the effect of seasonal variability in phytoplankton biomass in the ocean, under the specific initial conditions and forcing used for the model simulations.

Figure 4.8 shows the cumulative effect of biological feedback over several months, when the mixed-layer physics and biology evolved in the absence of modifications by seasonal changes in the surface currents or the atmospheric forcing. In reality, however, the evolution of mixed-layer physics and biology is frequently modified by events such as the passage of storms and horizontal advection that may deepen the mixed-layer and dilute, at least temporarily, the phytoplankton assemblages contained therein.

The physical-biological interactions simulated in this chapter are based on a one-dimensional model that cannot account for the effect of horizontal advection of properties either in the ocean or in the atmosphere. The parameters used to model the atmospheric component of the coupled model are representative of the climatological mean state of the atmosphere. Therefore, the effect of seasonal variability in the thermodynamic characteristics of the atmosphere is not taken into account. Seasonal variability in the moisture content of the atmosphere modifies its radiative and thermodynamic characteristics. Increased moisture content of the atmosphere will result in a decrease in the amount of solar radiation entering the ocean, and therefore in the external energy available for driving the physical-biological interactions.

FIGURE 4.12. The effect of fixed $Q(0)$ on the model evolution. In this figure, the mixed-layer depth and temperature from four model simulations are plotted. The differences between the results from the fully-coupled model (labeled as '4') and the partially-coupled model, in the presence of a time-dependent phytoplankton distribution (labeled as '3') are measures of the opposing effect of the ocean-atmosphere interaction on the physical-biological interaction.

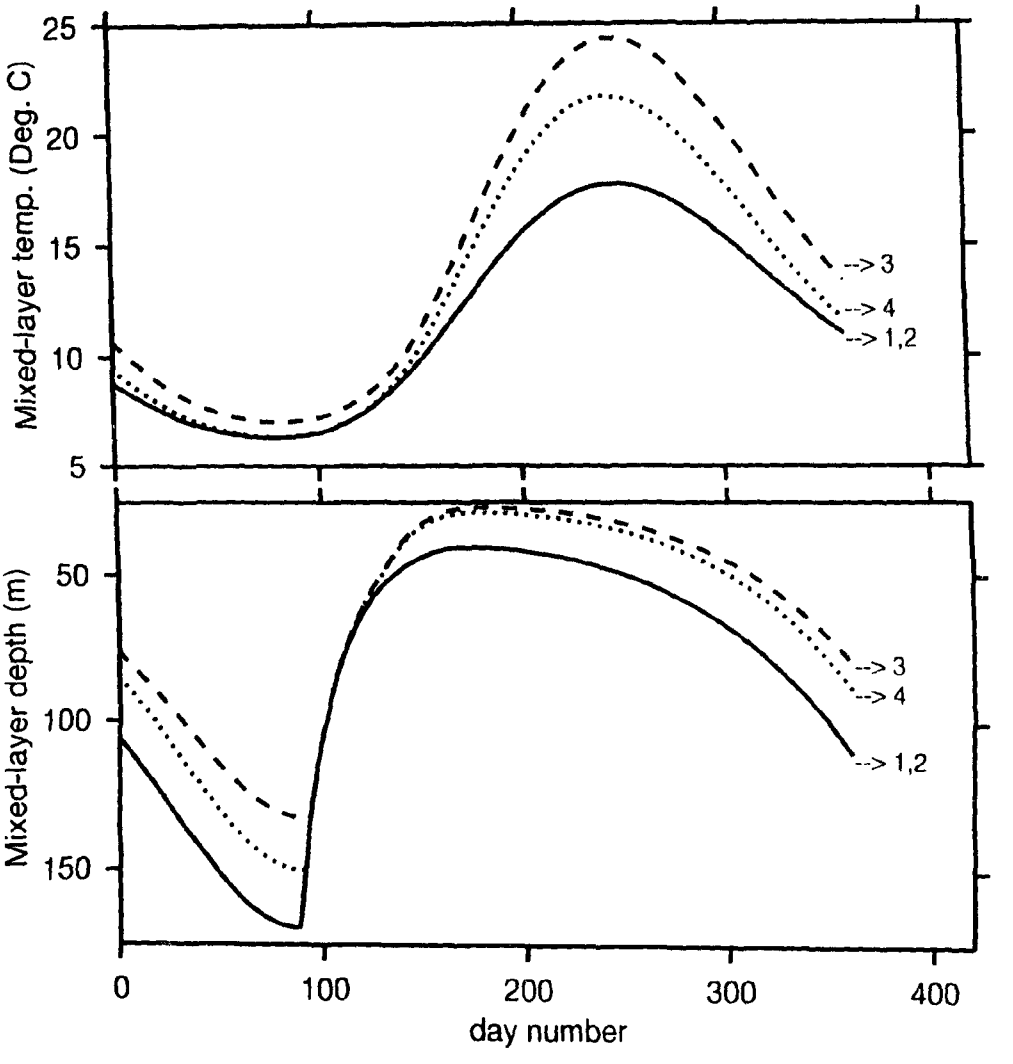

(1) Atmospheric feedback & No biological feedback
(2) Prescribed heat flux & No biological feedback
(3) Prescribed heat flux & Biological feedback
(4) Atmospheric feedback & Biological feedback

Figure 4.12

4.4 Effects of Air-Sea Heat Exchange

An increase in the attenuation coefficient of the mixed layer intensifies energy trapping in the upper ocean, shallows the mixed layer and increases its temperature. Because the air-sea heat exchange is a function of the mixed-layer temperature and the temperature difference across the air-sea interface, the heat exchange will also change. In this section, through a set of four model simulations, I examine how the modifications to air-sea heat exchange, in turn, affect the physical-biological interactions in the mixed layer. These simulations are designed to compare the contributions from biological feedback to the evolution of mixed-layer depth and temperature in the presence of free exchange of heat across the sea surface, with the layer depth and temperature that would prevail if free exchanges were prevented. Each one is a 365-day simulation with the same initial conditions and external forcing. The only differences between the simulations are those resulting from changes in the specifications of air-sea heat exchange and of biological feedback. All results correspond to situations in which nutrient availability is not a limiting factor.

In the first simulation, we calculate the mixed-layer depth and temperature in the absence of any feedback between ocean physics and ocean biology. The results are used as a benchmark for this series of simulations. Coupling between the physical and biological processes in the mixed layer is suppressed for this simulation; the phytoplankton concentration is held constant throughout the year as 0.01 mg chl-a m^{-3}. However, the ocean physics and the atmospheric physics are coupled by virtue of the free exchange of heat $Q(0)$ across the air-sea boundary. The time series of mixed-layer temperature and depth from this simulation are shown as curves labeled '1' in Figure 4.12. The time series of $Q(0)$ calculated during this simulation are used as input during the second and third simulations in the series.

In the second and third simulations, the free exchange of heat between the ocean and the atmosphere is suppressed. The heat exchange $Q(0)$ is prescribed,

rather than calculated directly, during each time step. In the second simulation, biological feedback is also suppressed, whereas in the third, it is allowed.

In the second simulation, $Q(0)$ is prescribed externally rather than calculated internally. It is prescribed according to the results of the first simulation. Also, as in the first simulation, biological feedback is suppressed. This experiment is included to confirm that we have correctly implemented the prescription of $Q(0)$. The results are shown in Figure 4.12 by curves labeled '2'. Not surprisingly, they are identical to those of the first simulation: the oceanic and atmospheric physics are the same in both cases. The prescribed values of $Q(0)$ convey information about the relevant physics. The way in which the model is implemented does not affect the results, provided that the physics does not change.

In the third simulation, $Q(0)$ is again prescribed rather than calculated at each time step. The prescription again follows the results of the first simulation. However, in this case, the physics will not be the same as in the first simulation because of the feedback from biology, which is now admitted. Note that the prescribed values of $Q(0)$ would not be consistent with the fully-coupled model including the biological feedback (see simulation 4). All of the increased input of solar energy into the mixed layer, as γ_m increases with season, is used to change the layer depth and its temperature. None is allowed to feedback to the atmosphere through a coupling between ocean physics and atmospheric physics. Note that in this case there is a genuine suppression of the expected modifications in air-sea heat exchange. The mixed-layer depth and temperature from this simulation are shown by curves labeled '3' in the Figure 4.12.

In the fourth and final simulation, all feedbacks are allowed to operate simultaneously. It is the most realistic of the four cases. Coupling between the ocean physics and biology determines the evolution of phytoplankton biomass and therefore of mixed-layer heating. Coupling between the oceanic and atmospheric physics

determines the value of $Q(0)$, which is calculated rather than prescribed, at each time step. The results of this simulation are shown in Figure 4.12 using the curves labeled '4'.

The results of this set of simulations can be used to describe characteristic features of the physical-biological interactions in general and the effect of air-sea heat exchange on it in particular. In the presence of a biological feedback, the mixed layer is shallower and warmer than it would be in the absence of feedback. In the presence of free heat exchange across the sea surface the effect of biological feedback on the layer temperature is less than it would be if the free heat exchange is suppressed using externally-prescribed values of $Q(0)$. This is because, in the presence of free heat exchange, some of the effect of biological feedback is lost to the atmosphere as heat flux. Figure 4.12 shows that the increase in the layer temperature and decrease in the layer depth associated with an increase in phytoplankton concentration is opposed by the air-sea heat exchange. It also shows that the air-sea heat exchange is not sufficient to neutralize the biological contribution to the mixed-layer physics. Otherwise, the first, the second and the fourth simulations would have produced identical time series of mixed-layer depth and temperature. Even though the air-sea flux will not be great enough to cancel the effect of biological feedback, it is nevertheless a significant effect and ought to be taken into account. Therefore, the accurate simulation of mixed-layer depth and temperature will require that the ocean-ecosystem model be coupled to an atmospheric model.

4.5 Implications for Mixed-Layer Modelling

The analyses presented in Section 4.4 have demonstrated that the biological processes in the ocean can initiate feedback mechanisms that influence the seasonal evolution of mixed-layer physics and air-sea heat exchange. In this section we

examine the implications of the biological feedback for the modelling and prediction of upper-ocean properties and the air-sea interaction processes.

In the past, coupled models of physical-biological interactions have been used to study the effect of phytoplankton variability on the evolution of sea-surface temperature (see for example, Simonot *et al.,* 1988; Stramska and Dickey, 1993). These models calculate the heat fluxes across the sea surface as a function of the temperature difference across the air-sea interface. With such a parameterization, the air-sea temperature difference is usually specified as the difference between the mixed-layer temperature predicted by the model and the air temperature as determined from time series observations at a station. The observed air temperature already contains information on the biological feedback that prevailed at the time of the observation. Hence, these models consider explicitly the interactions between mixed-layer physics and mixed-layer biology but treat implicitly the interactions between mixed-layer biology and atmospheric physics.

Models of upper-ocean thermal structure such as that of Martin (1985) and of Gaspar (1988), also use the air-sea temperature difference to calculate the surface heat flux components. These models generally assume a constant, time-independent attenuation coefficient for solar radiation in the mixed layer and therefore cannot account for the effect of biological feedback on the evolution of mixed layer depth and temperature. However, the observed air temperature used by these models to calculate the heat fluxes does carry implicit information about the effect of biological feedback, but no explicit information within the model formulation.

A third point of interest in the present analysis is the seasonal progression of mixed-layer depth and temperature predicted by coupled models of the ocean and the atmosphere, such as that of Davidson and Garwood (1984). These models assume a constant attenuation coefficient for the solar radiation and therefore do not take into account the effect of time-dependent biological feedback on the evolution

of mixed layer physics. Also, the air temperature is calculated from the heat budget of the atmosphere alone and therefore, contains no information about the biological feedback. Thus, such coupled models of the ocean and the atmosphere do not consider, either explicitly or implicitly, the effect of biological feedback.

Thus, there are four general approaches used for modelling the mixed-layer physics with respect to the incorporation of biological feedback. They are:

1 Explicit coupling of biological processes to the mixed-layer physics and explicit computation of the biological contribution to air-sea heat exchange (eg. the model developed in this chapter).

2 Explicit coupling of biological processes to the mixed-layer physics and implicit inclusion of the biological contributions to air-sea heat exchange (eg. Simonot *et al.*, 1988).

3 Implicit inclusion of the biological contribution to the air-sea interaction without consideration of coupling of biological processes to mixed-layer physics (eg. Martin, 1985, Gaspar, 1988).

4 Neglect of the coupling of biological processes to the mixed-layer physics and of the biological contributions to air-sea heat exchange (eg. Davidson and Garwood, 1984).

In the remainder of this section we will examine, through model simulations, the differences in the mixed-layer depth and temperature that would be predicted using each of these four approaches. The procedure followed is similar to that used in Section 4.4, in that the mixed-layer depth and temperature in the presence of free heat exchange between the ocean and the atmosphere and in the presence of biological feedback are compared with their corresponding values after suppressing the air-sea heat exchange and the biological feedback. However, the two sets of

FIGURE 4.13. The effect of specified T_a on the model evolution. In this figure the mixed-layer depth and temperature from four model simulations are plotted. The layer depth and temperature estimated by the partially-coupled model with constant phytoplankton concentration, using stored air temperature (labeled as '7'), are substantially different from those estimated using the fully-coupled model with constant phytoplankton concentration (labeled as '8'). The figure shows the effect of biological feedback through the alteration of surface air temperature and hence the surface heat flux, as well as the effects associated with the vertical distribution of radiative heating within the ocean.

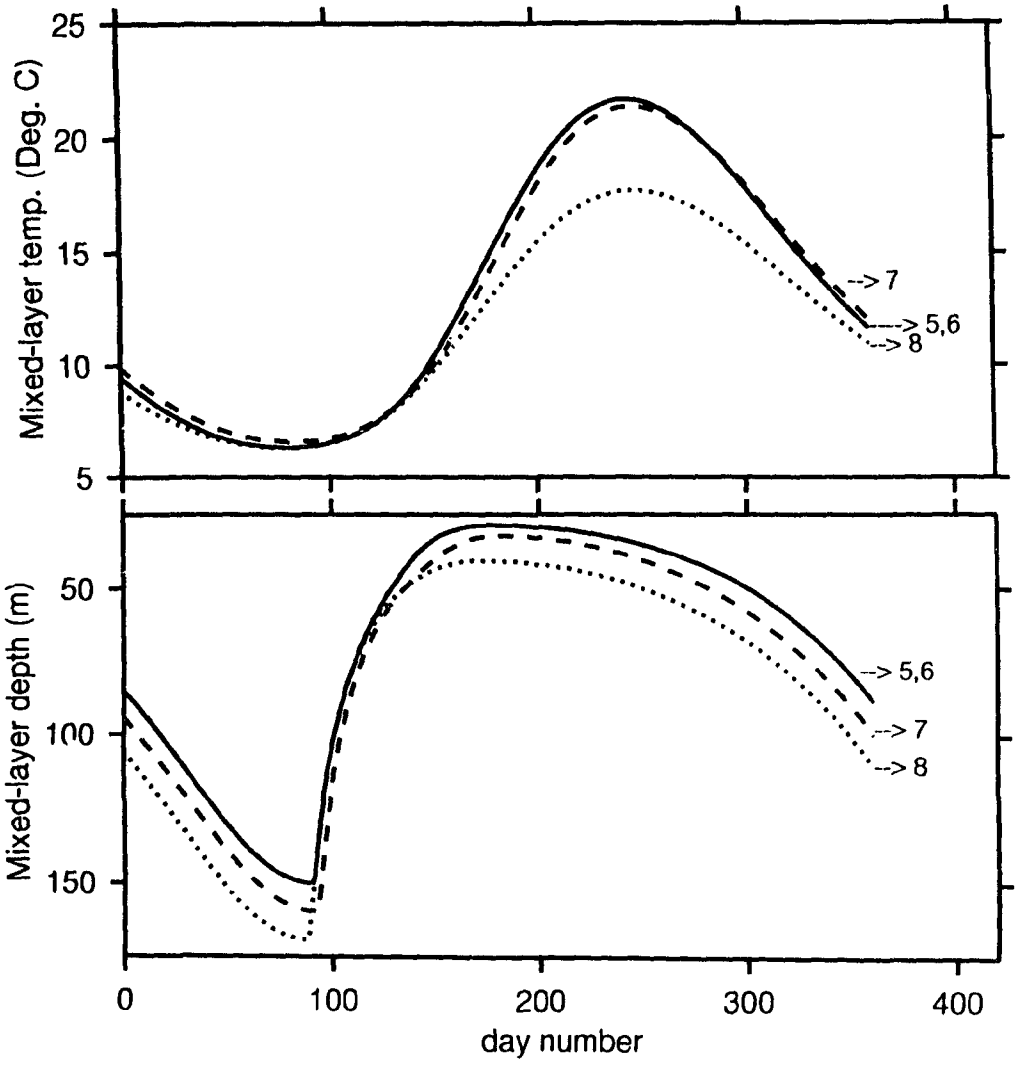

(5) Atmospheric feedback & Biological feedback
(6) Prescribed T_a & Biological feedback
(7) Prescribed T_a & No biological feedback
(8) Atmospheric feedback & No biological feedback

Figure 4.13

simulations differ from each other in the specification of the air-sea heat flux. In simulations 6 and 7, the full coupling between the ocean and the atmosphere is suppressed by prescribing externally the air temperature needed to calculate the net heat flux, rather than by specifying the net heat flux itself (as in the case of simulations 2 and 3). The new simulations are numbered from 5 to 8.

The fifth simulation examines the evolution of mixed-layer physics when both feedback processes are active. The daily values of mixed-layer depth and temperature from this simulation are shown by curves labeled '5' in Figure 4.13. These values are used as benchmarks to compare and contrast with the results from the next three simulations. The daily values of air temperature from this simulation are stored for use in the next two simulations, in calculation of the surface heat flux. (Note that the fifth simulation is identical to the fourth simulation shown in Figure 4.12. The same simulation is indexed differently to identify it as part of two distinct sets of experiments.)

In the sixth simulation, the coupling between the ocean and the atmosphere is suppressed by calculating the surface heat flux components using the prescribed values of air temperature rather than computing them as functions of the model-derived values of air temperature. The prescribed values used are the daily air temperatures stored during the fifth simulation. The biological feedback to the mixed-layer physics is retained in this simulation as it is in the previous one. The layer depth and temperature predicted by this simulation are analogous to those predicted by models of physical biological interactions in the ocean such as that of Simonot *et al.* (1988), as in both cases an externally-prescribed air temperature is used to calculate the heat fluxes. The results of this simulation are shown by curves labeled '6' in Figure 4.13. Even though the fifth and the sixth simulations differ from each other in the determination of the heat flux across the sea surface, the resulting heat fluxes are identical and the physical processes considered by the

models are identical. Therefore they give the same values of mixed-layer depth and temperature.

The seventh simulation differs from the sixth only in that the biological feedback is removed. That is, the mixed-layer depth and temperature are calculated assuming a constant biomass of 0.01 mg chl-a m^{-3}. As in the sixth simulation, the surface heat flux components are calculated using the prescribed values of air temperature, which in turn, are obtained from the fifth simulation. The depth and temperature predicted by the simulation are analogous to those predicted by thermodynamic models of the upper ocean such as that of Gaspar (1988). This is because, with the use of constant values of attenuation coefficient γ_m, both these models ignore the effect of biological feedback on mixed-layer physics. Also, they calculate the surface heat fluxes using prescribed values of air temperature. The results of this simulation are shown in Figure 4.13 using curves labeled '7': the predicted mixed-layer temperature is very close to that predicted in the fifth simulation. On the other hand, the mixed-layer depth is much different from that resulting from the fifth and sixth simulations.

In the final simulation, the evolution of mixed-layer depth and temperature in the presence of free exchange of heat between the ocean and the atmosphere is modelled without considering the biological feedback. That is, the coupling between the model ocean and the atmosphere is preserved but that between physical and biological processes in the mixed layer is removed through specification of a constant biomass of 0.01 mg chl-a m^{-3}. The evolution of mixed-layer depth and temperature predicted by this simulation is similar to what would be predicted by the Davidson and Garwood (1984) model. This is because, in both cases, the seasonal progressions of the mixed-layer physics and air-sea heat exchange are modelled without considering biological feedback. The curves labeled '8' in Figure 4.13 represent the mixed-layer depth and temperature produced by this simulation. Clearly,

the mixed-layer is much deeper and cooler than predicted in the previous three simulations.

The results of these simulations can be synthesized to give a general description of the effect of biological feedback, as follows.

The fifth simulation incorporates the effect of biological variability on the evolution of mixed-layer physics as well as on the seasonal progression of air-sea heat exchange. Therefore, the mixed-layer depth and temperature predicted by this simulation take into account all the effects of biological feedback (in the absence of nutrient limitation). The sixth simulation shows that coupled models of physical-biological interactions in the ocean, such as that of Simonot *et al.* (1988), can produce the same results through external prescription of the air temperature determined from observations, to the extent that the observed temperature reflects the contributions of the prevailing biological processes to the mixed-layer physics.

The mixed-layer temperature produced by the seventh simulation is very close to that resulting from the fifth simulation. Apparently, the mixed-layer temperature predicted by a model that incorporates the effect of biological feedback and a model that neglects it are almost identical. This result can easily be misinterpreted and therefore requires further explanation. The seventh simulation contains no reference to the effect of biological feedback on mixed-layer physics. Indeed, the biomass is maintained constant throughout. However, the prescribed values of air temperature were calculated by a model that did account for this feedback and, therefore, are higher than would be the case if the prescription was accomplished by a model that ignored it. The higher air temperature favours an increase in the transfer of heat from the atmosphere to the ocean, which in turn results in an increase in the layer temperature.

On the other hand, the layer depth predicted by the seventh simulation is much different from that produced by the fifth simulation. This is because the mixed-layer depth is controlled not only by the heat input to the layer but also by the vertical distribution of the penetrative component of solar radiation in the layer. When the biological feedback is neglected (simulation 7), the stratification within the mixed layer is weak and therefore the mixed-layer is deeper than it would be in the presence of biological feedback (simulation 5). The relative success of this model (simulation 7) in predicting the evolution of the layer temperature, even though the layer depth calculated by the model is incorrect, is analogous to the ability of mixed-layer models of constant depth to describe the seasonal evolution of the sea-surface temperature. In both cases, it is the seasonal evolution of the air temperature that dictates the evolution of the mixed-layer temperature.

In the last simulation, the effect of biological feedback is completely neglected. The results show that the mixed-layer depth and temperature predicted by the model are substantially different from those predicted by coupled models in which the biological feedback is explicit. This finding is relevant to the development of coupled models of the ocean-atmospheric system to simulate the large-scale characteristics of air-sea interactions. It suggests that, unless the seasonal evolution of biomass is incorporated explicitly into coupled models of air-sea interactions, the physical variables calculated by the model are likely to be in error.

4.6 Concluding Remarks

The principal goals of mixed-layer modelling are to estimate the temperature and depth of the mixed layer. With respect to the temperature, our experience with these simulations shows that reliable results will not be obtained unless the air temperature, a function of time, is specified or calculated with some accuracy. With respect to the depth of the mixed layer, there is a further requirement that the diffuse

vertical attenuation coefficient γ_m, also a function of time, be well specified if we are to have confidence in the results. In this context, well specified means carrying information on the local (time-, and space-dependent) biomass. The quality of the predictions for the temperature and depth of the mixed layer will always be constrained by the reliability of the data on, or models of, air temperature and attenuation coefficient used in the model.

What are the implications of these general observations for mixed-layer modelling? The best solution will be to use a fully-coupled, atmosphere-ocean-ecosystem model, as developed in this thesis. If for any reason the atmospheric component cannot be incorporated, the optimal approach will involve a coupled, ocean-ecosystem model with prescribed air temperature. Such a model will give good results for both the temperature and depth of the mixed layer, provided that the prescribed air temperature is accurate. Otherwise the results will be in error.

If we are also unable to incorporate the ecosystem model, it may still be possible to get reasonable results for temperature but the results of mixed-layer depth will be unreliable. Satisfactory estimation of mixed-layer depth requires that we know the local attenuation coefficient, a bio-optical property best obtained from an ecosystem model. A less perfect, but nevertheless viable alternative to coupling an ecosystem model would be to fix phytoplankton biomass from satellite data on ocean colour and use this to estimate the attenuation coefficient γ_m. If γ_m cannot be specified with confidence, either from an ecosystem model or by assimilation of remote-sensed data, the estimates of mixed-layer depth will be in error. The magnitude of the potential error will vary with time and place according to the amplitude of the seasonal signals in the biomass of phytoplankton.

CHAPTER 5

General Discussion and Conclusions

5.1 Introduction

Solar radiation penetrating the sea surface is one of the major sources of buoyancy in the upper ocean, which in turn, plays a critical role in the seasonal evolution of the depth and temperature of the surface mixed layer. The depth-dependent distribution of solar radiation in the ocean is taken into account in thermodynamic models of the upper ocean, such as that of Kraus and Turner (1967), by incorporating an attenuation coefficient into the model equations (see equations (2.1) and (2.2)). In reality, the attenuation coefficient is modulated spatially and temporally, according to the local biomass of phytoplankton. Therefore, mixed-layer depth and temperature are determined in part by the abundance of phytoplankton. Moreover, the rate of change of biomass depends on the mixed-layer depth itself. Hence, there is a potential for a positive feedback between phytoplankton dynamics and mixed-layer physics. In my thesis I have attempted to explore this feedback.

As a first step in this direction, a well-known mixed-layer model (Denman, 1973) is analyzed in Chapter 2, with respect to its sensitivity to the attenuation coefficient γ_m. The sensitivity analysis is used to explain how a given change in γ_m affects the deepening and shallowing of the mixed layer and how the layer temperature will respond to such a change. The principal conclusion of this analysis is that the effect of changes in γ_m on the evolution of the mixed-layer depth and temperature depends on the relative importance of solar radiation in the total buoyancy input to the ocean. In other words, the sensitivity of mixed-layer physics to changes in γ_m increases with increasing contribution from solar radiation to the

total buoyancy input to the mixed layer. Also, the results show that the evolution of mixed-layer depth and temperature are more sensitive to changes in γ_m when the layer is relatively transparent. A typical example occurs in high-latitude seas during Spring: in these conditions, a change in γ_m can play a critical role in determining the progression of the stratification. Because open-ocean waters are relatively transparent in comparison with coastal waters, small changes in γ_m in open-ocean waters can have a significant impact on the evolution of the layer depth and temperature.

Another important issue considered in Chapter 2 is the parameterization of γ_m itself. With few exceptions, existing mixed-layer models parameterize the attenuation of solar radiation in the ocean using an exponent that is independent of depth and wavelength. However, in Chapter 2, a method is developed to combine a mixed-layer model with spectral models of underwater irradiance. In particular, it allows Kraus-Turner-type models to be extended to account for the depth dependence of γ_m. Moreover, equations (2.48) and (2.49) can easily be adapted to deal with absorption by substances other than phytoplankton.

Bulk models of the mixed-layer are conceptually simple and computationally efficient. Therefore they are widely used in theoretical descriptions of upper-ocean thermodynamics and for incorporation of thermodynamic processes into large-scale circulation models. However, these models have been criticized for the assumptions used in their formulation, such as the existence of a density discontinuity at the base of the mixed layer. In Chapter 3, I have provided an alternative derivation of a bulk, mixed-layer model. The equations derived are more general than the conventional model equations. From a theoretical point of view, the significance of the model developed in Chapter 3 is that it is based entirely on the simple physical concept of the change in the potential energy of a water column resulting from vertical mixing. Also, each of the eight terms in the model equation can be identified with a physical process contributing to the evolution of the layer depth. From a practical

point of view, the model's significance is that it extends the range of applicability of bulk models to conditions that are beyond the scope of the conventional bulk models. Moreover, the model could be used to couple thermodynamic processes into large-scale circulation models of the upper ocean with improved heat conservation. Another important feature of the model developed in Chapter 3 is that when the energy inputs remain constant, the model results are not sensitive to the time step of integration. This is useful for developing mixed-layer models with larger time steps than permitted by conventional models.

Having developed a new model with the characteristics described above, one can now examine the central theme of the thesis: the potential feedback between biological processes and mixed-layer physics. However, one must be alert to the possibility that this feedback might be nullified by air-sea heat exchange. Therefore, in Chapter 4, I have developed a coupled model of mixed-layer physics, mixed-layer biology and the atmosphere. The numerical simulations with this coupled model show that, under the specific conditions considered, biological variability can produce up to 25 m change in the mixed-layer depth, up to 5°C change in the mixed-layer temperature and air temperature, and up to 15 W m^{-2} change in the heat flux across the sea surface. The study also shows that the effects of biological feedback on mixed-layer physics and atmospheric physics are not linear functions of phytoplankton biomass. Rather, they saturate with increasing biomass. It is noticed that the effect of biological feedback reaches its saturation as the biomass reaches above 10 mg chl-a m^{-3}, which is well within the range of variability that can be observed in the ocean. Furthermore, the effect of variations in biomass is maximum when the mixed layer is relatively transparent.

In Chapter 4, it is also shown that the air-sea heat exchange and the physical-biological interactions in the mixed layer have opposing roles in the evolution of the layer temperature. However, the modification in air-sea heat exchange is not

sufficient to neutralize the effect of physical-biological interactions. Thus the biological feedback to the mixed-layer physics is a real effect rather than a virtual one. Further, I have examined the consequence of neglecting biological feedback in models of upper-ocean thermodynamics and air-sea interactions. The results show that coupled models of mixed layer and atmosphere could significantly underestimate the seasonal evolution of mixed-layer depth, mixed-layer temperature, and air temperature, unless such models incorporated the effect of biological feedback.

5.2 A Conceptual Model of Physical-Biological Interactions

In Figure 5.1, the various components of the work presented in the previous chapters are synthesized and presented schematically to derive a qualitative description of physical-biological interactions in the ocean and their effect on heat exchange across the sea surface.

Shallowing of the mixed-layer results in an increase in the net growth rate of phytoplankton, which in turn leads to a net increase in the biomass in the mixed layer. As a consequence, the amount of solar radiation absorbed by the layer increases, as does the buoyancy input to the mixed layer. The mixed-layer depth therefore decreases further. Thus, the increase in the phytoplankton biomass in the mixed layer, subsequent modification of the attenuation of solar radiation in the layer, and the resulting decrease in the layer depth, represent a feedback loop of interactions, identified by region I of Figure 5.1, between the phytoplankton concentration and mixed-layer depth.

An increase in the attenuation coefficient of the mixed layer increases the layer temperature by increasing the amount of solar radiation absorbed by the layer. An increase in the stratifying tendency of the mixed layer associated with an increase in the attenuation coefficient can also cause a decrease in the layer depth.

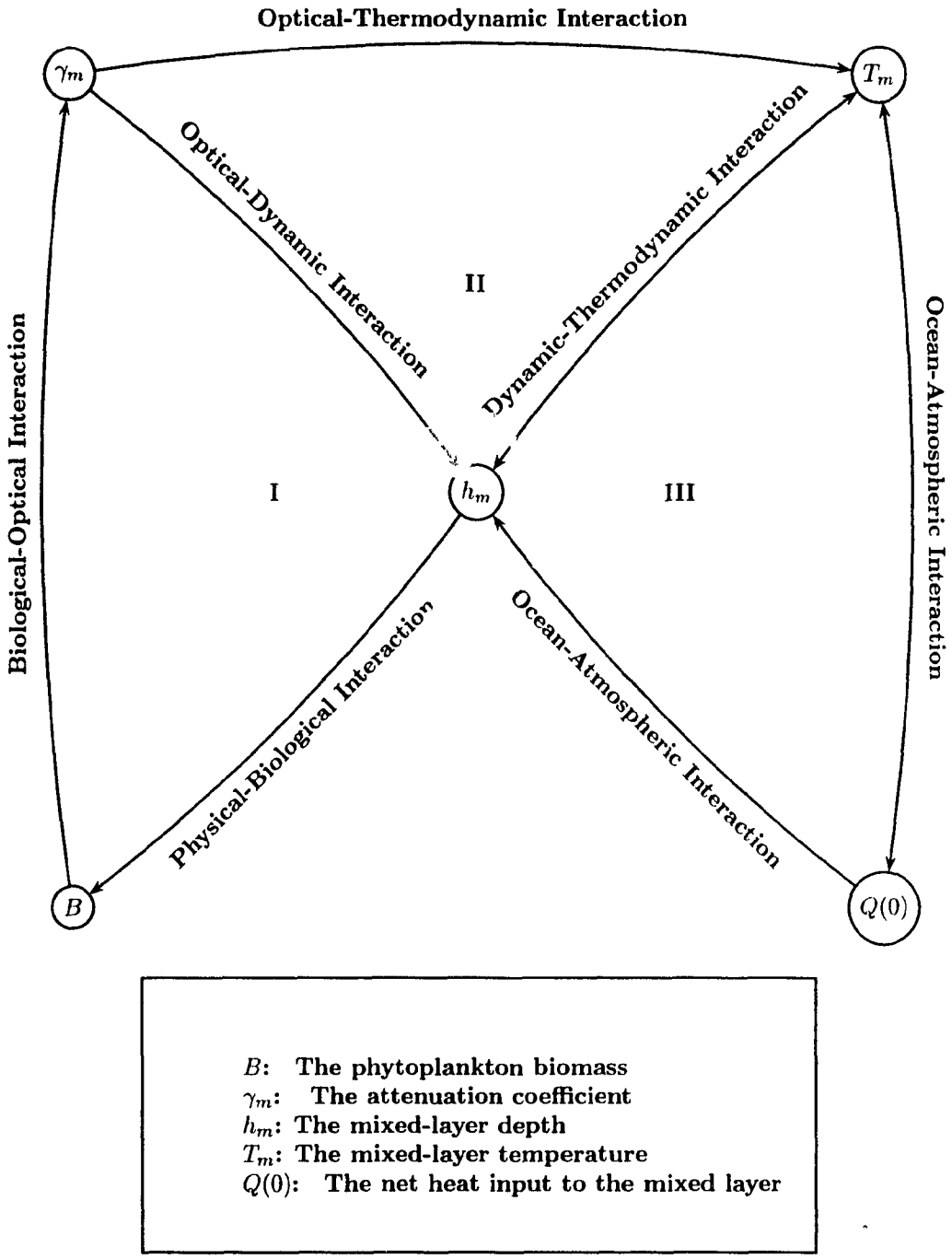

FIGURE 5.1. A conceptual model of physical-biological interactions in the ocean-atmosphere system.

Consequently the absorbed energy is distributed over a shorter vertical extent and therefore the mean temperature of the layer will increase further. These processes together constitute interactions identified by region II in Figure 5.1.

Interaction between mixed-layer thermodynamics and the atmospheric physics is represented by region III of the figure. An increase in the mixed-layer temperature increases the heat transfer to the atmosphere. The resulting heat loss from the mixed layer decreases the temperature of the layer, which increases the layer depth. This may lead to further decrease in the layer temperature as solar heating would now be redistributed over a greater vertical interval.

The interaction in the mixed layer between the biological and thermodynamic processes (identified as region I in Figure 5.1) and that between the mixed-layer thermodynamics and the atmosphere (identified as region III in the figure) act in opposite directions with regard to their effects on mixed-layer depth and temperature. If the net effects of the interactions represented by region I and III of the figure were equal in magnitude, biological processes would not cause any change in the mixed-layer depth, temperature or the heat exchange. But the results of model simulations indicate that air-sea heat exchange is not sufficient to neutralize the effects of interactions between the biological and thermodynamic processes in the mixed layer. Figure 4.12 shows that changes in mixed-layer depth and temperature are typically reduced by order of 50% through heat loss to the atmosphere, so the effect is definitely significant, although not dominant.

5.3 Limiting Conditions of the Interactions

a) Physical-biological interactions in the mixed layer

The shallowing of the mixed layer results in an increase in the phytoplankton

biomass in the layer. An increase in biomass further decreases the layer depth. Thus, the physical-biological interactions in a shallowing mixed layer are driven by a positive feedback between the shallowing of the layer and the increase in the phytoplankton biomass. I now consider whether this positive feedback can continue indefinitely, resulting in an unrestrained growth of phytoplankton and the disappearance of the mixed layer.

The depth of a shallowing mixed layer is given by equation (3.32). The effect of changes in the attenuation coefficient for solar radiation is incorporated into this equation through the function $f_{h_m^+}$. The dependency of this function on the phytoplankton concentration in the layer is identical to that of f_{h_m} shown in Figure 2.3. The range of $f_{h_m^+}$ is between 0 and 1. It is shown in Chapter 2 that, towards higher values of phytoplankton concentration, the change in $f_{h_m^+}$ is asymptotic; in other words, the rate of change in $f_{h_m^+}$ decreases sharply for higher biomass. Consequently, the sensitivity of mixed-layer depth to changes in the phytoplankton concentration decreases as the biomass increases.

The analyses presented in Chapter 4 suggest that when the initial biomass is relatively low, the positive feedback between the layer depth and the biomass is very strong, which results in a rapid shallowing of the layer and a rapid increase in the biomass. As the biomass increases, the feedback becomes weak and the layer depth becomes insensitive to further increase in the biomass. In other words, the positive feedback saturates as the phytoplankton concentration increases. This factor prevents the physical-biological interaction in the mixed layer from causing a runaway phytoplankton bloom or the disappearance of the mixed layer. The termination of the positive feedback is given by the limiting case of $\gamma \rightarrow \infty$ or $f_{h_m^+} = 1$. Under the limiting case, the depth of the mixed layer can be written as:

$$h_m^+ = \frac{\left[2C_p(G-D)\right]}{g\alpha\left[I(0)+Q(0)\right]}. \tag{5.1}$$

This equation is equivalent to the conventional definition of the Monin-Obukhov depth (Kundu, 1990).

b) Optical-thermodynamic interactions in the mixed layer

As seen above, when the attenuation coefficient of the mixed layer increases, the sensitivity of the mixed-layer depth to changes in the attenuation coefficient weakens. The sensitivity of mixed-layer temperature to changes in the attenuation also weakens as the attenuation increases. This is because an increase in the attenuation coefficient results in a decrease in the amount of solar radiation penetrating the base of the mixed layer. Once the amount of solar radiation penetrating the base of the mixed layer becomes negligible, the layer temperature becomes insensitive to further increases in the attenuation coefficient, provided that the layer depth remains constant. For a given amount of energy stored in the layer, the resultant temperature depends simply on the thickness of the layer over which the stored energy is distributed. The dependence of mixed-layer temperature on the layer depth is a fundamental effect that is important under all circumstances.

c) The relation between mixed-layer thermodynamics and the air-sea heat exchange

With increasing mixed-layer temperature, the heat transfer from the mixed layer to the atmosphere increases. The consequence of such an increase for the atmospheric heat budget is determined by the balance between the incoming solar radiation, $R(-h_a)$, and the outgoing longwave radiation, $L(-h_a)$, at the top of the atmosphere. As long as the heat input from solar radiation exceeds the heat loss from the emission of longwave radiation, $(H(-h_a) > 0)$, there will be an increase in the combined heat content of the ocean and the atmosphere. The model equations

for h_m and T_m are functions of the surface heat flux $Q(0)$, which itself is a function of T_m. Therefore, the evolutions of the surface heat flux $Q(0)$ and the layer temperature T_m always depend on each other.

5.4 Other Ways in Which Biological Processes may Influence the Physics of the Upper Ocean

Pollard and Regier (1990) have reported that the vertical motion associated with the conservation of potential vorticity in the upper ocean may be an important factor regulating mixed-layer evolution and formation of the seasonal thermocline. The distribution of potential vorticity in the upper ocean depends on the vertical stratification in the water column. Following Pollard and Regier (1990), the potential vorticity of the mixed layer q can be expressed as:

$$q = \frac{(f + \zeta')}{h_m} \frac{\Delta\rho_m}{\rho_m}, \tag{5.2}$$

where f and ζ' are the planetary and relative vorticities, ρ_m is the density of the mixed layer, $\Delta\rho_m$ is the density difference between the mixed layer and the underlying water and h_m is the depth of the mixed layer. The sensitivity analyses presented in Chapter 2 suggest that both $\Delta\rho_m$ and h_m in equation (5.2) are sensitive to changes in the phytoplankton concentration. An increase in the phytoplankton concentration will increase the amount of solar radiation absorbed within the mixed layer and therefore increase $\Delta\rho_m$. The increased stratification will decrease the layer depth. Thus, an increase in the phytoplankton biomass will result in an increase in $\Delta\rho_m$ and a decrease in h_m both of which are favorable for an increase in the magnitude of q.

Satellite data on ocean colour shows that many parts of the world ocean, including the North-West Atlantic, the Northern Arabian Sea and the Equatorial

Pacific, are subject to large-scale seasonal and spatial variability in the phytoplankton biomass (see McClain (1993) for a review). The argument presented above suggests that changes in the mixed-layer depth induced by modulations in phytoplankton concentration may modify the potential-vorticity field. The resulting vertical motion may contribute to horizontal variability in vertical mixing, nutrient input, phytoplankton production and even circulation. The magnitudes of these effects are yet to be determined.

Warm-, and cold-core rings are typical features associated with large-scale ocean circulation. Cold-core rings are generally regarded as regions of relatively high primary production as they are formed by the upwelling of nutrient-rich waters. On the contrary, warm-core rings are generally considered to be unproductive. However, Tranter *et al.* (1980) have reported that physical-biological interactions in a warm-core ring can be responsible for increased primary production within the ring. In the presence of strong surface cooling, convective overturning elevates the nutrient concentration within the ring. Subsequently, as the ring reaches regions of surface heating, a shallow layer is formed at the center of the ring. In this shallow layer, characterized by elevated nutrient concentration with respect to the surrounding waters, phytoplankton production exceeds losses, resulting in an increase in the biomass concentration. The feedback from phytoplankton variability can modify the temperature distribution within the ring and thereby influence the evolution of the ring.

Another potentially important aspect of the physical-biological interactions in the mixed layer is the effect of optical variability in the mixed layer on the heat input to the deep ocean (Lewis *et al.,* 1990; Webster, 1994). Because the mixed layer is in constant contact with the atmosphere, the heat stored in the layer is readily available for exchange with the atmosphere. In the presence of a shallow and relatively transparent mixed layer, a significant portion of the solar

radiation entering the ocean may be transferred beneath the mixed layer. This portion is temporarily removed from the energy budgets of the mixed-layer and the atmosphere. During the deepening phase of the mixed-layer evolution, the energy trapped in the thermocline may be re-introduced into the mixed layer. Or, subsurface currents, such as the equatorial undercurrents, can transport the trapped energy from one region to another, modifying the regional heat budget of the ocean and the atmosphere. The amount of solar energy trapped beneath the mixed layer depends on the optical properties of the mixed layer, which in turn, are influenced by the biological processes within the layer.

5.5 Concluding Remarks

If we want to make a reliable model of the surface mixed layer of the ocean for a particular station, variations in the the attenuation coefficient for the solar radiation (γ_m) should be accounted for. The better the determination of γ_m, the better the results will be. This is true for any region, irrespective of whether the changes in the light attenuation are dominated by sediment discharge from the continent, by dust input from wind or by modulations in phytoplankton biomass caused by changes in the environmental conditions. The principal contribution to variability in γ_m in the open ocean is overwhelmingly biological. The study presented in this thesis has shown that, after correcting for losses to the atmosphere, the biological modifications to γ_m can account for changes of up to 5°C in the mixed-layer temperature, under the specific energy-input conditions considered. Studies of air-sea interactions in the tropics have shown that even an error of about 0.5°C in the mixed-layer temperature can seriously limit our ability to predict the evolution of physical processes in the lower atmosphere (Kershaw, 1988). This is only one of many reasons that justify the incorporation of biological feedback in models of the seasonal evolution of the upper-ocean physics and the lower atmosphere.

In this thesis I have focused on the effects of temporal variability in the phytoplankton biomass on mixed-layer evolution and air-sea heat exchange. The effect of spatial variability in the biomass field is an equally important issue that requires further examination. Both the spatial and temporal variability in phytoplankton distribution in the ocean are controlled by the upper-ocean circulation. Therefore, an essential step for further understanding the physical-biological interactions in the upper ocean associated with phytoplankton variability is to extend the one-dimensional analysis presented in this thesis to three dimensions, by incorporating a thermodynamic model and a biological model into a circulation model of the upper ocean that is coupled to an atmospheric model.

REFERENCES

Antoine, D. and A. Morel, Modelling the seasonal course of the upper ocean pCO_2 (I). Development of a one-dimensional model, *Tellus*, *47B*, 103-121, 1995.

Archer, D., *Modeling* pCO_2 *in the upper ocean: a review of relevant physical, chemical and biological processes*, 63 pp., US Dept. of Energy, TRO50, 1990.

Ball, F. K., Control of inversion height by surface heating, *Quart. J. R. Met. Soc., 86*, 483-494, 1960.

Banse, K., Grazing, the temporal changes of phytoplankton concentrations, and the microbial loop in the open sea, In *Primary productivity and biogeochemical cycles in the sea*, edited by P. Falkowski and A. D. Woodhead, pp. 409-440, Plenum Press, New York, 1992.

Cherniawsky, J. Y., C. W. Yuen, C. A. Lin and L. A Mysak, Numerical experiments with a wind-and buoyancy-driven two-and-a-half-layer upper ocean model, *J. Geophys. Res., 95*, 16149-16167, 1990.

Davidson, K. L. and R. W. Garwood, Coupled oceanic and atmospheric mixed layer model, *Dynamics of Atmospheres and Oceans*, *8*, 283-296, 1984.

Denman, K L., *The response of the upper ocean to meteorological forcing*, Ph. D. thesis, 118 pp., University of British Columbia, Vancouver, B. C., 1972.

Denman, K. L., A time-dependent model of the upper ocean, *J. Phys. Oceanogr.*, *3*, 173-184, 1973.

Denman, K. L. and M. Miyake, Upper layer modification at Ocean Station *Papa*: observations and simulation, *J. Phys. Oceanogr.*, *3*, 185-196, 1973.

Dickey, T. D. and J. J. Simpson, The influence of optical water type on the diurnal response of the upper ocean, *Tellus*, *35B*, 142-154, 1983.

Fasham, M. J. R., H. W. Ducklow and S. M. McKelvie, A nitrogen-based model of plankton dynamics in the oceanic mixed layer, *J. Mar. Res.*, *48*, 591-639, 1990.

Foukal, P. and J. Lean, An empirical model of total solar irradiance variation between 1874 and 1988, *Science, 247*, 556-558, 1990.

Garwood, R. W., An oceanic mixed layer model capable of simulating cyclic states, *J. Phys. Oceanogr.*, *7*, 455-468, 1977.

Garwood, R. W., Air-sea interaction and dynamics of the surface mixed layer, *Reviews of Geophysics and Space Physics*, *17*, 1507-1524, 1979.

Gaspar, P., Modeling the seasonal cycle of the upper ocean, *J. Phys. Oceanogr.*, *18*, 161-180, 1988.

Gill, A. E., *Atmosphere-Ocean Dynamics*, 662 pp., Academic Press, San Diego, 1982.

Halpern, D., Upper ocean current and temperature observations along the Equator West of the Galapagos islands before and during the 1982-83 ENSO event, In *Papers from 1982/83 El Niño/Southern Oscillation Workshop,* edited by Witte, J., pp. 59-91, National Research Council, U.S.A., 1983.

Haney, R. L., Surface thermal boundary condition for ocean circulation models, *J. Phys. Oceanogr., 1,* 241-248, 1971.

Harrison, W.G., L. R. Harris and B. D. Irwin, The kinetics of nitrogen utilization in the oceanic mixed layer: nitrate and ammonium interactions at nanomolar concentrations, in press, *Limol. Oceanogr.,* 1996.

Heinrich, A. K., The life histories of plankton animals and seasonal cycle of plankton communities in the ocean, *J. Cons. Perm. Int. Explor. Mer, 27,* 15-24, 1962.

Iqbal, M., *Introduction to solar radiation,* 390 pp., Academic Press, Toronto, 1983.

Jerlov, N. G., *Marine Optics,* 231 pp., Elsevier, Amsterdam, 1976.

Joseph, P. V., B. Liebmann and H. H. Hendon, Interannual variability of the Australian summer monsoon onset: possible influence of Indian summer monsoon and El Niño, *J. Climate,* 4, 529-538, 1991.

Kantha, L. H. and C. A. Clayson, An improved mixed layer model for geophysical applications, *J. Geophys. Res., 99,* 25235-25266, 1994.

Kershaw, R., The effect of a sea surface temperature anomaly on a prediction of the onset of the south-west monsoon over India, *Quart. J. R. Met. Soc., 114*, 325-345, 1988.

Kim, J. W., A generalized bulk model of the oceanic mixed layer, *J. Phys. Oceanogr., 6*, 686-695, 1976.

Kirk, J. T. O., *Light and photosynthesis in aquatic ecosystems*, 401 pp., Cambridge University Press, Cambridge, 1983.

Kirk, J. T. O., Solar heating of water bodies as influenced by their inherent optical properties, *J. Geophys. Res., 93*, 10897-10908, 1988.

Kraus, E. B., Merits and defects of different approaches to mixed layer modelling, In *Small-scale turbulence and mixing in the ocean*, edited by J. C. J. Nihoul and B. M. Jamart, pp. 37-50, Elsevier, Amsterdam, 1988.

Kraus, E. B., and J. S. Turner, A one-dimensional model of the seasonal thermocline, II. The general theory and its consequences, *Tellus, 19*, 98-105, 1967.

Kundu, P. K., *Fluid mechanics*, 638 pp., Academic Press, San Diego, 1990.

Lampitt, R. S., Evidence for the seasonal deposition of detritus to the deep-sea floor and its subsequent resuspension, *Deep Sea Res., 32,* 885-897, 1985.

Large, W. G., J. C. McWilliams and S. Doney, Oceanic vertical mixing: a review and a model with a nonlocal boundary layer parameterization, *Reviews of Geophysics, 32,* 363-403, 1994.

Lewis, M. R., J. J. Cullen and T. Platt, Phytoplankton and thermal structure in the upper ocean: consequences of nonuniformity in chlorophyll profile, *J. Geophys. Res.*, *88*, 2565-2570, 1983.

Lewis, M. R., M. E. Carr, G. C. Feldman, W. Esaias and C. McClain, Influence of penetrating solar radiation on the heat budget of the equatorial Pacific Ocean, *Nature*, *347*, 543-545, 1990.

Martin, P. J., Simulation of the mixed layer at OWS November and Papa with several models, *J. Geophys. Res.*, *90*, 903-916, 1985.

McClain, C. R., Review of major CZCS applications: U.S. case studies, In *Ocean colour: theory and applications in a decade of CZCS experience,* edited by Barale V. and P. M. Schlittenhardt, pp. 167-188, Kluwer Academic Publishers, Dordrecht, 1993.

McCormick, M. J. and G. A. Meadows, An intercomparison of four mixed layer models in a shallow inland sea, *J. Geophys. Res.*, *93*, 6774-6788, 1988.

McCreary, J. P. and P. K. Kundu, A numerical investigation of sea surface temperature variability in the Arabian Sea, *J. Geophys. Res., 94*, 16097-16114, 1989.

McCreary, J. P., P. K. Kundu and R. L. Molinari, A numerical investigation of dynamics, thermodynamics and mixed-layer processes in the Indian ocean, *Prog. Oceanogr., 31,* 181-244, 1993.

Mellor, G. L. and P. A. Durbin, The structure and dynamics of the ocean surface mixed layer, *J. Phys. Oceanogr.,5*, 718-728, 1975.

Mellor, G. L and T. Yamada, A hierarchy of turbulent closure models for planetary boundary layers, *J. Atmos. Sci., 31*, 1791-1806, 1974.

Morel, A., Light and marine photosynthesis: a spectral model with geochemical and climatological implications, *Prog. Oceanogr., 26,* 263-306, 1991.

Morel A. and D. Antoine, Heating rate within the upper ocean in relation to its bio-optical state, *J. Phys. Oceanogr., 24,* 1652-1665, 1994.

Morris, A. H. Jr., *NSWC library of mathematics subroutines*, NSWCDD/TR-90/425, 609 pp., Naval Surface Warfare Center, US Navy, Virginia, 1993.

Niiler, P. P., Deepening of the wind-mixed layer, *J. Mar. Res.*, *33*, 405-422, 1975.

Niiler, P. P. and E. B. Kraus, One-dimensional models of the upper ocean, In *Modelling and prediction of the upper layers of the ocean*, edited by E. B. Kraus, pp. 143-172, Pergammon Press, Oxford, 1977.

Palmer, T. N., Response of the UK Meteorological Office general circulation model to sea surface temperature anomalies in the tropical Pacific Ocean, In *Coupled ocean atmosphere models*, edited by J. C. J. Nihoul, pp. 83-107, Elsevier, Amsterdam, 1985.

Paltridge, G. W and C. M. R. Platt, *Radiative processes in meteorology and climatology*, 318 pp., Elsevier Scientific Publishing Company, Amsterdam, 1985.

Platt, T., S. Sathyendranath and P. Ravindran, Primary production by phytoplankton: analytic solutions for daily rates per unit area of water surface, *Proc. R. Soc. Lond. B, 241*, 101-111, 1990.

Platt, T., D. F. Bird and S. Sathyendranath, Critical depth and marine primary production, *Proc. R. Soc. Lond. B, 246*, 205-217, 1991.

Platt, T., J. D. Woods, S. Sathyendranath and W. Barkmann, Net primary production & stratification in the ocean, In *The polar oceans and their role in shaping the global environment,* edited by O. M. Johannessen, R. D. Muench and J. E. Overland, pp. 247-254, Geophysical Monograph 85, American Geophysical Union, 1994.

Pollard, R. T. and L. Regier, Large variations in potential vorticity at small spatial scales in the upper ocean, *Nature, 348,* 227-229, 1990.

Price, J. F., R. A. Weller and R. Pinkle, Diurnal cycling: observations and models of the upper ocean response to diurnal heating, cooling and wind mixing, *J. Geophys. Res., 91,* 8411-8427, 1986.

Ramp S. R., R. W. Garwood, C. O. Davis and R. L. Snow, Surface heating and patchiness in the coastal ocean off Central California during a wind relaxation event, *J. Geophys. Res., 96,* 14947-14957, 1991.

Rasmusson, E. M. and T. H. Carpenter, The relationship between eastern equatorial Pacific sea surface temperatures and rainfall over India and Sri Lanka, *Mon. Weather Rev., 111,* 517-528, 1983.

Rosati, A. and K. Miyakoda, A general circulation model for upper ocean simulation, *J. Phys. Oceanogr., 18*, 1601-1626, 1988.

Sathyendranath, S., A. D. Gouveia, S. R. Shetye, P. Ravindran and T. Platt, Biological control of surface temperature in the Arabian Sea, *Nature, 349*, 54-56, 1991.

Sathyendranath, S. and T. Platt, The spectral irradiance field at the surface and in the interior of the ocean: a model for applications in oceanography and remote sensing, *J. Geophys. Res., 93*, 9270-9280, 1988.

Sathyendranath, S. and T. Platt, New production and mixed-layer physics, In Special Volume on *Biogeochemistry of the Arabian Sea: present information and gaps*, edited by D. Lal, pp. 177-188, Proc. Indian Academy of Sci., 1994.

Schopf, P. S. and M. A. Cane, On equatorial dynamics, mixed layer physics and sea surface temperature, *J. Phys. Oceanogr., 13*, 917-935, 1983.

Schopf, P. S. and D. E. Harrison, On equatorial waves and El Niño. I: Influence of initial states on wave-induced currents and warming, *J. Phys. Oceanogr., 13*, 936-948, 1983.

Shetye, S. R., A model study of the seasonal cycle of the Arabian Sea surface temperature, *J. Mar. Res., 44*, 521-542, 1986.

Simonot, J.-Y., E. Dollinger and H. L., Treut, Thermodynamic-biological-optical coupling in the oceanic mixed layer, *J. Geophys. Res., 93*, 8193-8202, 1988.

Simpson, J. H., C. M. Allen and N. C. G. Morris, Fronts on the continental shelf, *J. Geophys. Res., 83* 4607-4614, 1978.

Simpson, J. J. and T. D. Dickey, The relationship between downward irradiance and upper ocean structure, *J. Phys. Oceanogr., 11*, 309-323, 1981.

Smayda, T. J., The suspension and sinking of phytoplankton in the sea, *Oceanogr. mar. Biol., 8*, 353-414, 1970.

Stocker, T. F., D. G. Wright, and L. A. Mysak, A zonally averaged, coupled ocean-atmosphere model for paleoclimate studies, *J. Climate, 5*, 773-797, 1992.

Stramska, M. and T. D. Dickey, Phytoplankton bloom and the vertical thermal structure of the upper ocean, *J. Mar. Res., 51*, 819-842, 1993.

Sverdrup, H. U., On conditions for the vernal blooming of phytoplankton, *J. Cons. Perm. Int. Explor. Mer, 18*, 287-295, 1953.

Takahashi T., J. Olafsson, J. G. Goddard, D. W. Chipman and S. C. Sutherland, Seasonal variation of CO_2 and nutrients in the high-latitude surface oceans: a comparative study, *Global Biogeochem. Cycles, 7*, 843-878, 1993.

Taylor, A. H., A. J. Watson, M. Ainsworth, J. E. Robertson and D. R. Turner, A modelling investigation of the role of phytoplankton in the balance of carbon at the surface of the North Atlantic, *Global Biogeochem. Cycles, 5*, 151-171, 1991.

Thompson, R. O. R. Y., Climatological numerical models of the surface mixed layer of the ocean, *J. Phys. Oceanogr.*, *6*, 496-503, 1976.

Tranter, D. J., R. R. Parker and G. R. Cresswell, Are warm-core eddies unproductive?, *Nature*, *284*, 540-542, 1980.

Turner, J. S., A note on wind mixing at the seasonal thermocline, *Deep Sea Res.*, *16*, 297-300, 1969.

Wallace, J. M., and P. V. Hobbs, *Atmospheric science: an introductory survey*, 467 pp., Academic Press, San Diego, 1977.

Webster, P. J., The role of hydrological processes in ocean-atmosphere interactions, *Reviews of Geophysics*, *32*, 427-476, 1994.

Woods, J. D., W. Barkmann and A. Horch, Solar heating of the world ocean, *Quart. J. R. Met. Soc.*, *110*, 633-656, 1984.

Woods, J. D. and W. Barkmann, The response of the upper ocean to solar heating. I: The mixed layer, *Quart. J. R. Met. Soc.*, *112*, 1-27, 1986.

Wroblewski, J. S., *A model of spatial structure and productivity of phytoplankton populations during variable upwelling off the coast of Oregon*, Technical report, 116 pp., MASIG, Florida State University, 1976.

Zilitinkevich, S. S., D. V. Chalikov and Y. D. Resnyansky, Modelling the oceanic upper layer, *Oceanol. Acta*, *2*, 219-240, 1979.